EMTP-based Load Disaggregation at Feeder Levels

by

Shima Shojae

B.Sc., Sharif University of Technology, 2011

A THESIS SUBMITTED IN PARTIAL FULFILLMENT
OF THE REQUIREMENTS FOR THE DEGREE OF

Master of Applied Science

in

THE FACULTY OF GRADUATE AND POSTDOCTORAL STUDIES
(Electrical and Computer Engineering)

The University of British Columbia
(Vancouver)

September 2015

Abstract

Power distribution networks play an important role in electricity grid. Distribution system components require becoming smarter and more automated for the sake of improving their reliability and increasing their operational efficiency. Smart meters are one of the powerful devices that achieved this goal. However, their data are of minimal use — grid or load information obtained from smart meters are shallowly analysed. This thesis takes advantage of the shortcoming by accurately calculating the load information using EMTP-based load disaggregation method. The approach is applicable to residential loads at small scale and feeders at large scale.

In this thesis we first give our theoretical method for load disaggregation inspired by EMTP computational program. Then with simulation and experimental results, we demonstrate that our work outperforms past solutions by the following advantages:

1. EMTP-based load disaggregation is applicable at every point of interest, i.e., from distribution feeder down to the customer's entry point.

2. Unlike other methods, our method employs both transient and steady state load properties.

3. Last but not least, our solution is capable of determining load's electrical parameters.

In this thesis we stress on three major eigen-loads: (1) motor, (2) resistive, and (3) purely inductive. Then we report how much of the load is made of each eigen-load. We exampled our method on a number of PSCAD simulation cases and a few real appliance measurements. Our results prove load disaggregation shall assist power system engineers in evaluating the power flow on accurate load observations.

Preface

The originality of this thesis is based on the author's authentic research work. All theory, simulation, and experimental results have been produced in UBC Electrical Engineering Power Systems Lab exercised within the last two years.

Table of Contents

List of Tables

List of Figures

Glossary

The following are abbreviations and acronyms used in this thesis, listed in alphabetical order:

SCADA supervisory control and data acquisition

AGC Automatic Generation Control

DMS Distribution Management System

VVO Voltage VAR Optimization

SG Smart Grid

DS Distribution System

OLTC On Load Tap Changer

LPF Linear Power Flow

ALM Appliance Load Monitoring

NILM Non Intrusive Load Monitoring

NALM Non Intrusive Appliance Monitoring

ILM Intrusive Load Monitoring

THD Total Harmonic Distortion

REDD Residential Energy Disaggregation Data

STFT Short Time Fourier Transform

SVM Support Vector Machine

ANN Artificial Neural Network

DWT Discrete Wavelet Transform

LPF Linear Power Flow

SFA Shifted Frequency Analysis

AMI Advanced Metering Infrastructure

Acknowledgements

First, I would like to thank my supervisor, Professor Dr. Jose Marti. I had such an honour to meet Dr. Marti when for the first time, I visited UBC in 2013. I am super grateful to have Dr. Marti recruiting me, especially during hard times of this research. He never stopped motivating me yet encouraged to work harder. I remember whenever I was stuck in uncharted areas of the work, he kept telling that, there always has to be a solution. He was right, there was a solution. Without his constructive feedback, technical support, patient guidance, and his big heart, I would have not been able to finish this work.

Second, I would like to thank my graduate course instructors, in particular, Dr. Hermann Dommel, Dr. Nagpal Mukesh, Mr. Nathan Ozog, and Dr. Ebrahim Vaahedi. I learned a lot in their classes. They opened up my eyes in the power system world, the challenges and the solutions. They provided me technical insight.

Third, my thanks go to UBC power systems lab graduate students. We all were like a family working together and pushing each other towards reaching our goals. In particular, Dr. Hamed Ahmadi, I had a close collaboration with him during my research. He always spot me with difficult questions, which triggered to think deeper to find genuine answers.

Fourth, my parents, the angles of my life. Whoever I am today and I will be in future, undoubtedly is because of them. My father was my role model from the beginning of my education. I learned his hard working while inherited his sharpness and patience. Due to his treat, I have always been number one in school to enter Sharif. He taught me to work hard for our goals to achieve them. My mom, the symbol of scarification who supported me emotionally during every stage of my life. I am indebted and proud of these two wonderful people for the whole rest of my life.

Lastly and the most importantly, many many thanks to my handsome and kindhearted Mehdi. He is the one who wants me have the best, makes me laugh hard and be the

luckiest girl. Mehdi always pushes for stretching the boundaries to get closer to my big dreams. Without him, this thesis could have never come together. During the past six months, he did a lot for me specificity patiently walking with me for writing my thesis.

Chapter 1

Introduction

Every power systems network is comprised of three main sections: (1) Generation, (2) Transmission, and (3) Distribution. Generation takes care of producing electrical power from the potential water accumulated behind dams or burning the coal or natural gas. Transmission is the process of transferring the generated power to feeders — electrical power is transmitted at high voltage through overhead transmission lines. Distribution is about dividing the electrical power to lower voltages to supply residential and industrial customers. In this thesis target domain is distribution. Distribution networks, as the last part of a power system chain are reportedly less studied [1], thus require more attention. This chapter gives the background overview of power distribution network then the main motivation behind the thesis work. In the following, Section 1.1, an overview of the power system network is provided, then in Section 1.2, the problem statement and fundamental needs for this thesis are discussed.

1.1 Power Distribution Networks

Power distribution compared to generation and transmission is less studied [1]. This is while distribution networks play a key role in distributing the energy where monitoring the quality of power and voltage is significantly important. However adding monitors in distribution networks carry some challenges. Traditional distribution networks, consist of feeder elements such as reclosers, switches, fault indicators, capacitor banks, and voltage regulators that are incapable of sending critical information to the control center. Besides, the major obstacle is the lack of communication infrastructure across the distribu-

tion systems. There basically is no or little possible communication way between control centres and distribution network equipment. There certainly is a need for automation involvement in distribution similar to transmission network — in transmission, faults' propagation is managed by monitoring, localizing, and predicting the fault through automation.

To overcome the shortage, utilities launched deployment of smart meters. Smart meters, collect customers' consumption information regularly. Smart meters emergence, since last decade, encourages most or all sections of a network to become automated and intelligent. This thesis will cover more on smart meters in Section 1.2.2. However, more work needs to be done to have a smart, automated and efficient Distribution Management System (DMS). An automated DMS will fulfil the following requirements for future grids:

1. Integration of distributed renewable energy resources in substitute of traditional fossil fuels.
2. Providing management for optimising demand, i.e., providing incentives for customers to use electrical energy in a more efficient manner.
3. Improving Automatic Generation Control (AGC) system due to the peak demand rise, especially for emerging demand of electrical vehicles.
4. Managing fast-response behaviour of power electronics components of the grid versus slow-response nature of synchronous generators.

Additionally, industry has developed the following smart tools for main parts of a distribution system. Some of these smart tools are:

1. Voltage VAR Optimization (VVO) : VVO algorithm, optimises the voltage profile along the distribution feeders and customers to avoid voltage flickers and fluctuations. VVO is not practical without being informed about description of the load.
2. Stochastic load and generation forecasting in consideration of large renewable penetration.
3. Optimal network reconfiguration: Providing an optimum switching manoeuvre for the feeder. Disconnecting some parts of the feeder compromised to reduce the energy loss and supply more critical loads. Load disaggregation reveals descriptions of feeder connected loads beneficial to network reconfiguration.

Having less accurate real time measurement devices, not accessing to the efficient algorithms corresponding to the real time data management, and possessing no accurate load models restrict the distribution system's future improvement. To improve the operational behaviour of the distribution network, feeder planning, outage prediction and customers' reliability improvement are well advised. Figure 1.1 shows a basic schematic of a smart distribution network. Figure 1.2 shows a typical radial distribution feeder layout.

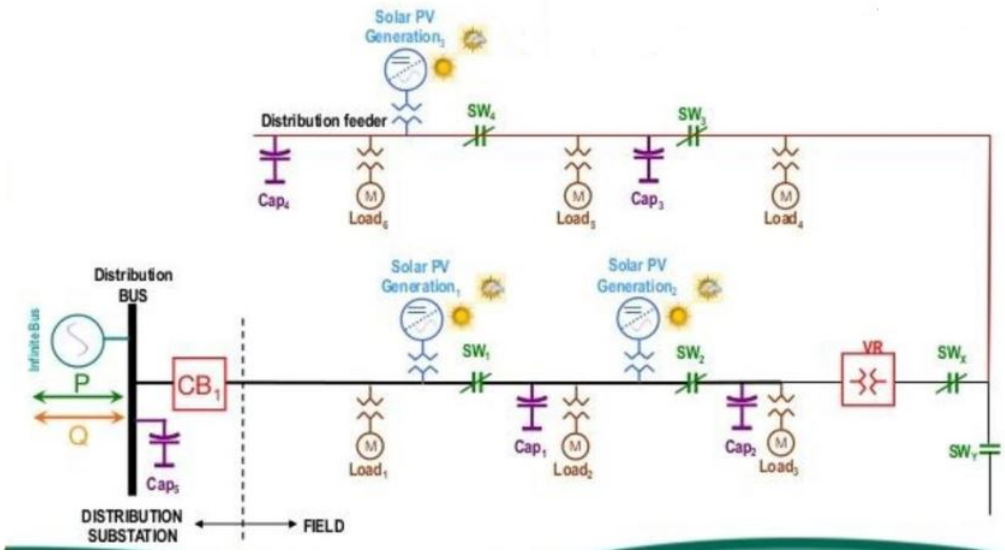

Figure 1.1: Distribution network from substation to feeders from [2].

In following section, BC-Hydro distribution network as an example is discussed.

1.1.1 An Example of Distribution: BC-Hydro Distribution Network

A typical BC-Hydro distribution network consists of an infinite bus, which is connected via a primary distribution line to the distribution substation. The low voltage bus at the substation is generally regulated with one of the following elements:

1. Automatic load tap changer (LTC) with a set point of about 124 V (7.44/12.89 kV or 14.88/25.77 kV).

2. 3-phase 300/400 Amp feeder position voltage regulator.

3. Bus regulator with a set point of 122-123 Volt (120.0 Volt on a secondary basis is

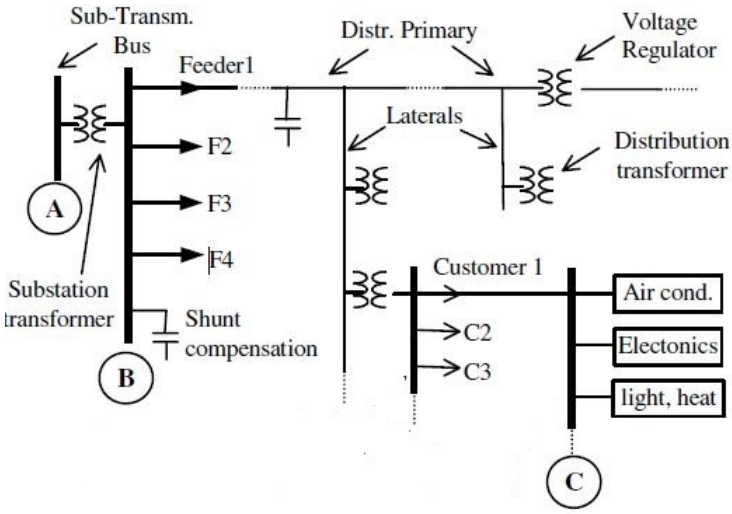

Figure 1.2: Typical distribution feeder schematic.

equivalent to Bc-Hydro nominal primary voltages of 7.2/12.47 kV and 14.4/25.0 kV) [3].

To this end, we introduced the structure of a typical distribution network. We pointed out the difference between traditional distribution network and a smart distribution network as well.

Distribution system dynamic behaviour is all about the nature of its loads. Load disaggregation function is to separate the aggregated load to its components. Knowing the components of the total load, supports power engineers towards a more efficient power system's operation and maintenance.

1.2 Motivation

The basic goal of a power system cycle is to supply different types of the load. Thus, having an accurate information about customer loads plays a critical role in the distribution system planning and operation. On the other hand, advent of distributed generators such as solar panels, onshore/offshore wind farms and PVs forces conventional grid to

operate more dynamically, thus capturing load's dynamic behaviour turns into be more crucial matter. In the following Sections 1.2.1 and 1.2.4, the most important application need of load disaggregation are discussed.

1.2.1 Energy Management

Today, energy management is challenging due to the fast growing nature of energy demands (loads). Electricity demand is increasing twice as fast as overall energy use. On the other hand, energy supplies are declining to two thirds by 2035 as shown in Figure 1.3. This increasing need and decreasing energy production, coupled with the fact that coal fuels are 40% of energy supply contributor, makes electricity energy generation as the highest cause of CO2 emission. Hence, world needs to increase electricity energy supply preferably clean energy resources for the next 20 years [4]. Accessing adequate

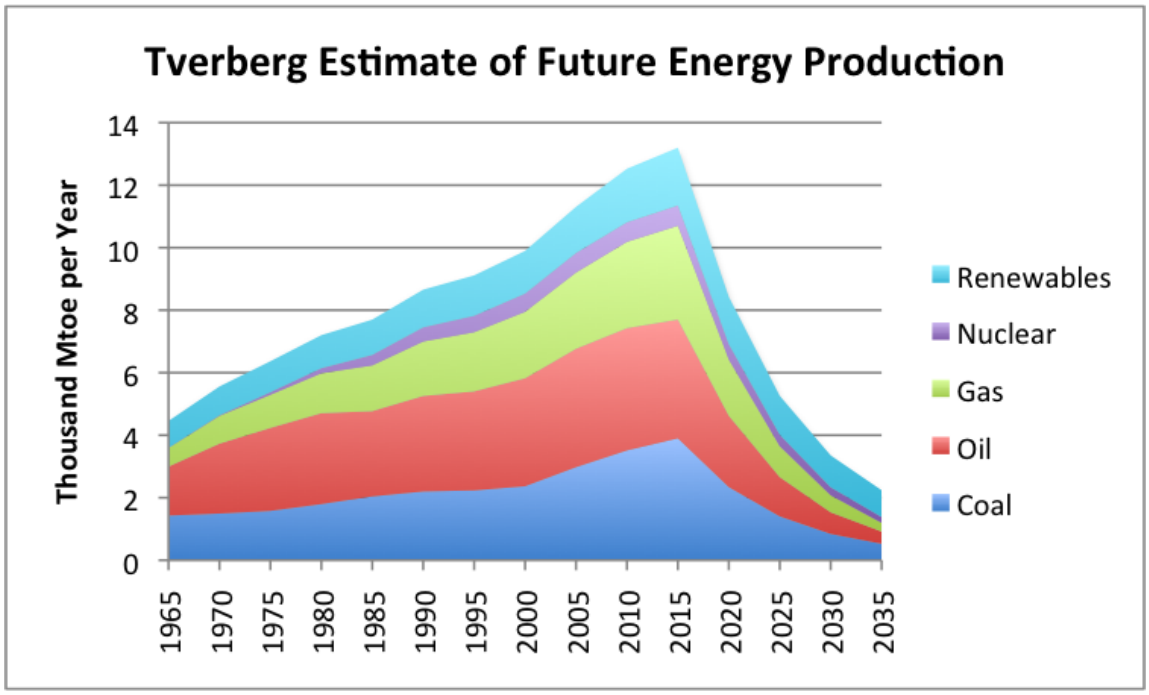

Figure 1.3: World's total primary energy supply from 1965 to 2035 by fuel [5].

clean energy supply resources without tackling demand side management is not practical. Thereby, to cope with the growing energy demand while producing less greenhouse gasses, it is important to understand the type of loads connected to the grid as the main

players' demand type. Real-time information helps out in having a less lossy distribution network and a more stable and reliable transmission system thus saving energy.

1.2.2 Smart Grid

Smart grid refers to a modernized and smart healing network. Smart Grid (SG) answers most of the upcoming challenges which Distribution System (DS) is facing since 20th century. SG adds up communication and automation features to grid's elements [6]. Strong communication capability enables utilities, substations, and distribution customers monitor each other in real-time. For example, if a contingency occurs and one generator or transmission line trips, distribution system is able to get updated in less than a second reducing outage duration.

Smart Meter

Smart grid development, brought smart meters and in-home energy displays as the solution to address the issue of accessing customers' real-time demands information. Smart meters are intelligent energy meters that obtain customer load's information and send it back to control centre. Meter measures time domain voltage and current waveforms for a customer and sends the obtained data for evaluation to supplier [7]. Received real-time data are analysed for the following purposes:

1. Giving customers an insight of their energy consumption.
2. It offers tariff models in electricity market.
3. Providing customers with incentives about the time of usage.
4. Enabling the utilities to monitor the grid's aggregated load and energy in real time.
5. Helping out distribution engineers in optimising VVO techniques.

Load disaggregation exploits smart meter readings to provide customers with an intuitive quantitative understanding of the amount of energy consumed by them. The main aim of load disaggregation is energy saving.

Distribution Management System

With the addition of millions of new data resources in DS, it is imperative for utility operators to monitor and control a high volume of real-time data in an optimum manner.

DMS is the decision support tool, which collects data all over from smart measurement devices. It takes the data back to the control centre. Operators assess the grid based on received data. The most important application of DMS is that, it improves operators and distribution engineers' visibility to the distribution system. DMS is valuable because of its application in the following:

1. Advanced control of the voltage and reducing network's loss through the automatic distribution optimized reconfiguration.

2. Integration of distributed renewable resources.

3. Integration of dynamic loads and having dynamic feeder protection.

In other words, DMS is an effective mechanism of managing the AMI data and performing complex analysis and calculation [8]. Figure 1.4 shows a large picture of a DMS network including all subsystems and devices incorporated together. Load disaggregation

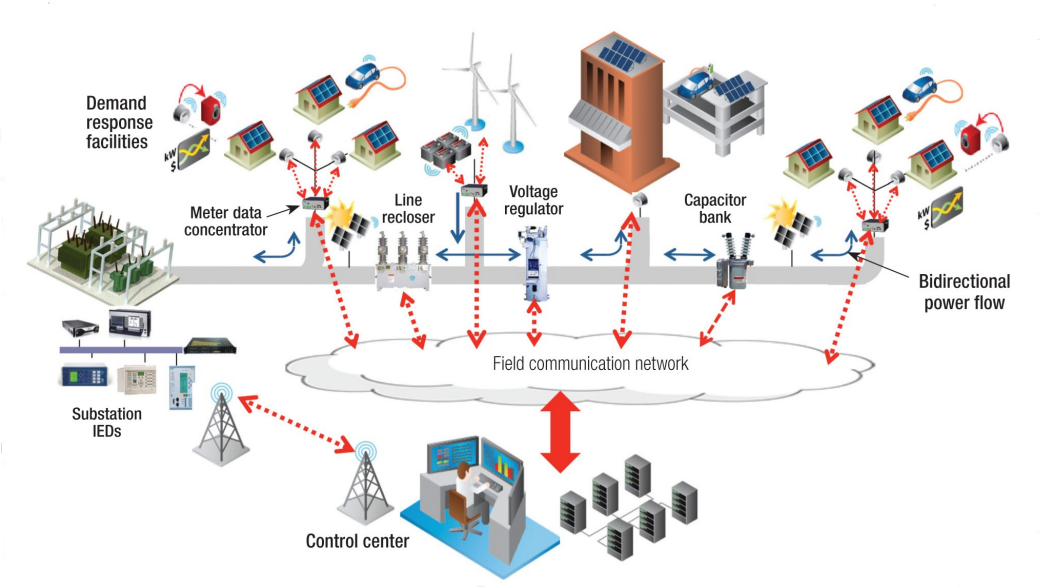

Figure 1.4: DMS (Distribution Management System) schematic [9].

algorithm has to be embodied in a DMS, towards achieving a better performance from all sections of the DMS platform.

1.2.3 VVO

VVO Definition

VVO is defined as maintaining the voltage level at a standard range (+/- 15% nominal voltage according to CSA standard) through the distribution network. VVO has been of great interest by utilities for many years. Load's behaviour and consequently voltage/-VAR level are changing throughout the day. Therefore, distribution engineers need to apply different methods to control the voltage at the feeders. Deployment of voltage regulators and shunt capacitors are the two common methods of controlling the voltage within a limit. Voltage and reactive power have a proportional relation, meaning that increasing the reactive power leads to voltage rise and reactive power drop will cause voltage drop as well. Because of this, inductive and capacitive loads play an important role in controlling the voltage profile of the system. Recently, with advent of Advanced Metering Infrastructure (AMI), engineers try to leverage real time data achieved from smart meters to control the voltage along the feeders more realistically. Voltage regulators, capacitor banks and On Load Tap Changer (OLTC) are common equipment employed, to control the voltage and the reactive power. OLTC increases and decreases the voltage level according to the load changes. For example, if load increase across the feeder, tap changers will increase the voltage to account for the excessive voltage drop on the feeder. Voltage regulators and capacitor banks perform the same.

Load Disaggregation Role in VVO Definition

Loads play an important role in VVO techniques. Motor loads form more than 80% of the total load. They have inductive characteristics. They absorb Q from the feeder which leads to a voltage drop. Also, for a capacitive load case, they generate reactive power which may cause a voltage rise in the system. Thus, loads nature has a direct impact on the system voltage and power levels. Being able to detect the accurate type of load helps VVO to control the system more accurately.
supervisory control and data acquisition (SCADA) enables optimising the voltage and reactive power, according to the load changes.
All in all, we need load voltage and power information at the feeder level to adjust the voltage and reactive power along a feeder [10].

1.2.4 Linear Power Flow (LPF)

Power flow calculation is one of the strongest tools to analyse distribution network. Power flow study solves a group of non-linear equations to calculate the bus voltage magnitudes and phase angles. Advance distribution system automation should be fast enough to meet the real time demand response. Linearising the power flow algorithm gives this opportunity to analysis the distribution system faster and more efficiently. Linear Power Flow (LPF) is introduced for the first time in [11]. There are different load models that are used in solving a power flow problem as described in following section.

Load Models

Loads modelling has not been taken into serious consideration for the last 2 decades in power systems area [12]. Based on BC-Hydro experimental results, there is 0.6 percent KWh (active power P) reduction per 1 percent load's voltage reduction, and a 3 percent KVAR (Reactive power Q) reduction per 1 percent voltage reduction which brightens the significance of Loads models [13]. Loads are classified to two types of load modelling methodologies:

1. Static: So far, static load models are integrated in a power flow solution. Static load models are not dependant on time, i.e. static models express P&Q relationship to voltage at the same time instant while dynamic approaches describe P and Q as a function of voltage at each time instant. Power system study tools mostly use polynomial and exponential load models under the static group.

2. Dynamic: Dynamic loads characteristics change in time. So, they should be modelled in real time.

For static models, Equation 1.1 formulates the voltage dependency of load characteristics by an exponential model.

$$\begin{aligned} P(V) &= P_0(\frac{V}{V_0})^a \\ Q(V) &= Q_0(\frac{V}{V_0})^b \end{aligned} \tag{1.1}$$

Polynomial models (ZIP model) also are widely used for load's behaviour formulation. There are three major components in (ZIP model), (1) constant power, (2) constant current,

(3) constant impedance. They are formulated in Equation 1.2.

$$\begin{aligned} \frac{P(V)}{P_0} &= F_z(\frac{V}{V_0})^2 + F_I(\frac{V}{V_0}) + F_p \\ \frac{Q(V)}{Q_0} &= (F_z')(\frac{V}{V_0})^2 + F_I'(\frac{V}{V_0}) + F_p' \end{aligned} \tag{1.2}$$

Where, F_Z, F_I, F_P are constant impedance, constant current and constant power respectively. Both polynomial and exponential models add non-linearity to the power flow equations. A new static load model is proposed in [11], which demonstrates a linear presentation of load's behaviours. Equation 1.3 describes the new load model (ZI model). It assumes a load, as the combination of constant impedance (Z) and constant current (I), which leads to a linear power flow formulation.

$$\begin{aligned} \frac{P(V)}{P_0} &= C_z(\frac{V}{V_0})^2 + C_I(\frac{V}{V_0}) \\ \frac{Q(V)}{Q_0} &= (C_z')(\frac{V}{V_0})^2 + C_I'(\frac{V}{V_0}) \end{aligned} \tag{1.3}$$

Where $(C_I + C_Z = 1) \text{and} (C_I' + C_Z') = 1$.
C_I, C_Z, C_1', C_Z' are derived from measurement data. A curve fitting will determine the values of C and C′. It is a matter of solving a fitting optimization problem as formulated in Equation 1.4.

$$\text{minimize} \sum_{i=1}^{N} (C_z(V_i)^2 + C_I V_i - P(V_i))^2 \tag{1.4}$$

subject to $C_z + C_I = 1$. Figure 1.5 shows a comparison between three different explained load modelling forms, applied on a three phase induction motor with the ratings of: 460 V, 3-phase, 1.4 hp, 1725 r/min .

Load Disaggregation Application in LPF

Loads are behaved as voltage dependent instead of constant P and Q as described in Equatuion 1.3. Voltage dependency characteristics of the loads are required for solving a linear power flow (LPF). Different type of loads have different voltage dependency indexes. Therefore, we should know the type of a load to estimate its voltage dependency

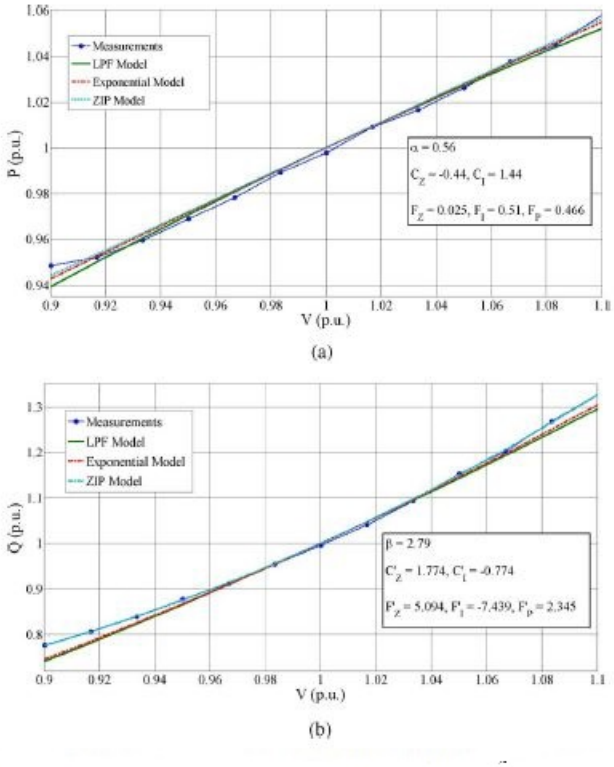

Figure 1.5: Comparison of the exponential, ZIP and proposed LPF load models. [11].Data in this figure are from [14].

behaviour. Load disaggregation result is fed into the LPF problem. EPRI (Electric Power Research Institute) conducted a study on how to derive voltage dependency of different type of loads from laboratory measurements [15]. Above mentioned factors motivated us to devise an innovative tool to recognize grid connected types of loads. The main focus of this thesis is load disaggregation.

Chapter 2

Literature Review

This chapter provides previous work made in research and industry. In Section 2.1, based on surveyed literature, appliance load monitoring as the first topic discussion for load disaggregation is discussed. In Section 2.2, based on a collection of papers, load disaggregation main elements are listed and the contributions in each domain are reviewed. Finally, in Section 2.3, popular studies in the area of load disaggregation are discussed.

2.1 Appliance Load Monitoring

Appliance Load Monitoring (ALM) is essential for energy management. It allows to obtain appliance specific energy consumption. It is approachable in the following two methods:

1. Intrusive Load Monitoring (ILM) which is known as distributed sensing method.
2. Non Intrusive Load Monitoring (NILM) which is known as single point sensing method [16].

In the following, these two methods are reviewed.

2.1.1 ILM

ILM requires deploying smart power outlets on every appliance due to extra hardware cost and installation complexity. However, it is accurate in measuring appliance's specific energy consumption.

2.1.2 NILM

NILM, also called, load disaggregation, is an area in computational sustainability that tries to discern what electrical loads (i.e. appliance) are running within a physical area. Such areas can include communities, industrial sites, office towers, buildings, homes, or even within an appliance [17].
NILM receives the aggregated load data from home entry electrical panel with no need to install sensors for each appliance inside the home. George W. Hart was the first one coming up with this idea about load disaggregation [18].

NILM History

NILM is initiated almost two decades ago by Hart [18]. He suggested to install Non Intrusive Appliance Monitoring (NALM) devices connected to the total load circuit. Based on switching on/off events and specific signatures for each individual load, he was able to determine the nature and number of loads connected. Moreover, he was able to check out each load's active and reactive power consumption and its time of the day variation. Figure 2.1 shows the power consumption versus the time of a single family for 40 minutes

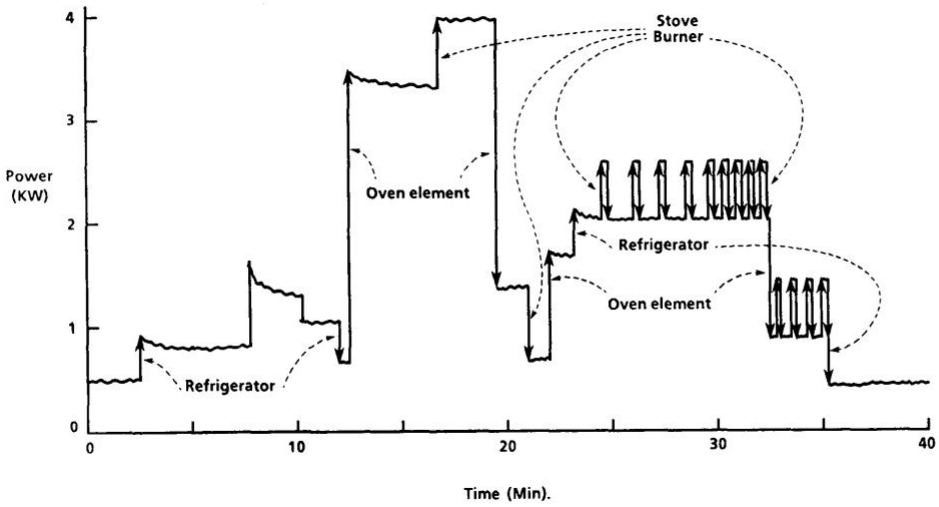

Figure 2.1: Power consumption of a single family for 40 minutes [18].

period. There are four step changes in the active power consumption. This states existence of four different appliances. However, with knowing each individual load's consumption

pattern, we can say when each load is switched on or off and for how long. Figure 4.2

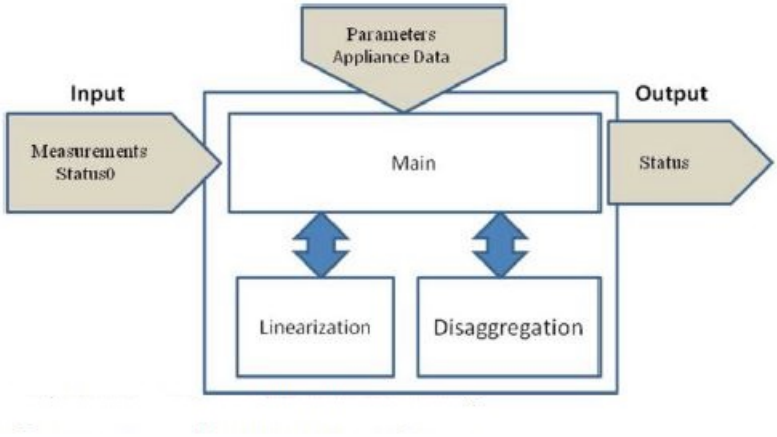

Figure 2.2: Overview diagram of NILM [19].

presents NILM as a block diagram which is fed in with two main inputs, measurements and appliance data information. NILM connects with the total load using standard meter user socket. It measures information such as voltage, current, P, Q and Total Harmonic Distortion (THD) for total load of a house entry. Appliance data block contains specific appliance's information such as P signatures, Q signatures and also type of the appliance obtained by the manufacturer [19]. The output of NILM process is the daily status of the analysed appliance.

2.2 Load Disaggregation Elements

This section elaborates three main elements of a load disaggregation process: (1) data acquisition, (2) feature extraction and (3) learning/classification.

Researchers working in load disaggregation domain, argue about different techniques and state of the art algorithms which are applicable in any of the three major modules. Most researchers consider the active and reactive power patterns as the appliance distinct features, to distinguish between different types of home appliances. The common property among most of the load disaggregation studies, is to report the types of loads looking at a single customer's point of entry. Their algorithm will state which appliances turn on or off at each moment.

2.2.1 Data Acquisition

Data Acquisition receives loads electrical waveforms measured at smart meters. Different energy meters have different sampling rates. We need to choose the appropriate sampling frequency based on the type of signal chosen for load's feature. For example, if steady state real power and reactive power are the metrics, low sampling rate (i.e., 120 Hz) is adequate. But If harmonics are studied as loads signatures, we need to sample the measured data at a higher frequency rate. For instance, to capture the harmonics up to 6, the minimum sampling frequency should be 360 Hz. The other important point to consider is Nyquist-Shannon criteria. Nyquist theorem states that sampling frequency has to be more than twice of the highest harmonic frequency in a signal. Since there is no higher than 11th harmonics available, maximum sampling rate is between 1.5-02 KHz [20]. Higher frequency meters are useful in capturing more accurate information of a signal to reach high accuracy of load detection. They are able to capture "Microscopic" features such as harmonics and instantaneous signal values. In compare with Microscopic signatures, power consumption changes are "Macroscopic" features, which can be detected with low frequency meters.

2.2.2 Feature Extraction

After obtaining load data, we have to choose a distinguishable feature of the load. Raw data received from meter needs to be processed towards achieving a load feature metric, to distinguish between different types of loads. Loads' signatures are classified into steady state and transient categories.

1. Steady state features: RMS values of a waveform like voltage and current and an event change in a metric like power consumption are examples of steady-state features. Sampling time of equal or larger than 1 second in adequate to extract steady state features. For example power consumption changes usually happens whenever an appliance turns on or off. This happens in more than one second time duration. Capturing this type of slow changing load properties does not need high volume of memory or fast paced measurement devices. This is known to be the advantage of using **steady state** load features as far as they are able to differentiate between different types of loads. The other dominance property is that they do not require repeatable patterns unlike transients signals [18] and [21].

2. Transients features: An appliance's starting current, starting power, shape and duration of high order harmonics and also some other transient load's characteristics that happen in less than one milliseconds are examples of transient features. Transient features recognize the non-linear type of loads. Interestingly, transient signals contain some unique characteristics of the load since, some characteristics, happen in high frequencies [22] [23] [24] [25] [26]. Figure 2.3 demonstrates different categories of load features.

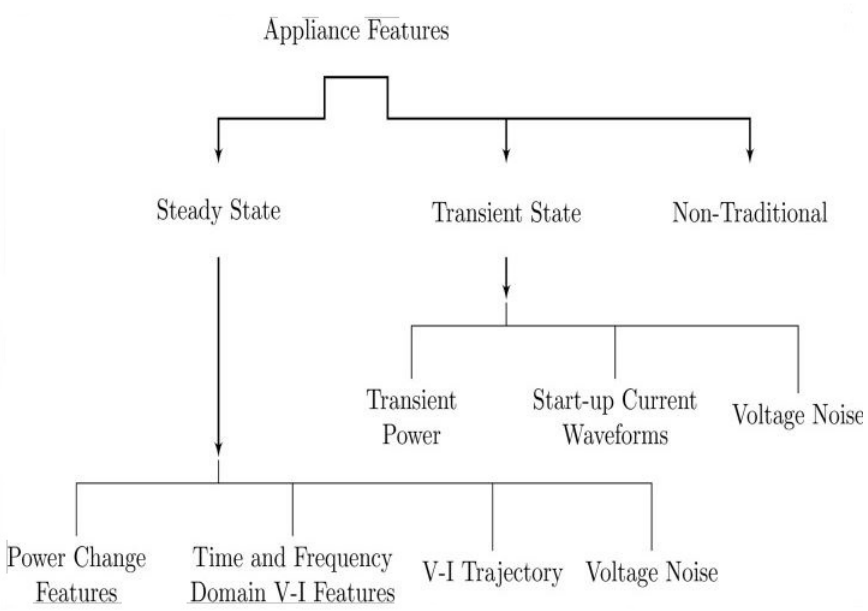

Figure 2.3: Load electrical features categorization [27].

Selecting an appropriate method either time domain approaches or frequency domain, depends on the level of disaggregation accuracy required and also the meter type. For example, if harmonics are chosen as appliances' distinctive features, we employ frequency domain analysis (fft, dft).

2.2.3 Load Classification

Learning process is grouped into two categories:

1. Supervised Learning Approaches (Classification)
2. Unsupervised Learning Approaches (Clustering)

Supervised Learning

Supervised classification algorithms, assign a label for each input data. Given a training data in the form of x_i which represents ith example data, and y_i which is the ith class label, the algorithm finds a model in which $A(x_i) = y_i$. The extracted load features are analysed with an optimization method, or with a pattern recognition (machine learning) technique. Researches in this domain, usually pattern recognition technique to train a seen library of data and detect the unseen load based on trained data information. Learning system allows training a classifier based on available load measurements signals. Any pattern recognition composes of three major steps:

1. Selecting a category of load features which are distinctive enough to classify between different types of loads.
2. Synthesizing a training set of feature's data.
3. Training a classier with the observed data towards identifying the new type of load after training.

Supervised learning uses KNN, Byes theorem, SVM, Neural Networks and Optimization methods as the classification tools to make the distinctive clusters of different load types. In following, each of above mentioned classifiers are briefly introduced.

KNN KNN works based on the smallest distance between the input data and trained one. Accordingly the class label assigned to smallest k, is given to that input.

Byes Theorem Byes theorem assigns the class which has the highest probability is assigned to the observed data [21] [28]. We can assign class c to an unknown example within feature sets: $X = (x_1, \cdots, x_n)$ such that: $c = \max_c P(C = c \mid x_1, \cdots, x_N)$.
The P probability can be formulated as : $P(C = c \mid x_1, \cdots, x_N) = \frac{P(C=c).P(x_1,\cdots,x_N|C=c)}{P(x_1,\cdots,x_N)}$

SVM SVM is mainly used for binary classification. SVM method separates an 'n' dimensional space into two classes. However, since data set is not always linearly separable, sometimes kernel-induced feature space is introduced to cast the space into higher dimensional one [23] [25] [26].

Neural Network Neural network works based on three layers of trained neurons: (input layer, hidden layer and output layer). Observed data set is fed into the input layer. Different weights are assigned to the input data due to a function which could be designed based on problem's objective. Input data it passed through the hidden layer. Finally, Output layer is a value which shows the class label of the corresponding input. To illustrate more on this one,in order to identify an event associated with operation of an new appliance, we match data set which includes all available event based appliances' signatures, with new load's event based value. There are many literature arguing different available recognition techniques [22] [26] [29] [30].

Optimization methods Optimization methods consider load disaggregation problem as an optimization problem. It works well when we need to identify an unknown single load which is not present in the data set. It compares the new measured feature vector like p(t), to the feature vectors which exist in the data set library. The objective is to reduce the matching error. The optimization problem is formulated in Equation 2.1

$$\text{class} = arg\min_{i} || \, y_i^{\wedge} - y_i \, || \tag{2.1}$$

In which y_i is the new measured feature vector and y_i' is the feature vector which exists in the load library. The limitation appears when, when we are working with an unknown aggregated load data. The reason arises form the fact that, an optimization problem can has one objective function at each time instant. To identify the components of an aggregated load, the method should consider all possible combinations of the appliances present in the data set, which are probable to synthesis the unknown signal. The combination, which leads to the least matching error will be selected as the components of the total load. Integer programming and generic algorithms are the examples of an optimization problem's solvers [31]. However, in the presence of a complex load feature vector, it is getting computationally expensive and time consuming to approach the load disaggregation as an optimization problem.

Un-Supervised Learning

Recently, researchers are developing unsupervised learning techniques to resolve some of supervised learning algorithm's drawbacks. Supervised learning system is expensive and not efficient due to the fact that preparing a complete data set covering all the possible

types of loads, needs new meters and sometimes sensors' installation. Unlike supervised methods, unsupervised algorithms, tackles the load disaggregation, in a smarter way with no need to the data set pool. K-means and clustering approaches, are two examples of an unsupervised learning method [32] [33] [34]. For example in Figure 2.4 P and Q are selected as the main load features to constitute the major load clusters. The goal behind

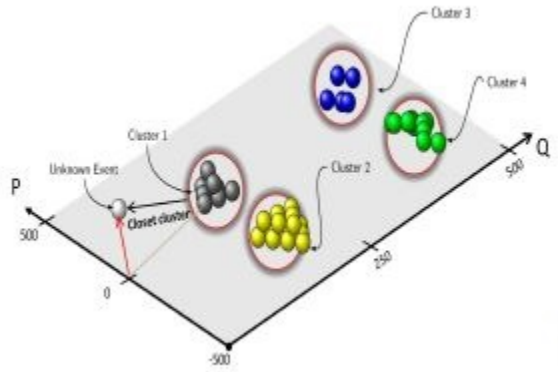

Figure 2.4: Load clustering using P and Q [16].

any unsupervised learning approach, is to achieve the minimum distance between an unknown load and the existing clusters in order to recognize, which main category of loads, the new load belongs to.
Most of unsupervised load disaggregation methods, need to full fill following criteria due to their application with smart meters and due to having a more simplified computation effort.

1. Power consumption data should be captured in real time.
2. No training dataset is necessary.
3. Number of total appliances usually does not exceed 20-30.
4. These methods cover ON/OFF appliances, multi state appliances, continuous consuming appliances and permanent consuming appliances.
5. Methods are scalable in a sense of robustness.

2.3 Literature Reviews of Previous Studies

Hart adopted active power as the main signature of loads. NILM's task is to decompose the P value in Equation 2.2, into its single load's power components [16]. Total value of active power mainly is formulated as the sum of all the individual load's consumption as following:

$$[P(t) = p_1(t) + p_2(t) + ... + p_n(t)] \tag{2.2}$$

Where p_i is the power consumption of individual appliance and n is the total number of appliances. There are literatures which employs unsupervised learning methods to capture a load's type. Dominik Egarter, takes advantage of HMM (Hidden Markov Model) for the appliance modelling and FHMM (Factorial Hidden Markov Model) for the household consumption modelling. All the hidden states of appliances, which are generated with HMM, are transferred to FHMM. FHMM aggregates the appliance's power consumption. He proposes popular Monte Carlo (Partial Filtering) estimation method, to estimate the disaggregated appliance's states. Partial Filtering calculates the weighted particles to obtain PDF values for each state. Particles are propagated over time to obtain the new particles and new the weights [32]. For the validation, this method is, tested on a household synthetic power draw numbers. It was capable of recognizing up to 18 different appliances. He evaluated his approach on Residential Energy Disaggregation Data (REDD) data set.
REDD contains detailed power usage information from several homes [35]. Figure 2.7 demonstrates how to install a REDD box inside a house.

We conclude that unsupervised learning methods, are advantageous because they do not need any training library. They require a general knowledge about the appliance structures such as, the number of operations (whether on/off and multi state appliances) and also, power demand measured values of each appliance.

In [33] load disaggregation is viewed as a single channel source separation problem. In this study, tensor (Multi-way array) factorization algorithm is applied for the electrical source modelling. Multi-way array considers the power consumption of each load at each smart home as a tensor. The Goal is to achieve all appliance's significant information through the available measurements data resulted from tensors factorization. Authors in this paper intend to develop a model based on a non-negative sparse coding, in particular a non-negative matrix factorization algorithm, which enforces the sparsity conditions to

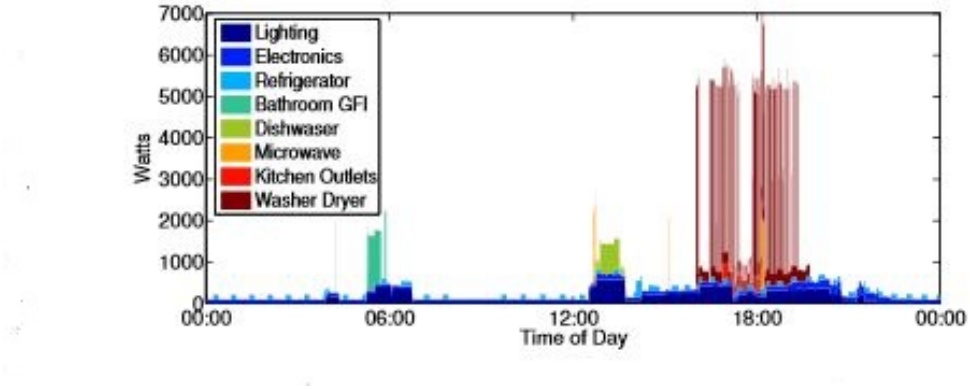

Figure 2.5: An example of energy consumption during a day for one of the house [35].

Figure 2.6: REDD box instalment inside a house

the load models. This approach learns a sparse model for each load, which is later used for the purpose of disaggregation. This method assumes an aggregated power consumption signal $x(t)$, corresponding to the sum of all of the appliance's usage over time period of T:

$$x(t) = f(x_1(t), ..., x_k(t)) \tag{2.3}$$

In Equation 2.3, f is assumed as a linear combination of constitution load. In this case we can formulate f as :

$$x(t) = \sum x_i(t) \tag{2.4}$$

To solve a single source separation problem, all the load's models are used to extract the significant characteristics of each source x_i. Load's models can be learned using On-line measurement data if available. Otherwise Matrix Factorization is a common method for source modelling. $x_i(t)$ is modelled as sum of the products of the main characteristic's matrix and activation matrix as formulated in Equation 2.5.

$$x_i(t) = \sum a(t) * b(t) \tag{2.5}$$

In which $x_i(t)$ is the power consumption of the ith appliance at time instant t. a(t) contains main features of appliance i and matrix b is the activation matrix. Figure 2.7 shows the three way tensor. Note that, different matrices x_1 to x_k across the devices direction, are source models for appliances 1 to k. This decomposition extracts information about the three directions (time of the day, days of the week, type of electrical appliance). RMSE (Root-Mean-Square-Error) is the evaluation metric in this approach which measures the error between predicted and actual measured power consumption as formulated in Equation 2.6.

The restriction of this model is that each source is independently modelled, ignoring the dependency characteristics existing between different appliances. In other words, if two different appliances are turned on simultaneously, the algorithm, is not able to distinguish between them.

$$RMSE(\bar{X}, \hat{\bar{X}}) = \sqrt{\frac{\sum_{t=1}^{T} \sum_{d=1}^{m} (\bar{X} - \hat{\bar{X}})^2}{T * m}} \tag{2.6}$$

In which $\bar{X}$ is the actual aggregated signal and $\hat{\bar{X}}$ is the predicted value. m is the number of days for training. The other popular approach to load disaggregation problem is adopting probabilistic methods.

Kim Etal was the first person to use probabilistic method for solving load disaggrega-

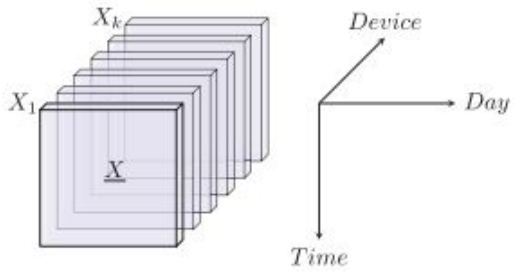

Figure 2.7: Load three dimensional characteristics[36].

tion problem. He applied FHMM as the main method. He also, considered modelling the coupling between dependant appliances. His method, incorporates a non-geometric parametric distribution of discrete-time ON durations. Even though his algorithm takes advantage of the time-ON statistics information to address the overlapping problem, but it still suffers form the computational complexity which increases exponentially with the number of appliances [34]. In [28] Zeifman, applied probabilistic approaches to meet the smart meter's requirements as following:

1. Load's selected features have to be compatible with the smart meters.
2. Algorithm is able to detect near real time appliances status.
3. Disaggregation accuracy should not drastically drop when the number of appliances is increasing.

In this paper, Semi-Markov model is selected as the mathematical solution for load disaggregation problem. The candidate of appliances are chosen between the one which has the overlap in the power draw for the sake of decreasing the complexity of problem. The idea is, to consider a group of two appliances i and i+1, with different time off durations. The probability of that an observed power change corresponds to the appliance i, depends on whether the appliance i+1 is turned on or off and for how long. Briefly explained, the algorithm is able to determine the starting time and the ending time of an appliance, with having an aggregated metered data. For example, Figure 2.8 shows the measured power consumption versus the reconstructed power pattern of a refrigerator and a dish-washer using Probabilistic method.

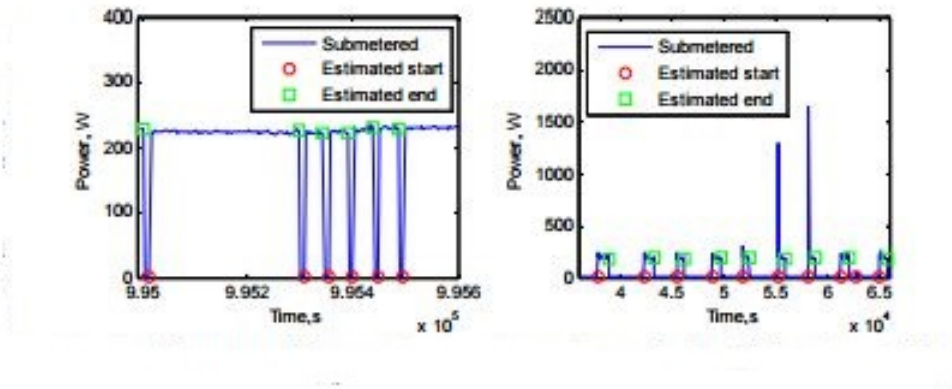

Figure 2.8: Metered vs reconstructed consumption of a dish washer and refrigerator using probabilistic method [28].

In article [26], researches use "V-I" trajectory, (the mutual locus of instantaneous voltage and current waveforms) towards separating an aggregated power data to its eigen-loads as shown in Figure 2.9.
They also tested different numbers of learning algorithms such as feed forward Artificial Neural Network (ANN), Hybrid learning algorithm and Support Vector Machine (SVM) to evaluate the precision and robustness of different classification algorithms. Energy consumption data is needed for this method to extract instantaneous voltage and current waveforms information. This method is considered as the high frequency approach since it needs to sample voltage and current signals at a rate of 100 samples per second. Extracted data is for the purpose of training which means, system learns different load's behaviours based on these sampling points.

This method, suffers from its requirement for a huge learning data set. It also, needs clustering methods, to pre-process the dataset in order to apply V-I trajectory method on it . Jin-Wen University researchers, proposed analysis of load's transient operational characteristics named as transient time and transient energy to detect power demand and load operation. Study applies DWT (Discrete Wavelet Transform) to the frequency-time domain features vectors to analyse the behaviour of a specific type of loads. This research asserts that using steady state features is less accurate in compare with employing transient features of the loads. Because, in the event based methods, (steady state information

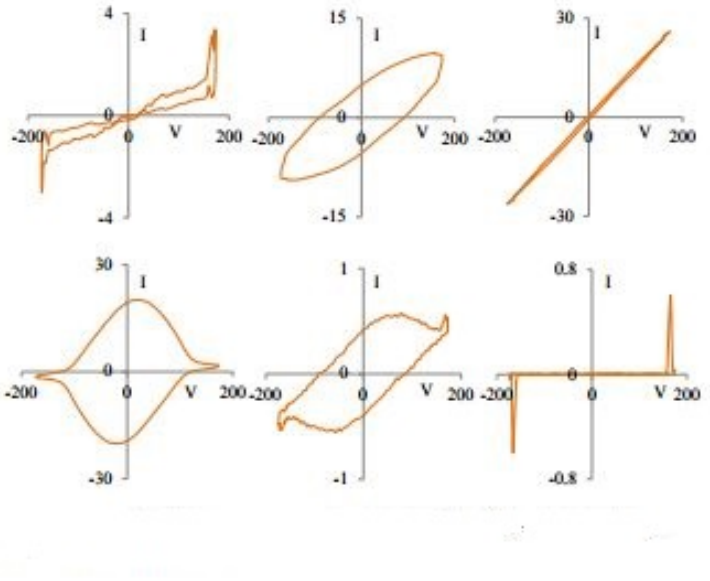

Figure 2.9: Graphical illustration of voltage-current trajectories from six different appliances from REDD household 3 [26].

are captured after an event like switching ON/OFF happens)whenever two different appliances have the same switching time or when the power of a certain load equals the total power of the other load, it is not possible to distinguish between the two loads. Following Equation 2.7 shows how to calculate the transient energy function of an aggregated load.

$$V_k = v_k - v_{k-1} I_k = \frac{i_k + i_{k-1}}{2} U_t = U_{1phtransient} = \sum_{k=0}^{K} V_k I_k \tag{2.7}$$

in which $V_k and V_{k-1}$ are derived from the transient voltage for Kth and (k+1)th samples. I(k) is the average of transient current received from smart meter measurement. This study, compares the results of the Short Time Fourier Transform (STFT) and Discrete Wavelet Transform (DWT) of the turn on transients of three different loads. Figure 2.10 shows the result of applying short term Fourier transfer on transient current of three different categories of loads. The transient response time of each load can be identified from the ending time and the starting time based on Figure 2.10.

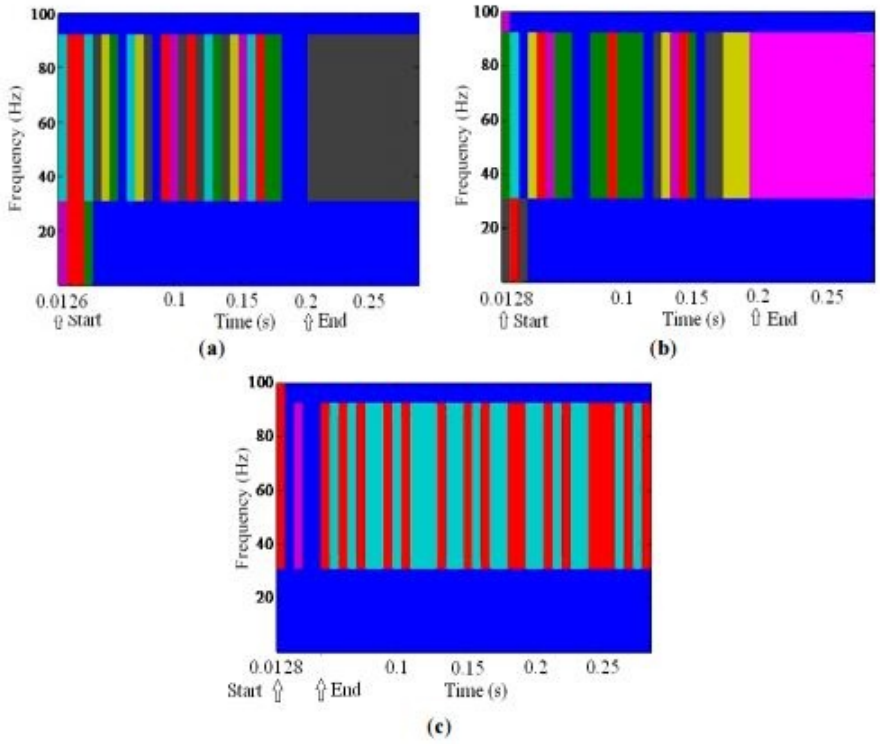

Figure 2.10: The STFT results on turn on current transients. (a) 160 horse power induction motor, (b) 123 horse power induction motor driven by variable voltage driver. (c) A bank of loads supplied by a six-pulse thyristor rectifier for AC power [37].

In order to compare STFT method with DWT method, Wavelet transform of same three waveforms are captured and pictured as following: DWT is more robust since it should not use fixed window frame same as STFT. Size of the window is scalable in DWT which enables this method to capture all information from starting point to ending point (same starting time and end time as load's signal).

In Figures 2.11, 2.12 and 2.13, first picture is instantaneous power waveforms of turn-on transients for a 160 hp induction motor, a 123 hp induction motor driven by variable-voltage drivers and a bank of loads supplied by a six-pulse thyristor respectively and 2nd plot demonstrates discrete wavelet coefficients which are distinguishable for different

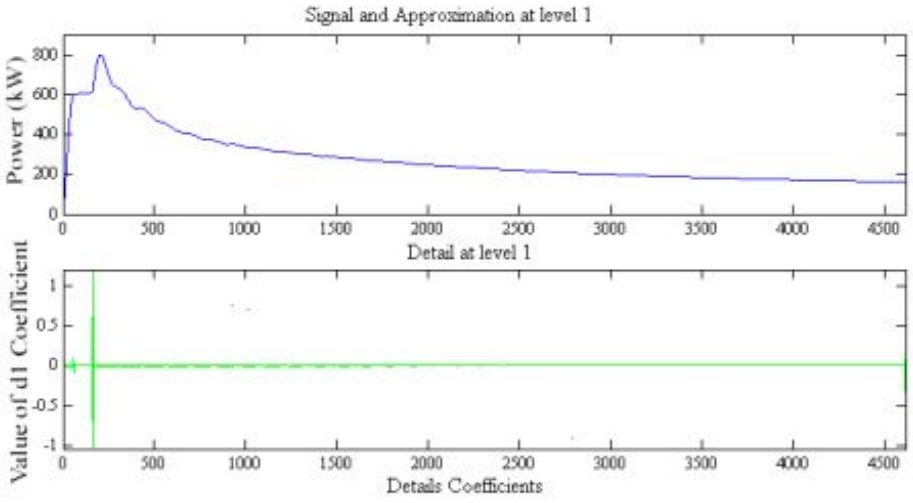

Figure 2.11: The DWT results of turn on instantaneous power transients for a 160 hp induction motor [37].

appliances.

High frequencies harmonics envelopes are the other strong descriptor for detecting a specific type of load in particular, power electronic types. Many loads, inherently draw non-sinusoidal, distorted current due to their physical characteristics. Taking Fourier transform of their current waveforms, aims to compute "spectral envelopes" which uniquely characterises the specific type of the load. In [38] a computer and an incandescent light bulb got detected in the ΔP, ΔQ and Δ3rd harmonic, coordinate system as shown in Figure 2.14.

In [25] matrix pencil method is used to represent the current in time value in terms of conjugate poles and residues. 1st, 3rd and 5th current harmonics are studied for over 9 different load classes including, incandescent Lamp, halogen Lamp, economy Lamp, water heater, electric convector, oven, hot Plate (one and two burners), television, Computer) and PC. There is a data set of 900 samples prepared to be passed in to a selected classifier.

The drawn current by each appliance is the sum of M complex valued sinusoid signals weighted by complex residues expressed in Equation 2.8.

$$i_t = \sum_{m_1}^{M} r_m.exp(a_m + j2\pi.f_m)t + b(t) \tag{2.8}$$

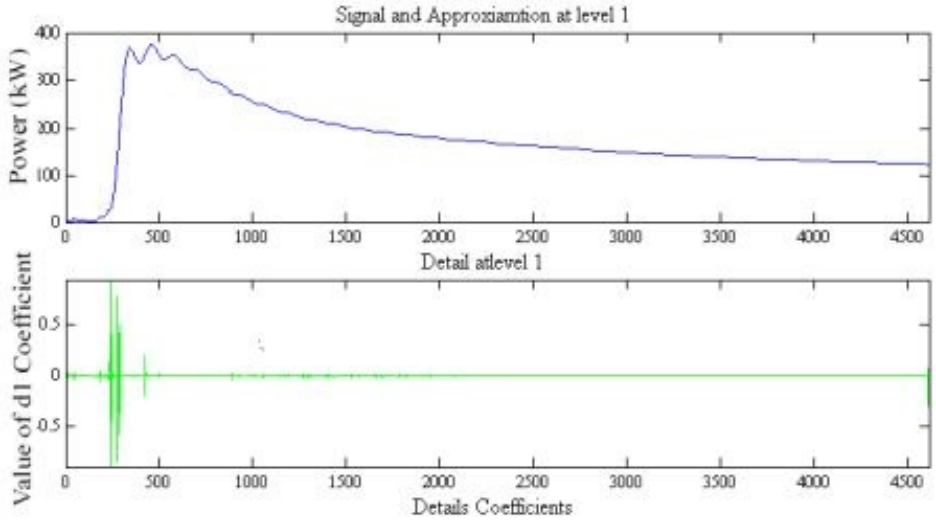

Figure 2.12: The DWT results of turn on instantaneous power transients for a 123 hp induction motor driven by variable voltage driver [37].

The discrete current signal is expressed in Equation 2.9:

$$i_k = \sum_{m_1}^{M} r_m . z_m^k + b(k) \qquad k = 1,2,\cdots,N \tag{2.9}$$

Where

$$z_m = exp(a_m + j2\pi . f_m)t_s \qquad m = 1,2,\cdots,M \tag{2.10}$$

In Equation 4.1, a_m is the attenuation factor, f_m is frequency, t_s is the sampling time and r_m is the residue of mth component.
The other innovative approach to load disaggregation arises from harmonic energy coefficients. This study, carried out different measurements to deduce that steady-state harmonics contents, are more repeatable than transients harmonics contents. Therefore, they concluded that steady state harmonics are more reflective of the loads behaviour. For this reason, just before and after an event, steady state harmonics contents, should be examined. This method measures currents harmonics content of the electrical loads, from a three-phase environment. A vector of length 27 corresponds to the first 8 harmonics plus

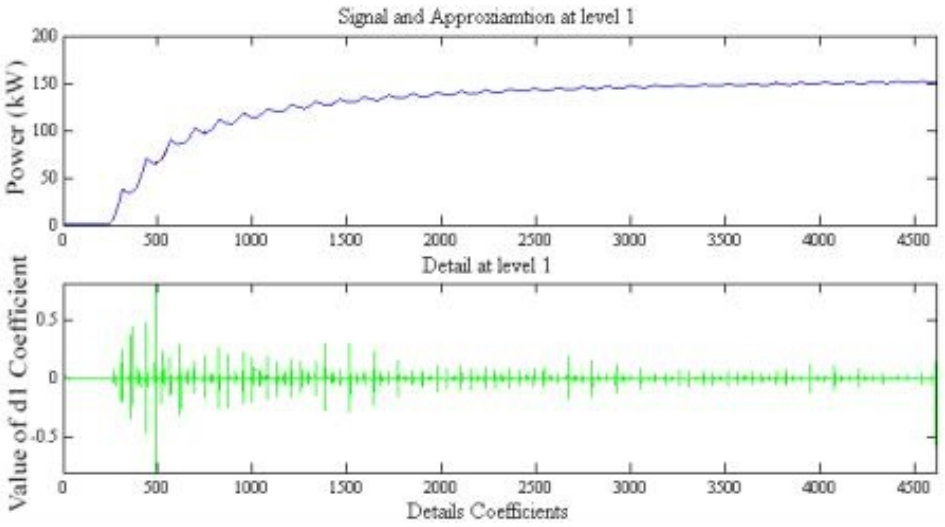

Figure 2.13: The DWT results of turn on instantaneous power transients for a bank of loads supplied by a six-pulse thyristor rectifier for AC power [37].

the fundamental frequency content, for all three phases is developed as the load's feature's database. An observed new load is identified with comparing its harmonics energy content to the reported library's harmonics vectors and minimizing the match error [24]. In [22] researchers assert that a load's current waveform polluted with harmonics can be represented as a normalized energy vector consisting of five elements. They took samples of three loads (personal computer, fluorescent lamp and dimmer for incandescent) current waveforms at the rate of 10 KHz with total period time of 51.2 ms. then, 5 level decomposition of wavelets has been applied for analysis. It is shown that for each type of load the wavelet coefficients curves give distinctive signatures and they used these signatures to identify each specific type of load. The other innovative approach, considers the steady-state starting noise of each appliance as a distinctive load feature. approach uses single plug in sensor, to detect both the abrupt noise created with an abrupt switching operation, and also the noise created by the certain devices in operation. The single plug-in model connects to a PC and PC records the generated noise caused by an appliance's switching ON or OFF as shown in Figure 2.15. Learning classifier, learns the certain characteristics of the noise to detect what appliance is turned ON or OFF in future. Authors in this paper, categorise the noise into two categories named as transient noise and steady

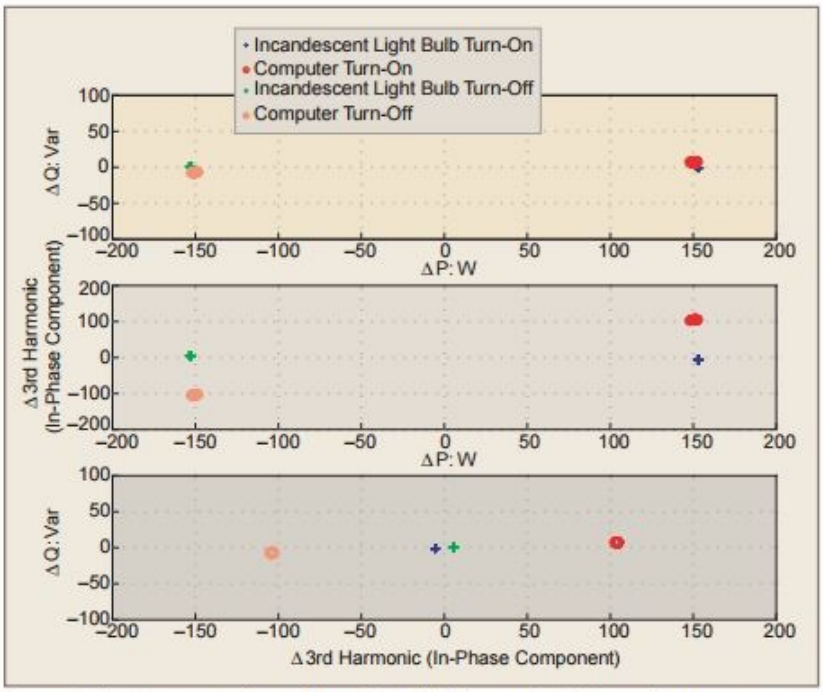

Figure 2.14: A computer and an incandescent light bulb in the Δ P, Δ Q and Δ 3rd harmonic coordinate system [38].

state noise. transient noise pulse is created while a large motor load such as a fan is turned on while, transient noises last only for microseconds and contain rich spectrum of the frequency components which is ranged from 100 Hz-10 KHz.

This study assumes noise signature of a particular device depends on both type of the device and the transmission line behaviour of the interconnecting power line. They capture both contributors in the load identification process. Three main classes of electrical residential loads, are considered in this research.

1. Pure resistive loads such as light bulbs and stoves, do not create detectable amount of electrical noise.

2. Motor loads like blender and fan which produce transient voltage noise synchronous to 60 Hz.

3. Power electronic appliances, such as microwave, PC and chargers which emit the

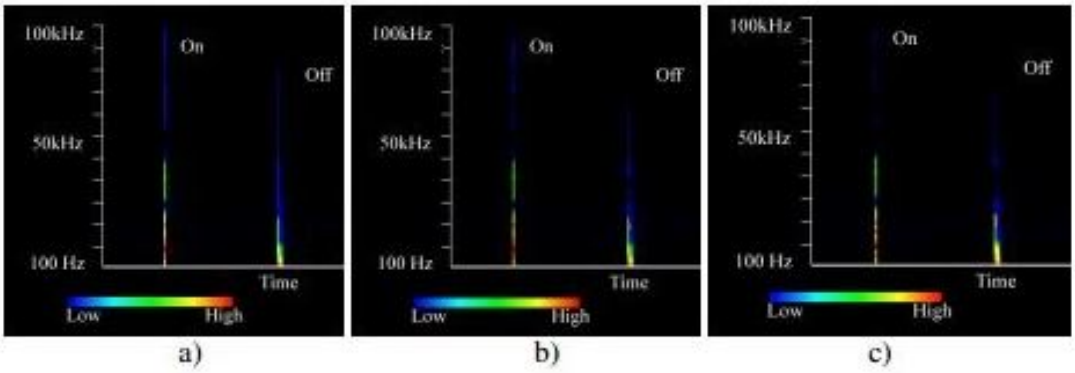

Figure 2.15: Frequency spectrum of a particular light switch being toggled (on and off events). Graphs indicate amplitude at each frequency level. Events at (b) were captured two days after (a). (c) events are captured one week after (a). On and off events are different enough to be distinguished.

steady-state noise synchronous to the internal oscillator.

This study was able to classify the various electrical events using SVM learning algorithm with accuracies ranging from 85-90% [23].

2.4 Chapter Summary

This chapter, summarized previous research and studies in the area of load disaggregation. Each method has its own advantages and disadvantages as explained. The mutual limitation in all above algorithms, is that in most of them, we need to have a large accurate load library, including different types of loads in order to train a classifier which will detect a new type of load based on seen signatures in future. Also, none of the methods, consider disaggregating the total load from the distribution feeder level, which is more efficient from an electrical grid point of view.

Chapter 3

Theory

As discussed in Chapter 2, researchers did not come up with an efficient algorithm to detect all power grid connected loads. Most of the studies focus on load identification based on a supervised learning method, meaning that a learning system observes training data set's behaviour, thereafter it recognizes a new observed load type. This sort of approach is restricted from the fact that if a new observed load is not operationally similar to the ones which system already is trained with, it will not detect the correct load's type. The other shortcoming arises from the fact that non of recent researches look at load disaggregation problem from distribution feeder point of view. In other words, the ability to detect total load's components connected to a specific feeder at each time instant. As yet, people who are working in this domain, are looking at each customer's entry in particular residential loads.

This thesis proves that looking at aggregated load from distribution feeder instead of each customer's entry point will benefit both the power system engineers and also the customers. It helps Distribution and Transmission engineers to capture a larger picture of connected load's structure. Because all consumer's load information is gathered together and each feeder's data is sent back to control centre for analysis.

The thesis introduces an algorithm to obtain feeder level load structures and electrical parameters using EMTP discrete time based solutions. This is the first time that there is a connection between Load Disaggregation problem and EMTP analysis solution.

We developed a method which enables engineers at control centre to know exactly how many percent of the aggregated load is motor type, purely resistive or purely inductive. We are able to report the load type for all feeders. This will help in a sense that most

powerful tools in power systems need to know the exact type of load at a large picture. Estate estimation, power flow studies, stability related studies, etc. all need to know total load's major components.
This thesis employs EMTP technique that helps predict the order of total load. Additionally, the thesis adopts network synthesis methods for the sake of recognizing exact parameters of aggregated load constitutes.
In Section 3.3 different electromagnetic transient program integration (discretization) rules are described and compared. In Section 3.5 Foster and Cauer methods are introduced and considered to construct load's electrical circuit based on **Z** (aggregated load impedance) and **Laplace transform function** formulated from EMTP coefficients.
But before starting the theory, I give a brief overview of the two power analysis tools, EMTP and PSCAD in Sections 3.1 and 3.2 respectively, because these two power tools are the foundation of my thesis.

3.1 EMTP Software

This section gives an overview of the EMTP solution with the purpose to provide the sufficient background to reach a full understanding of the proposed method.
EMTP (Electro Magnetic Transient Program) is a general purpose computer program for simulating transient events in power system. The program features wide variety of modelling capabilities. The beauty and uniqueness of EMTP solution are rooted in the nature of the discretization process. It focuses on discrete domain and offers solution methods encompassing Trapezoidal, Backward Euler, Forward Euler, etc. Herman Dommel developed EMTP in late 1960s at Bonneville Power Administration (BPA) which considered the program as a digital computer [39].
EMTP solution, first, defines discretization of each elements of the network instead of discretizing the circuit's full sets of differential equations. In other word, in the EMTP every component's relationship between voltage and current is modelled with a discreet time equivalents circuits consisting of resistance and source combinations. The values depend on the integration method and sampling ratio.
This thesis assumes every single load a combination of passive elements R, L and C, which are connected together to make a load's circuit. Therefore, we behave a load like an electrical circuit consisting of R, L and C components which can be solved via EMTP discrete-time solutions. The initiative idea behind our solution for load disaggregation problem

is in form of EMTP-like solution techniques. EMTP can solve networks consisting of interconnections of resistances, inductances, capacitances, distributed- parameter lines and other certain elements. Another reason motivated employing EMTP as the main algorithm is small discretizing time step used in simulations. Small discretzation helps, trace the instantaneous value of our signals in real time. Smart meters are based on the same technique, i.e., they send out real time voltage and current values to the control centre. Popularity of smart meters enthused this thesis toward employing EMTP technique.

3.2 PSCAD

System's behaviour, can be studied in time domain or frequency domain. EMTDC (electromagnetic transients including DC) is the most powerful electro-magnetic transients simulation engine for time domain simulations [40].
This engine started becoming a power tool in 1975, at Manitoba Hydro by Dennis Woodford (Executive Director of the Centre 1986 - 2001), which at the time was sufficiently powerful and flexible to study the Nelson River HVDC power system.
PSCAD software is the advanced graphical user interface (GUI) of EMTDC which enables user to model the circuit, run it and analyse data extracted from the software in other types of environment such as Matlab. EMTDC serves time domain electromagnetic transient solution engines for the family of PSCAD software. PSCAD is widely used to analyse, model and study power system including DC systems, AC ones and also power electronics.
PSCAD is the main simulator in our research since it is accurate, user friendly, and compatible with Matlab. More importantly it is written based on EMTP solution techniques. The main idea appears in 1969 by Dr. Hermann Dommel published at [39]. Electromagnetic transient solution methods considers a fixed or variable time step (in our case is fixed) to solve differential equations representing network behaviour in time domain. The solution is the step by step proceeding along the time axis. Each step depends on its previous value in time, i.e., history parameters. In other words, state of the system is measured during $t = 0, t = \Delta t, t = 2\Delta t, \cdots, t = n\Delta t$. At each state we need to examine previous time steps as well.

3.3 Discretization Methods

There are various methods applied to solve the differential equations using different integration rules. The common benefit in all these methods is the capability of converting differential equation to a simple algebraic one including voltage, current and some history values. EMTP software converts electrical circuit to the simple equivalent resistive and then applies integration rules to calculate voltage and injected current. The main purpose is to model lumped passive components (resistance, inductance and capacitance) which is easily solved in discrete time domain afterwards.

Integration rules transform differential equations describing steady state and transient behaviours of the system's components to the discrete time models at finite time increments. A complete network is then formulated to solve for the system conditions at each time step. Following Figure 3.1 shows the table of different integration methods.

Integration method	Integration formula	Order of approximation
Forward Euler	$x_{n+1} = x_n + h * f(x_n, t_n)$	1
Backward Euler	$x_{n+1} = x_n + h * f(x_{n+1}, t_{n+1})$	1
trapezoidal	$x_{n+1} = x_n + \frac{f(x_{n+1}, t_{n+1}) + f(x_n, t_n)}{2} * h$	1
Simpson's rule	$x_{n+1} = x_{n-1} + h/3 * (f(x_{n-1}, t_{n-1}) + 4f(x_n, t_n) + f(x_{n+1}, t_{n+1}))$	2
Gear's 2nd order	$x_{n+1} = 4/3 x_n - 1/3 * x_{n-1} + h * [2/3 f(x_{n+1}, t_{n+1})]$	2

Figure 3.1: Different integration methods description.

3.3.1 Forward Euler

Forward Euler is based on calculating the area under polygons between two endpoints of the integral. In other words, forward Euler approximated the integral value by production of value of function at x_n i.e.,$f(x_n)$times $h = x_n - x_{n-1}$. Figure 3.2 illustrates the method it more clearly [41].
In fact it is the expansion of Taylor series in two terms [41].
x_{n+1}=$x_n + h/1!f(x_n, t_n) + h^2/2!f'(x_n, t_n) + h^3/3!f^{(2)}(x_n, t_n) + ... \rightarrow x_{n+1}$=$x_n + h * f(x_n, t_n)$

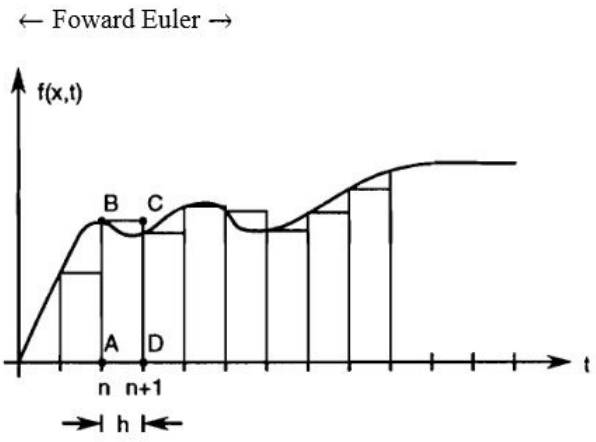

Figure 3.2: Approximation of x(t) by Forward-Euler method [41].

3.3.2 Backward Euler

Backward Euler is so similar to Forward Euler in a sense that, both considers the area under polygons embedded by integral endpoints, but in Backward Euler the integral value equals the production of $h = x_n - x_{n+1}$ into $f(x_{n+1})$ as you can see in Figure3.3.
x_{n+1}=$x_n + h * f(x_{n+1}, t_{n+1})$

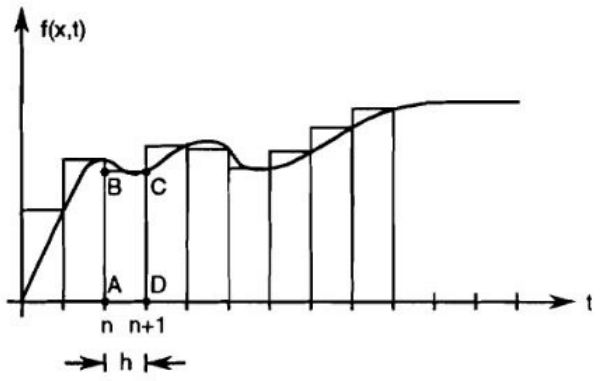

Figure 3.3: Approximation of x(t) by Backward Euler method [41].

A quick review of these two methods shows that forward Euler gives larger value than the real one while backward Eulers output is less than real value of function.

3.3.3 Trapezoidal

Here is where Trapezoidal rule kicks in by taking average of two values $f(x_{n+1})$ and $f(x_n)$. In other words the value of integral between x_n and $f(x_{n+1})$ is the area under trapezoid ABCD shown in Figure 3.4.

x_{n+1}=$x_n + \frac{f(x_{n+1},t_{n+1})+f(x_n,t_n)}{2} * h$

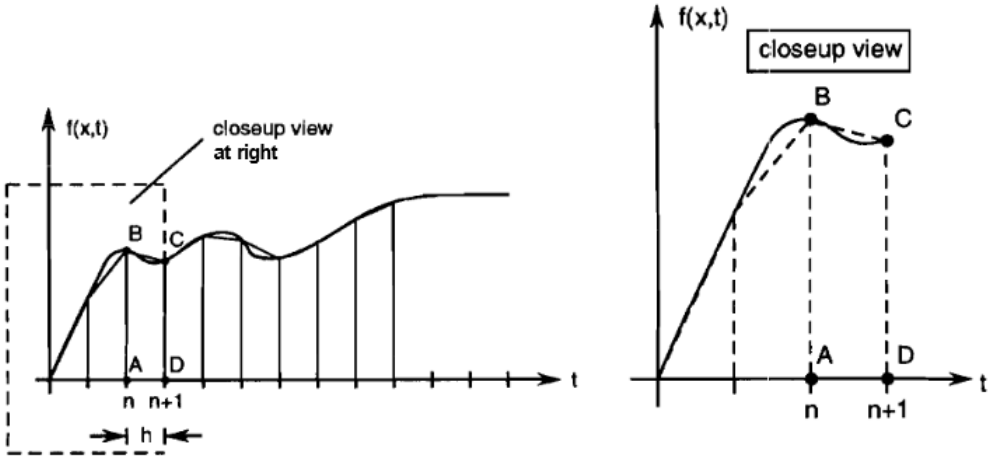

Figure 3.4: Approximation of x(t) by Trapezoidal method [41].

In fact in each integration step the average value of the intervals beginning and end is taken into account. It is the most accurate 2nd order integration method.

3.3.4 Simpson's

The other integration rule is called Simpsons rule which is Newton-Cotes formula using second order parabolas in estimating integral value. It uses quadratic polynomial instead of piecewise linear segments as in trapezoidal method. As can be followed in Figure 3.5 that the approximation for the integral function is the following:
x_{n+1}=$x_{n-1} + h/3 * (f(x_{n-1}, t_{n-1} + 4f(x_n, t_n) + f(x_{n+1}, t_{n+1})$
All these methods instead of giving continues solution of transients, aggregates snapshots of all discrete intervals with width of Δt as the solution. These integration methods described in Sections 3.3.1, 3.3.2 and 3.3.4 cause truncation error leading to numerical instability. Trapezoidal integration rule as described in section 3.3.3, is selected as my adopted method to distinguish load's circuits behaviour because it is simple, accurate and numerically stable [39].

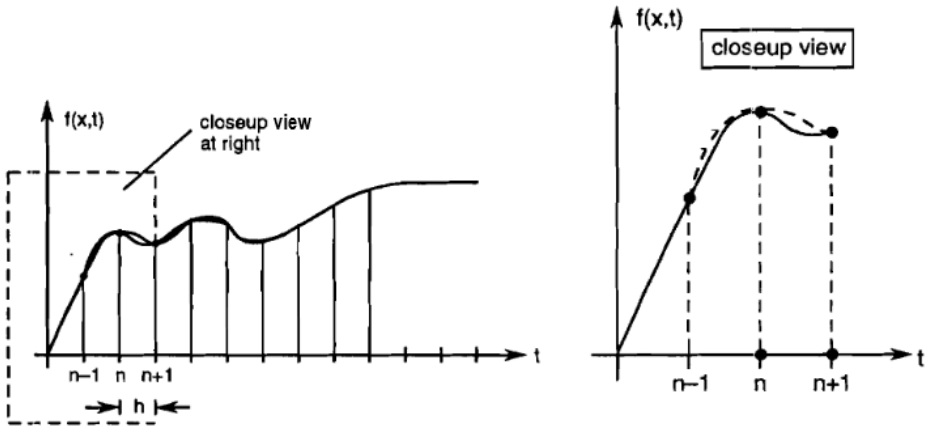

Figure 3.5: Approximation of x(t) by Simpson method

In this thesis our main focus is predicting load types based on their unique equivalent circuit. Motor types, lighting types and heating ones are our main three classes. All types of residential, commercial and industrial loads are categorized under motor, heating or lighting categories. Motor class represents induction motors. Lighting is symbolic of inductance types of loads. And lastly, heating is illustrative of resistive one. Our first assumption is that lighting types are modelled by "L", heating ones are represented by "R" and motor are modelled using equivalent model of an induction motor. Further investigation shows that we can assume load circuits as different combinations of L, R and in lumped form. Then we apply Trapezoidal rule to solve the time domain equation.

Trapezoidal Equivalent Models

In the following, I first, provide RLC trapezoidal equivalent models analysis to show how three main components of our study (R, L and C) are modelled in EMTP using Trapezoidal integration method. Then, we will calculate discrete time coefficients for complex combinations of RLC elements in the form of an induction motor equivalent circuit and etc.

Inductance Model

For the case of an inductor, it is modelled as demonstrated in Figure 3.6. The relation between voltage and current across is given by following calculations:

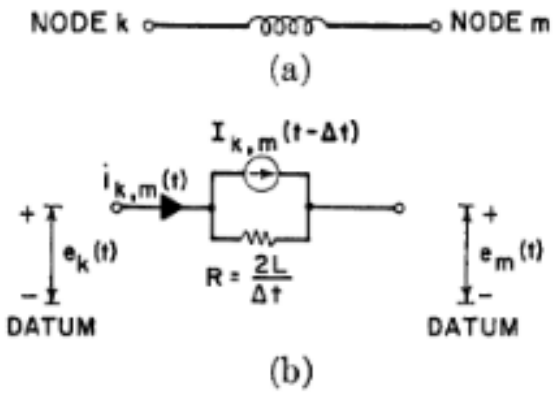

Figure 3.6: Inductance equivalent EMTP model.

$$V_{12}(t) = L.\frac{di_{12}}{dt}$$

$$V_{12}(t).dt = Ldi_{12}(t)$$

$$\int_{t-\Delta t}^{t} V_{12}(t)dt = L.\int_{t-\Delta t}^{t} di_{12}(t)$$

$$\int_{t-\Delta t}^{t} V_{12}(t)dt = L.[i_{12}(t) - i_{12}(t-\Delta t)]$$

Where Δt is the descretization time step.

$$\xrightarrow{Trapezoidal\,Discretization} \frac{V_{12}(t)+V_{12}(t-\Delta)}{2}.\Delta t = L.[i_{12}(t) - i_{12}(t-\Delta t)]$$

Then the voltage across the inductor is:

$$\rightarrow v_{12}(t) = \underbrace{\frac{2L}{\Delta t}}_{\text{Equivalent Impedance}} \quad i_{12}(t) - \underbrace{\frac{2L}{\Delta t} i_{12}(t-\Delta t) - v_{12}(t-\Delta t)}_{\text{History Terms}(e_h(t))} \tag{3.1}$$

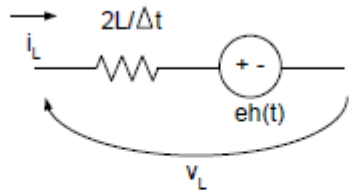

Figure 3.7: Voltage across the inductor [42].

Equation 3.1 describes the equivalent impedance value as a function of inductance (L) and time step Δt. Also, voltage value across the inductance at time t depends on history term which includes current value at previous time step and voltage value at t=t-Δt

Capacitance Model

For the case of a capacitor it is modelled as demonstrated in Figure 3.8. Equation 3.2 describes the equivalent impedance value as a function of capacitance (C) and time step Δt. Also, voltage value across the capacitance at time t depends on history term which includes current value at previous time step and voltage value at t=t-Δt.

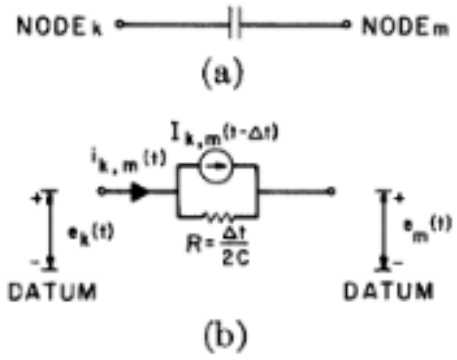

Figure 3.8: Capacitance equivalent EMTP model.

$$i_{12}(t) = C dv_{12}(t) dt$$

$$\int_{t-\Delta t}^{t} i_{12}(t)dt = C.\int_{t-\Delta t}^{t} dv_{12}(t)dt$$

$$\int_{t-\Delta t}^{t} i_{12}(t)dt = C.[v_{12}(t) - v_{12}(t-\Delta t)]$$

$$\xrightarrow{Trapezoidal Discretization} \frac{i_{12}(t)+i_{12}(t-\Delta t)}{2}.\Delta t = C.[v_{12}(t) - v_{12}(t-\Delta t)]$$

Then the voltage across the capacitance is:

$$\rightarrow v_{12}(t) = \underbrace{\frac{\Delta t}{2C}}_{\text{Equivalent Impedance}} \underbrace{i_{12}(t) + \frac{\Delta t}{2C} i_{12}(t-\Delta t) + \frac{v_{12}(t-\Delta t)}{C}}_{\text{History Terms}(e_h(t))} \tag{3.2}$$

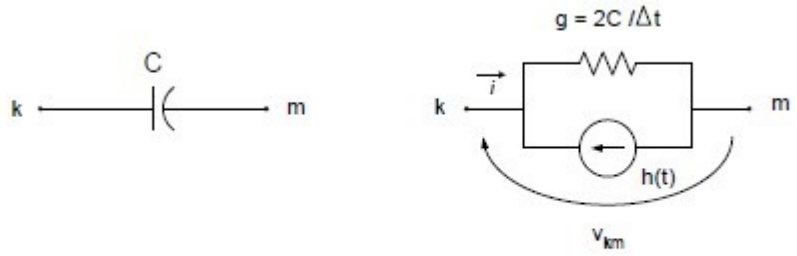

Figure 3.9: Voltage across the capacitance [42].

Resistance Model

For the case of a resistor it is modelled as demonstrated in Figure 3.10. The relation between voltage and current across is described in Equation 3.3.

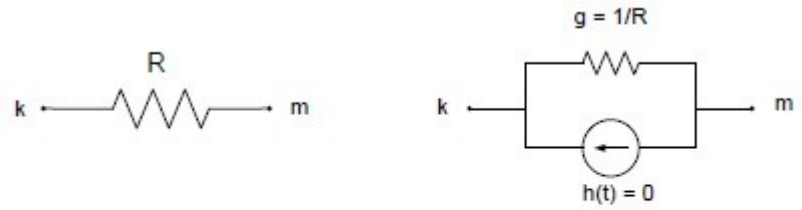

Figure 3.10: Voltage across the resistance [42].

For the case of a resistance the relation between voltage and current across it is given by:

$$V(t) = R.i(t) \tag{3.3}$$

3.4 The Thesis Method Discussion

In this thesis hereafter, all the current coefficients are annotated by letter 'a' and all voltage coefficients are annotated by letter 'b'. Starting from $i(t)$, the first coefficient is a_1, then for $i(t-\Delta t)$ the corresponding coefficients is a_2 and so on for $i(t-n.\Delta t)$ which is a_n. Same for voltage coefficient's notation, we have b_1 for $v(t-\Delta t)$, b_2 for $v(t-2\Delta t)$ and b_n corresponding to $v(t-n\Delta t)$. Substituting each passive element with its trapezoidal model leads to the following well known EMTP formulation which relates voltage and current time series values:

$$\begin{aligned} &a_0 i(t) + a_1 i(t-\Delta t) + a_2 i(t-2\Delta t) + \cdots + a_n i(t-n\Delta t) = \\ &b_0 v(t) + b_1 v(t-\Delta t) + b_2 v(t-2\Delta t) + \cdots + b_n v(t-n\Delta t) \end{aligned} \tag{3.4}$$

For $t = 0, \Delta t, 2\Delta t \cdots, n\Delta t$

In order to solve Equation (3.4), all terms are brought to one side of the equation except term $v(t)$. The new form of equation is as following:

$$\begin{aligned} v(t) = {} & a'_0 i(t) + a'_1 i(t-\Delta t) + a'_2 i(t-2\Delta t) + \cdots + a'_n i(t-n\Delta t) \\ & + b'_0 v(t-\Delta t) + b'_1 v(t-2\Delta t) + \cdots + b'_n v(t-(n+1)\Delta t) \end{aligned} \tag{3.5}$$

For $t = 0, \Delta t, 2\Delta t, \cdots, n\Delta t$

In order to find $a'_0, a'_1, \cdots, a'_n, b'_0, b'_1, \cdots, b'_n$ values, we need instantaneous voltage and current values at ($t = 0$,Δt, $2\Delta t$,$\cdots$,$n\Delta t$) as the known parameters. Voltage and current coefficients will be the unknown variables. Before solving Equation 3.6, we need to determine the order of the load circuit. The load's order is determined with solving $z(t) = \frac{v(t)}{i(t)}$ equation. Trapezoidal discretization rule will be applied on $z(t)$ same as in Sections 3.3.4 and 3.3.4. Integration of the impedance function using trapezoidal rule, we will derive an equation in the same form as Equation (3.4). The largest Δt index where $x = 1, \cdots, n$, will be the load order. Equation (3.5) is in the form of $AX = B$ or $(AX - B = 0)$ where two main matrices A and B include instantaneous values of voltage and current at time $t, t-\Delta t, t-2\Delta t, \cdots, t-n\Delta t$. The rows include $i(t-\Delta t)\cdots, i(t-n\Delta t)$and also $v(t-\Delta t)\cdots, v(t-n\Delta t)$ terms for one specific sampling scenario while number of columns is determined by the order of the load and interprets the total number of sampling points. Here is a symbolic representation of A and B matrices:

A=$\begin{bmatrix} i_{s1}(t) & i_{s1}(t-\Delta t) & \dots & i_{s1}(t-n\Delta t) & v_{s1}(t-\Delta t) & v_{s1}(t-2\Delta t) & \dots & v_{s1}(t-n\Delta t) \\ i_{s2}(t) & i_{s2}(t-\Delta t) & \dots & i_{s2}(t-n\Delta t) & v_{s1}(t-\Delta t) & v_{s2}(t-2\Delta t) & \dots & v_{s2}(t-n\Delta t) \\ \vdots & \vdots & \vdots & \vdots & \vdots & \vdots & \vdots & \vdots \\ i_{sn}(t) & i_{sn}(t-\Delta t) & \dots & i_{sn}(t-n\Delta t) & v_{s1}(t-\Delta t) & v_{sn}(t-2\Delta t) & \dots & v_{sn}(t-n\Delta t) \end{bmatrix}$
Where "n" is the order of our load. Depending on the order matrix size is defined. $s_1, s_2, \dots, s_n$ defines sample numbers, i.e., first sampling point, second sampling point and so on. Rows correspond to the samples and columns correspond to different time steps values. B=$\begin{bmatrix} v_{s1}(t) \\ v_{s2}(t) \\ \vdots \\ v_{sn}(t) \end{bmatrix}$
B matrix has n rows where n is again number of samples (or order of circuit) and it always has one column including voltage values at time t. Inverse (A)*B gives the solution matrix for Equation (3.6) which describes the numerical relationship between voltage and current in time.

$$\begin{bmatrix} i_{s1}(t) & i_{s1}(t-\Delta t) & \cdots i_{s1}(t-n.\Delta t) & v_{s1}(t-\Delta t) & v_{s1}(t-2\Delta t) & \cdots & v_{s1}(t-n.\Delta t) \\ i_{s2}(t) & i_{s2}(t-\Delta t) & \cdots i_{s2}(t-n.\Delta t) & v_{s2}(t-\Delta t) & v_{s2}(t-2\Delta t) & \cdots & v_{s2}(t-n.\Delta t) \\ \vdots & \vdots & \vdots & \vdots & \vdots & \vdots & \\ i_{sn}(t) & i_{sn}(t-\Delta t) & \cdots i_{sn}(t-n.\Delta t) & v_{sn}(t-\Delta t) & v_{sn}(t-2\Delta t) & \cdots & v_{sn}(t-n.\Delta t) \end{bmatrix} * \begin{bmatrix} a_0 \\ a_1 \\ a_2 \\ \vdots \\ a_n \\ b_0 \\ b_1 \\ \vdots \\ b_n \end{bmatrix} = \begin{bmatrix} v_{s1}(t) \\ v_{s2}(t) \\ \vdots \\ v_{sn}(t) \end{bmatrix} \tag{3.6}$$

Basically, the result of $Inv(A) * B$ is a matrix with $(2n+1)$ rows and one column where the first $(n+1)$ coefficients correspond to current characteristics and the rest n coefficients are numerical descriptor of voltage terms. Note that order of the circuit takes a decision of number of sampling points required. For example if we have a circuit with order=n, numbers of sampling points required to calculate the matrices A and B is $(2n+1)$.

3.4.1 Load's Electrical Circuit Order Determination Knowing the Structure of the Load

Here is a general sequence summarizing how the order of an electrical load is obtained **knowing** the structure of the load's circuit:

1. Equivalent Z (impedance) of load's circuit is calculated in the form of Laplace domain (S domain). (Writing down the impedance of load in the form $Z(s) = \frac{V(s)}{I(s)}$, then expanding the formula, we get $V(s) = Z(s).I(s)$.
   Resulted S domain expanded equation is converted to a discrete time domain expanded equation by substituting S parameter with d/dt, s^2 with d/dt^2 up to replacement of s^n with d/dt^n.

2. Integrating on both sides of the main equation and applying Trapezoidal discretization, results in a same format equation same as Equation (3.4).

3. the maximum coefficient of Δt appeared among history terms, determines the order of the circuit.

Up to this point, we discussed how to determine a load network's order with having its structure. Now it is time to determine the order of load's circuit with having no information about the load's topology. Because the main aim of this research is to develop an algorithm detecting feeder connected load's structures.

3.4.2 Load's Electrical Circuit Order Determination Unknowing the Structure of the Load

We summarize the process of predicting an electrical circuit's order having no knowledge about the topology of the circuit.
There are two distinct features about resultant discrete time coefficient which makes them an excellent candidates to be chosen as for the load distinctive signatures.

1. Since we assume an aggregated load as one single electrical circuit at each time step, for **different harmonics** scenarios these resultant matrix from $Inv(A) * B$ are equal. In other words, these time series coefficients are only function of circuit parameters (load passive elements) which are constant for one specific type of load, and also Δt which is the same for different harmonics as far as we use the same sampling frequency being able to capture major signal information of that circuit.

2. For **different sampling scenarios (of course which samples to take is important)** as discussed previous statement, corresponding coefficients are function of constant circuit passive elements and Δt.
   Again, choosing the same sampling frequency with selection of **same initial sample points with different sampling windows**, or **different initial samples but with the same window length** we get the same values as for these coefficients.

In this thesis, both approaches are evaluated on different combinations of loads in PSCAD simulation which lead to the same results. The first approach is more simple and practical for types of loads which produce harmonics such as power electronics types. Extracting at least two different frequency content both from voltage and current signals and calculating discrete time coefficients for each set, will give the order of the connected load. But looking an ideal power system world, goal is to reduce the harmonics effects, nowadays. Accordingly, second approach is considered as the main validation method for the rest of this study. In favour of predicting a connected load's order based on our approach, an initial order is considered, starting from order=0 (it happens for resistive loads). At least two distinguishing groups of coefficients derived from different sampling scenarios as demonstrated in Figures 3.11 and 3.12 are taken into account. If the obtained discrete time coefficient values for the selected scenarios, were equal, it means that guessed order was correct. Otherwise, order is increased by one and the same process is followed for the new order of the circuit. The process is repeated until for an order, the output matrix ($Inv(A) * B$) shows unequal values for different sets of sampling points. We started validating this idea based on simulations at PSCAD. In order to create different test case scenarios being able to compare different sets of coefficients, three sampling schemes are introduced:

1. Various width windows having same start point. (Sliding windows along time axis). We achieve this situation by changing the distance between sampling points as shown in Figure 3.11.

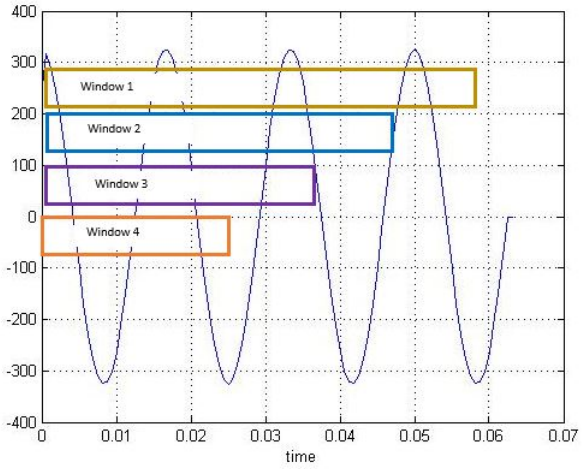

Figure 3.11: Different length windows having the same initial point as one of "voltage/current sampling points" selection method.

2. Windows with different starting point while having the same length as shown in Figure 3.12.

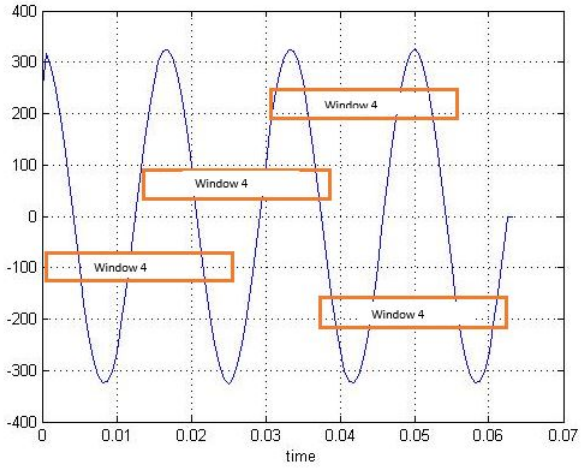

Figure 3.12: Same length windows having different initial point as one of "voltage/current sampling points" selection method.

3. Analysing two 1st and 2nd voltage and current harmonics as an input, calculating the corresponding Matrix for both sets which is not employed in this thesis.

Flowchart in Figure 3.13 exhibits this research's algorithm. The first step is receiving time series voltage and current data. The next step is prediction of load's order and finally, network synthesis methods help calculating load's parameters. In the following section,

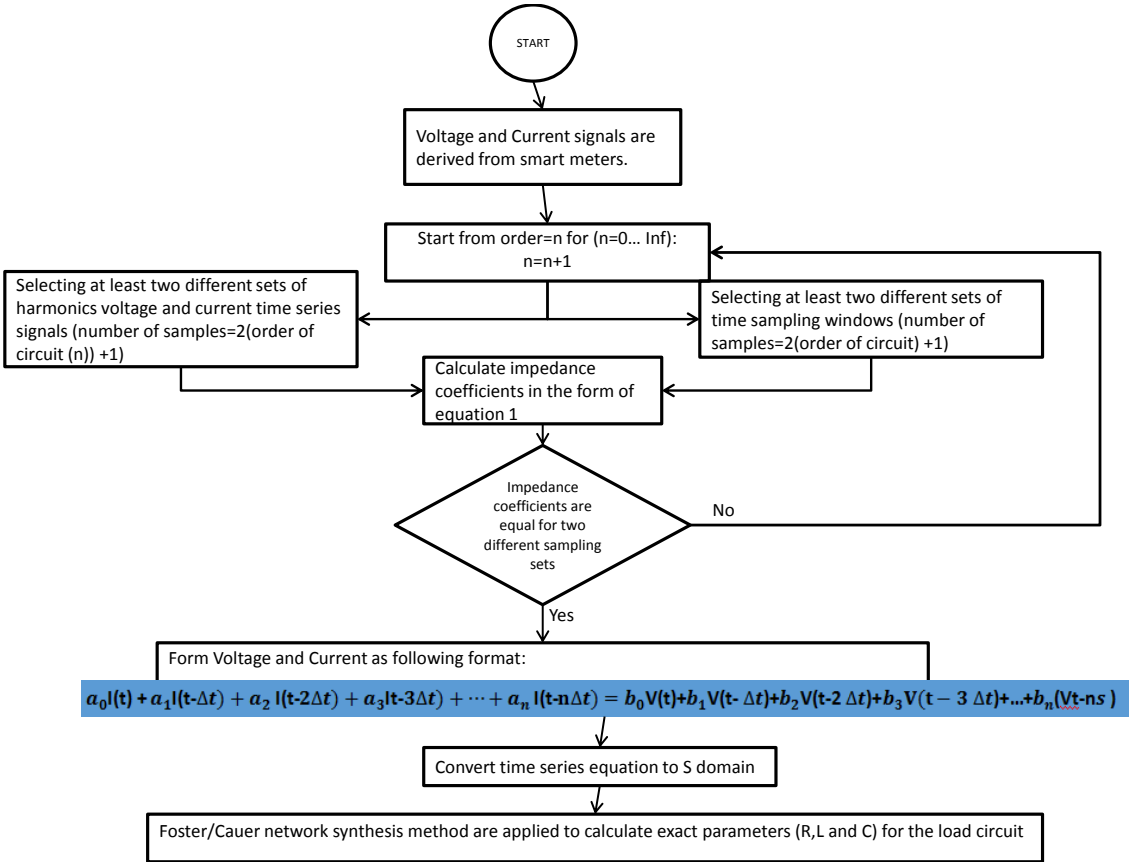

Figure 3.13: Proposed method: Process from smart-meter data capturing to load identification.

examples of parametric discrete time coefficients, describing the relation between voltage and current are calculated for few major load types.

3.4.3 Examples of Parametric Equivalent RLC Circuits Trapezoidal Models

Case One: Inductive Load-First Order Example

This example is already analysed in equation 3.1. Maximum Δt appeared in the expanded equation form is one, which confirms that a purely inductive load is a first order system with following coefficients: $a_0 = \frac{2L}{\Delta t}$
$a_1 = -\frac{2L}{\Delta t}$
$b_0 = -1$ This example calculates time series voltage and current coefficients for an "Inductor" . This category of load represents lighting eigen-loads.

Case Two: RL Parallel Load-First Order Example

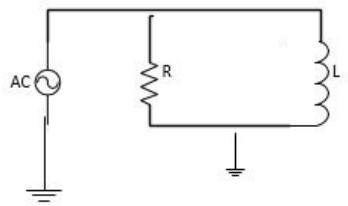

Figure 3.14: Parallel RL case.

$\frac{V(s)}{I(s)} = \frac{RL(s)}{R+LS} \rightarrow$

$RV(S) + LSV(s) = RLsI(s) \xrightarrow{convert-to-time-domain}$

$RV(t) + L(dV/dt) = RL.(di/dt) \rightarrow$

$\int_{t-\Delta t}^{t} RV(t) + L(dV/dt)dt = \int_{t-\Delta t}^{t} RL.(di/dt)dt$

$\xrightarrow{Trapezoidal-integration} R[\frac{V(t)+V(t-\Delta t)}{2}.\Delta t] + L[V(t) - V(t-\Delta t)] = RL[i(t) - i(t-\Delta t)] \rightarrow$

$V(t)[\frac{R.\Delta t}{2} + L] + [\frac{R.\Delta t}{2} - L].V(t-\Delta t) = RLi(t) - RLi(t-\Delta t)$

$\rightarrow V(t) = [\frac{1}{\frac{R.\Delta t}{2}+L}].[RLi(t) - RL\, i(t-\Delta t)\,] - \frac{[\frac{R.\Delta t}{2}-L]}{[\frac{1}{\frac{R.\Delta t}{2}+L}]}.\, V(t-\Delta t)\,] \rightarrow$

Voltage and current coefficeints are :

$a_0 = \frac{RL}{\frac{R.\Delta t}{2}+L}$

$a_1 = \frac{RL}{\frac{R.\Delta t}{2}-L}$

$b_0 = \frac{[\frac{R.\Delta t}{2}-L]}{\frac{R.\Delta t}{2}+L}$

In this case highlighted terms in Red are the largest Δt history terms. Based on our algorithm, first order is determined as the correct order for his type of load. For a resistance load, no Δt term will appear since impedance is a constant value of R, no history terms exist in this situation. Therefore, for all resistive loads, order=0 is assumed. Adding a resistive load in parallel or series with other loads will not change the original order of circuit.

Case Three: LC Parallel With A Resistance Load-Second Order Example

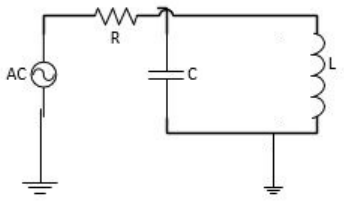

Figure 3.15: A parallel LC in series with a resistance case.

$\frac{V(s)}{I(s)} = \frac{RLCS^2+LS+R}{LCS^2+1} \rightarrow$

$LCs^2.V(s) + V(s) = RLCs^2.I(s) + LSI(s) + RI(s) \xrightarrow{convert-to-time-domain}$

$V(t) + LC.d^2V/dt^2 = RLC.d^2i/dt^2 + L.di/dt + Ri(t) \rightarrow$

$\int_{t-\Delta t}^{t}[V(t) + LC.d^2V/dt^2]dt = \int_{t-\Delta t}^{t}[RLC.d^2i/dt^2 + L.di/dt + Ri(t)]dt \xrightarrow{trapezoidal-integration}$

$LC[dV/dt - dV(t-\Delta t)/dt] + [\frac{V(t)+V(t-\Delta t)}{2}.\Delta t] = RLC[di/dt - di(t-\Delta t)/dt] + L[i(t) - i(t-\Delta t)] + R.[\frac{i(t)+i(t-\Delta t)}{2}.\Delta t]$

$\xrightarrow{trapezoidal-integration} RLC.[i(t) - i(t-\Delta t)] - RLC.[i(t-\Delta t) - i(t-2\Delta t)] + (L + \frac{R.\Delta t}{2}).[\frac{i(t)+i(t-\Delta t)}{2}.\Delta t]$

$+ (\frac{R.\Delta t}{2} - L).[\frac{i(t-\Delta t)+i(t-2\Delta t)}{2}.\Delta t] = LC.[V(t) - V(t-\Delta t)] - LC.[V(t-\Delta t) - V(t-2\Delta t)] + \frac{\Delta t}{2}.[(\frac{V(t)+V(t-\Delta t)}{2}.\Delta t)$

$+ (\frac{V(t-\Delta t)+V(t-2\Delta t)}{2}.\Delta t)] \rightarrow$

$i(t)[RLC + (L + \frac{R.\Delta t}{2}).\frac{\Delta t}{2}] + i(t-\Delta t).[-2RLC + (L + \frac{R.\Delta t}{2}).\frac{\Delta t}{2} + (-L + \frac{R.\Delta t}{2}).\frac{\Delta t}{2}]$

$+ i(t-2\Delta t).[RLC + (-L + \frac{R.\Delta t}{2}).\frac{\Delta t}{2}] = v(t).[LC + \frac{\Delta t^2}{4}] + v(t-\Delta t).[-2LC + \frac{\Delta t^2}{2}] + v(t-2\Delta t).[LC + \frac{\Delta t^2}{4}] \rightarrow$

$i(t).[R.\frac{\Delta t^2}{4} + L\frac{\Delta t}{2} + RLC] + i(t-\Delta t).[R.\frac{\Delta t^2}{2} - 2RLC] + i(t-2\Delta t).[R.\frac{\Delta t^2}{4} - L\frac{\Delta t}{2} + RLC] = v(t).[LC + \frac{\Delta t^2}{4}] + v(t-\Delta t).[-2LC + \frac{\Delta t^2}{2}] + v(t-2\Delta t).[LC + \frac{\Delta t^2}{4}] \rightarrow$ Voltage and current coefficeints are :

$a_0 = \frac{[R.\frac{\Delta t^2}{4}+L\frac{\Delta t}{2}+RLC]}{[LC+\frac{\Delta t^2}{4}]} = \frac{R.[\frac{\Delta t^2}{4}+LC]+L\frac{\Delta t}{2}}{[LC+\frac{\Delta t^2}{4}]} = R + \frac{L\frac{\Delta t}{2}}{[LC+\frac{\Delta t^2}{4}]}$

$a_1 = \frac{[R.\frac{\Delta t^2}{2}-2RLC]}{[LC+\frac{\Delta t^2}{4}]}$

$a_2 = \frac{[R.\frac{\Delta t^2}{4}-L\frac{\Delta t}{2}+RLC]}{[LC+\frac{\Delta t^2}{4}]} = \frac{R.[\frac{\Delta t^2}{4}+LC]-L\frac{\Delta t}{2}}{[LC+\frac{\Delta t^2}{4}]} = R + \frac{-L\frac{\Delta t}{2}}{[LC+\frac{\Delta t^2}{4}]}$

$b_0 = -\frac{[-2LC+\frac{\Delta t^2}{2}]}{[LC+\frac{\Delta t^2}{4}]}$

$b_1 = -\frac{[LC+\frac{\Delta t^2}{4}]}{[LC+\frac{\Delta t^2}{4}]} = -1$

Highlighted terms in Red show $2\Delta t$ terms which determines this circuit as being the 2nd order system.

Case Four: Motor Load-Second Order Example

This example calculates time series Voltage and Current coefficients for an "Induction Motor" . Figure 3.16 represents all motor types load which is one of 3 major eigen-loads in this study. Highlighted history terms have the largest index for Δt which confirms motor loads as being 2nd order systems.

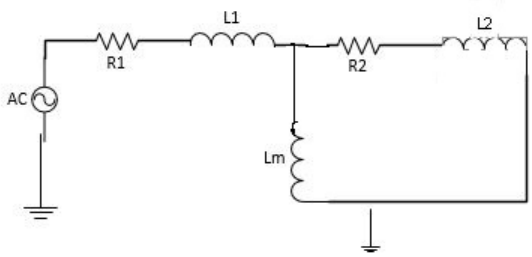

Figure 3.16: Induction motor type.

$$\frac{V(s)}{I(s)} = [(R_2 + L_2 \parallel L_m S] + [R_1 + L_1 S] = \frac{R_1.R_2 + S.[R_2.L_1 + R_1.L_2 + R_1.L_m + R_2.L_m] + S^2.[L_1.L_2 + L_1.L_m + L_2.L_m]}{R_2 + S.[L_m + L_2]}$$

$$\rightarrow R_2.V(s) + [L_m + L_2].SV(S) = R_1.R_2.I(s) + [R_2.L_1 + R_1.L_2 + R_1.L_m + R_2.L_m].SI(s) + [L_1.L_2 + L_1.L_m + L_2.L_m].S^2 I(S)$$

$$\xrightarrow{convert-fromS-domain-to-t-domain} R_2.v(t) + [L_m + L_2].\frac{dv(t)}{dt} = R_1.R_2.i(t) + [R_2.L_1 + R_1.L_2 + R_1.L_m + R_2.L_m].\frac{di(t)}{dt}$$

$$+ [L_1.L_2 + L_1.L_m + L_2.L_m].\frac{d^2 i(t)}{d^2 t} \rightarrow$$

$$\int_t^{t-\Delta t}[R_2.v(t) + [L_m + L_2].\frac{dv(t)}{dt}]dt = \int_t^{t-\Delta t}[R_1.R_2.i(t) + [R_2.L_1 + R_1.L_2 + R_1.L_m + R_2.L_m].\frac{di(t)}{dt} + [L_1.L_2 + L_1.L_m + L_2.L_m].\frac{d^2 i(t)}{d^2 t}]dt$$

$$\xrightarrow{Trapezoidal-integration} R2.(\frac{v(t)+v(t-\Delta t)}{2}.\Delta t) + [L_m + L_2].[v(t) - v(t-\Delta t)]$$

$$= R1.R2.(\frac{i(t)+i(t-\Delta t)}{2}.\Delta t) + [R2L1 + R1.L2 + R1Lm + R2Lm].[i(t) - i(t-\Delta t)] + [L1.L2 + L1.Lm + L2.Lm].[\frac{di(t)}{d(t)}$$

$$- \frac{di(t-\Delta t)}{dt}] \rightarrow [R2.\frac{\Delta t}{2} + [Lm + L2]].V(t) + [R2.\frac{\Delta t}{2} - [Lm + L2]]V(t-\Delta t)$$

$$= [R1.R2.\frac{\Delta t}{2} + R2.L1 + R1.L2 + R1.Lm + R2.Lm].i(t) + [R1.R2.\frac{\Delta t}{2} - [R2.L1 + R1.L2 + R1.Lm + R2.Lm]].$$

$$i(t-\Delta t) + [L_1.L_2 + L_1.L_m + L_2.L_m].[\frac{di(t)}{dt} - \frac{di(t-\Delta t)}{dt}] \xrightarrow{Trapezoidal-integration} [R2.\frac{\Delta t}{2} + [Lm + L2]].[\frac{V(t)+V(t-\Delta t)}{2}.\Delta t]$$

$$+ [R2.\frac{\Delta t}{2} - [Lm + L2]].[\frac{V(t-\Delta t)+V(t-2\Delta t)}{2}.\Delta t] = [R1.R2.\frac{\Delta t}{2} + R2.L1 + R1.L2 + R1.Lm + R2.Lm].[\frac{i(t)+i(t-\Delta t)}{2}.\Delta t]$$

$$+ [R1.R2.\frac{\Delta t}{2} -]R2.L1 + R1.L2 + R1.Lm + R2.Lm]].[\frac{i(t-\Delta t)+i(t-2\Delta t)}{2}.\Delta t]$$

$$+ [L_1.L_2 + L_1.L_m + L_2.L_m].[i(t) - i(t-\Delta t)] - [L_1.L_2 + L_1.L_m + L_2.L_m].[i(t-\Delta t) - i(t-2\Delta t)] \rightarrow \frac{[R2.\frac{\Delta t}{2} + [L2+Lm]].\Delta t}{2}.v(t)$$

$$+ \frac{R2.\Delta t^2}{2}.v(t-\Delta t) + \frac{[R2.\frac{\Delta t}{2} - [L2+Lm]].\Delta t}{2}.\boxed{v(t-2\Delta t)} = [\frac{R1.R2.\frac{\Delta t}{2} + [R2.L1+R1.L2+R1.Lm+R2.Lm].\Delta t}{2} + [L_1.L_2 + L_1.L_m + L_2.L_m]].i(t) -$$

$$2[L_1.L_2 + L_1.L_m + L_2.L_m].i(t-\Delta t) + [\frac{R1.R2.\frac{\Delta t}{2} - [R2.L1+R1.L2+R1.Lm+R2.Lm].\Delta t}{2}$$

$$+ [L_1.L_2 + L_1.L_m + L_2.L_m]].\boxed{i(t-2\Delta t)} \rightarrow a_0 = \frac{[\frac{R1.R2.\frac{\Delta t}{2} + [R2.L1+R1.L2+R1.Lm+R2.Lm].\Delta t}{2} + [L_1.L_2 + L_1.L_m + L_2.L_m]]}{\frac{[R2.\frac{\Delta t}{2} + [L2+Lm]].\Delta t}{2}}$$

$$a_1 = \frac{-2[L_1.L_2 + L_1.L_m + L_2.L_m]}{\frac{[R2.\frac{\Delta t}{2} + [L2+Lm]].\Delta t}{2}}$$

$$a_2 = \frac{[\frac{R1.R2.\frac{\Delta t}{2} - [R2.L1+R1.L2+R1.Lm+R2.Lm].\Delta t}{2} + [L_1.L_2 + L_1.L_m + L_2.L_m]]}{\frac{[R2.\frac{\Delta t}{2} + [L2+Lm]].\Delta t}{2}}$$

$$b_0 = -\frac{\frac{R2.\Delta t^2}{2}}{\frac{[R2.\frac{\Delta t}{2} + [L2+Lm]].\Delta t}{2}}$$

$$b_1 = -\frac{\frac{[R2.\frac{\Delta t}{2} - [L2+Lm]].\Delta t}{2}}{\frac{[R2.\frac{\Delta t}{2} + [L2+Lm]].\Delta t}{2}}$$

Discussion Based on Parametric Calculations

As earlier discussed in this chapter, our new developed model recognizes three major types of loads as eigen-loads which includes induction **motor**, **inductive** and **resistive**. The reason of choosing these three categories of loads is that each of these types have their own voltage dependency characteristic. UBC Power Systems Lab invented a new LPF (Linear Power Flow) formulation instead of non-linear power flow solution. In their method, loads are modelled considering their voltage dependence characteristics which allows for a load representation with a **constant-impedance** and a **constant-current** synthesis (Z-I model) [11]. Above mentioned voltage dependence is determined with knowing type of feeder connected loads. This fact triggered this thesis to investigate about load disaggregation more deeply and come up with an efficient pattern. As a result, the algorithm is able to detect motor, inductive and resistive contribution in the total load. Based on few example calculations performed for a motor, an inductor and a resistor, we figured out that "Resistive loads" do not change the circuit. "Inductive loads" are increasing the total order by one. Motor loads are increasing the total load's order by two. The only limitation of this method is that, for the case of an inductor and a resistor, we cannot say how many inductors or resistances are in parallel to result in the achieved aggregated load. Following Table 3.1 is a summary of different category of loads with corresponding orders:

Table 3.1: Different loads order prediction.

Type of Load	Order of Load)
Resistance	0
Inductance	1
Motor	2
Resistance parallel with Inductance	1
Resistance parallel with Motor	2
Inductance parallel with Motor	3
n parallel Resistance	0
n parallel inductance	1
n parallel Motor	2n

So far, we have obtained the order of load circuit. Now it is time to calculate the

electrical parameters of the load. For this reason, we select network synthesis to realize the load network having its equivalent impedance transfer function.

3.5 Network Synthesis

In this section network synthesis is explained. Two general methods namely, Foster and Cauer are discussed for the synthesis of networks having two kinds of elements (LC, RC, or RL).
Network synthesis is the opposite way of network analysis. In any network synthesis problem engineers deal with three quantities namely, input, output and network.
Note that, we use the calculated discrete time impedance coefficients of a load, in the form of the impedance "Z" domain transfer function. The next step is to covert the discrete time transfer function to the continuous time transfer function. Applying network synthesis techniques to impedance Laplacian transfer function, outcomes electrical parameters of the load.
The question is, what is the network topology for a given impedance or admittance transfer function.

3.5.1 Network Synthesis Description

Network synthesis is a block which is fed with a driving point such as impedance or admittance as the input and the output is the equivalent network composed of passive elements. In other words, it simplifies the interpretation of a closed loop driving point impedance or admittance.
There are several techniques, which can be found in electrical engineering literature for the synthesis of two terminal network from the driving point (impedance/admittance function) [43] [44] [45] [46]. We employ the main two common network synthesis methods, Foster forms and Cauer forms in this thesis [47] [48] [49].
The oldest and most widely used synthesis forms, are implemented on LC, RC and RL networks. LC networks topologies can be generalized to the RL and RC forms as well.
The first method introduced in Section 3.6 is Foster method which is based on partial fraction expansion of the impedance or admittance transfer function [50]. in the following section, the synthesis of LC one port networks (i.e., LC networks having a prescribed driving-point impedance/admittance) will be described.

3.6 Foster Forms

First Foster Form

First foster method realizes Z_{LC} in the form of circuit in Figure 3.17.
Realization of Z_s in the form of Figure 3.17 was first introduced by Foster. As a consequence, this form of realization is named the First Foster form or F_1 form.

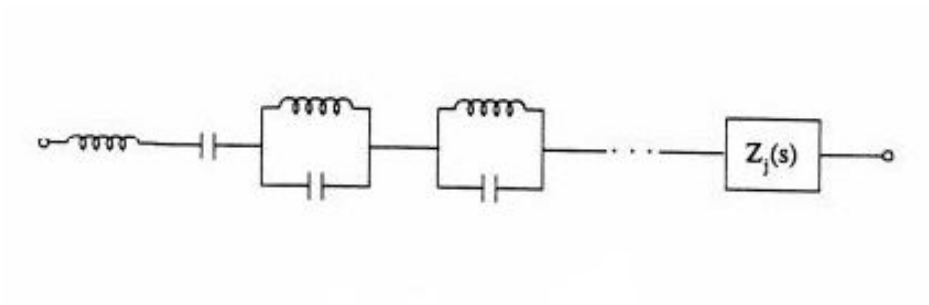

Figure 3.17: First Foster form-partial fraction expansion in the impedance form. The components are connected in series [51].

The equivalent impedance which is seen from the input port of the circuit in Figure 3.17 can be formulated as :

$$Z(s) = a_1 s + \frac{a_2}{s} + \sum_{i=3}^{j-1} \frac{2.a_i s}{s^2 + w_i^2} + z_k(s) \tag{3.7}$$

Equation 3.7 can be reformulated in a general form as Equation 3.8.

$$Z(s) = \frac{H.(s^2 + w1^2)(s^2 + w3^2)\cdots(s^2 + wm^2)}{(s^2 + w2^2)(s^2 + w4^2)\cdots(s^2 + wr^2)} \tag{3.8}$$

Figure 3.17 is the result of applying 1st Foster technique on impedance Equation 3.8.

Second Foster Form

Second foster method realizes Y_{LC} in the form of circuit in Figure 3.18.

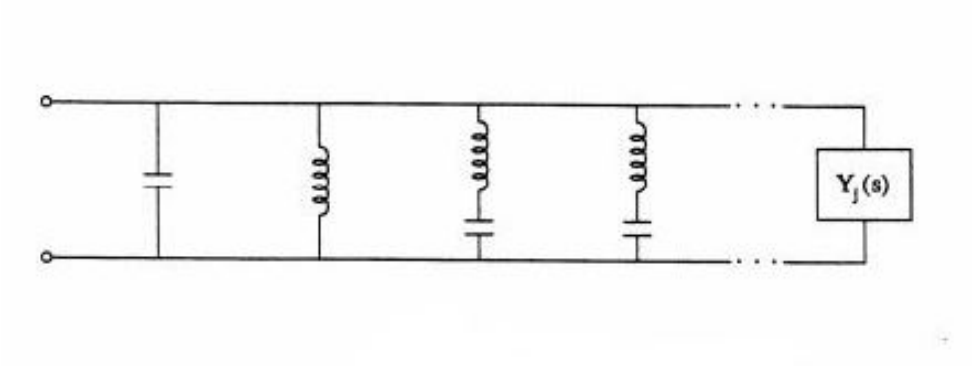

Figure 3.18: Second Foster form-partial fraction expansion in the admittance form. The components are connected in parallel [51].

The equivalent admittance which is seen from the input port of the circuit in Figure 3.18 can be formulated as :

$$Y(s) = a_1 s + \frac{a_2}{s} + \sum_{i=3}^{j-1} \frac{2.a_i s}{s^2 + w_i^2} + Y_j(s) \tag{3.9}$$

3.7 Cauer Forms

Cauer methods apply **Continued Fraction** on impedance or admittance transfer functions to realize the LC circuits. First Cauer and Second Cauer topologies are shown in Figures 3.20 and 3.21 respectively.
Cauer network configurations, which are in the form of the ladder circuits, were first introduced by Cauer and named as Cauer forms.
The expansion of Z_{LC} in the first Cauer form is accomplished through the alternate use of F1 (First Foster) and F2 (second Foster) forms. Cauer configurations are obtained through expansion of Z_{LC} in a continued fraction by the process of continued division.
There are continued Fraction expansion about infinity and continued fraction expansion about zero which form these two Cauer forms.
Continued Fraction expansion about infinity process follows the following steps:

1. Z(s) is written in a form that there is a pole at infinity. This pole is removed by long division leaving Z1(s).

2. Z1(s) is inverted, yielding Y1(s) which has a pole at infinity.

3. Each subsequent cycle consists of an inversion and the removal of a pole at s-infinity.

4. The resultant is a circuit with capacities in series and inductors in parallel which describes the 2nd Cauer form.

Continued fraction expansion about zero is similar to the continued Fraction expansion about infinity except that at each subsequent it consists of an inversion and the removal of a pole at zero. The resulting network has the same structure but with capacitors in series and the inductors in parallel which is describes the 1st Cauer form.
To get a better insight about continued fraction process toward Cauer forms synthesis, consider Figure 3.19 which has the series arms as the impedances and the parallel arms as the admittances.

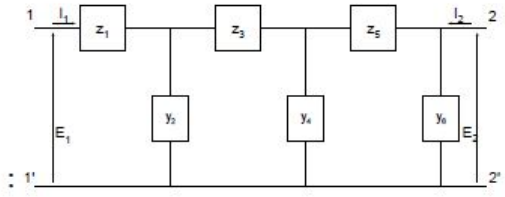

Figure 3.19: Ladder network topology [52].

To compute driving point of equivalent impedance for the circuit in Figure 3.19, we follow the following steps:

1. The impedance of the last term $Z6 = \frac{1}{Y6}$

2. The impedance of the last two arms $Z5 + \frac{1}{Y6}$

3. The impedance of the last three arms $\frac{1}{y_4 + \frac{1}{Z_5 + \frac{1}{y_6}}}$

Proceeding in this manner results: $Z = z_1 + \frac{1}{y_2 + \frac{1}{z_3 + \frac{1}{y_4 + \frac{1}{z_5 + \frac{1}{y6}}}}}$

Realization of LC driving point functions as in first and second Cauer forms are demonstrated in Figures 3.20 and 3.21.

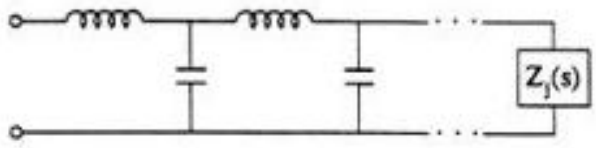

Figure 3.20: First Cauer form continued fraction expansion about infinity. When applied to the impedance of a positive LC network which results in a chain of series inductors and parallel capacitors [51].

$$Z(s) = L_1.s + \frac{1}{C_2.s + \frac{1}{L_3.s + \frac{1}{C_4.s + \cdots}}} \tag{3.10}$$

Figure 3.20 shows the obtained circuit network resulted from 1st Cauer synthesis method being applied on Equation 3.10.
Figure 3.21 shows the obtained circuit network resulted from 2nd Cauer synthesis method being applied on Equation 3.11.

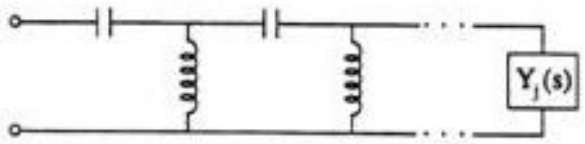

Figure 3.21: Second Cauer form continued fraction expansion about zero. When applied to the impedance of a positive LC network which results in a chain of series capacitors and parallel inductors [51].

$$Z(s) = \frac{1}{C_1.s} + \frac{1}{\frac{1}{L_2.s} + \frac{1}{\frac{1}{C_3.s} + \frac{1}{L_4.s + \cdots}}} \tag{3.11}$$

Figure 3.22 summarizes Foster and Cauer synthesis methods explained so far:

	1st Foster form	2nd Foster form	1st Cauer form	2nd Cauer form)
partial fraction of impedance function	✓			
partial fraction of admittance function		✓		
continued fraction expansion about a point of infinity			✓	
continued fraction expansion about the origin				✓

Figure 3.22: First Foster, 2nd Foster, first Cauer and 2nd Cauer forms method summary.

Table 3.2 gives the general forms of the expansions for all 4 types of Foster and Cauer methods.

Table 3.2: Foster and Cauer impedance/admittance expansions

partial fraction of impedance function	$Z(s) = K_0 + \frac{K_1}{s-s_1} + \frac{K_3}{s-s_3} + \cdots + \frac{K_n}{s-s_n}$
partial fraction of admittance function	$Y(s) = k_\infty s + k_0 + \frac{K_2}{s-s_2} + \frac{K_4}{s-s_4} + \cdots + \frac{K_m}{s-s_m}$
continued fraction expansion about a point of infinity	$Z = a_1 + \cfrac{1}{b_2 s + \cfrac{1}{a_3 + \cfrac{1}{b_4 s + \cfrac{1}{a_5 + \cdots}}}}$
continued fraction expansion about the origin	$Z = \cfrac{1}{a_1 s} + \cfrac{1}{b_2 + \cfrac{1}{a_3 s + \cfrac{1}{b_4 + \cfrac{1}{a_5 s + \cdots}}}}$

Up to here, we explained how to derive a LC circuit employing Foster and Cauer methods. In Section 3.8 we will discuss about applying network synthesis methods toward RL and RC circuits derivation.

3.8 RL-RC Network Synthesis

The synthesis of RC and RL networks is essentially identical. With the change of variables, RC and RL topologies will be converted to LC topology and vice versa. Either Foster or Cauer techniques can be applied to RL and RC networks.

3.8.1 Realization of Z_{RC} in Foster 1 Form:

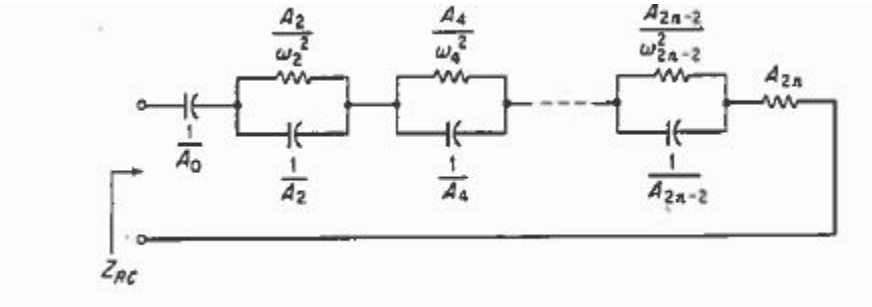

Figure 3.23: Realization of Z_{RC} in F1 form [53].

Evidently, to obtain the F1 form of an RC network, it is necessary to expand Z_{RC} in the partial fraction form as:

$$Z_{RC}(s) = \frac{A_0}{s} + \frac{A_2 P}{s+w_2^2} + \frac{A_4 P}{s+w_4^2} + \cdots + \frac{A_{2n-2} P}{s+w_{2n-2}^2} + A_{2n}$$

All residues $A_{2k}(k = 0,1,\cdots,n)$ and all poles $[w_{2k}^2](k = 1,2,\cdots,n-1)$ are positive and all poles are simple. Hence, all residues of Z_{RC} are positive and all its poles occur at $s = -w_{2k}^2(k = 0,1,\cdots,n)$ where $s = -w_{2k}^2$ is real and negative. Therefore all poles of Z_{RC} are simple, lie on the negative real axis (the -$\sigma axis$) and have positive residues.
Realization of Z_{RC} in F1 form is summarized as following:

1. Expand Z_{RC} into partial fractions.
2. Synthesis Z_{RC} as a series connection of impedance terms in the partial fraction form

3.8.2 Realization of Z_{RC} in Foster 2 Form:

to obtain the F2 form of a RC network, it is necessary to expand Y_{RC} in the partial fraction form as:

$Y_{RC}(s) = A_1 + \frac{A_3 s}{s+w_3^2} + \frac{A_5 s}{s+w_5^2} + \frac{A_7 s}{s+w_7^2} + \cdots + \frac{A_{2n-1} s}{s+w_{2n-1}^2} + A_{2n+1} s$
All A's and all w's are positive so that all poles of Y_{RC} are simple and lie on -$\sigma axis$.
Expansion of Y_{RC} leads to the circuit configuration in Figure 3.24.
Realization of Z_{RC} in F2 form is summarized as following:

1. Expand $\frac{1}{s}.Y_{RC}$ into partial fractions.
2. Form Y_{RC} by multiplying each term of the partial fraction expansion by s.
3. Synthesis Z_{RC} as a parallel connection of admittance terms in the partial fraction form

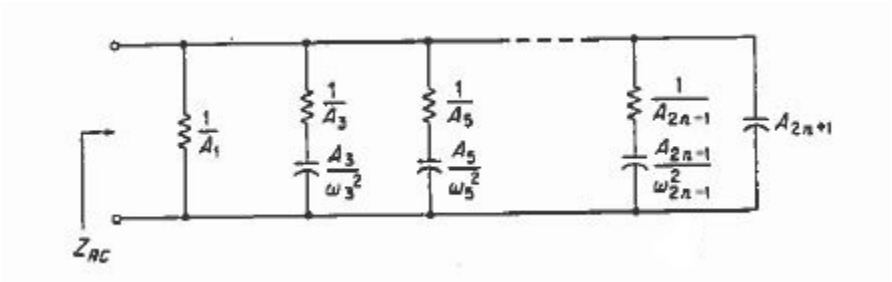

Figure 3.24: Realization of Z_{RC} in F2 form [53].

3.8.3 Realization of Z_{RC} in Cauer 1 Form:

Expansion of Z_{RC} leads to the circuit configuration in Figure 3.25.
Realization of Z_{RC} in C1 form is summarized as following:

1. Arrange the numerator and denominator polynomials in descending order.
2. perform continued division
3. Assign the quotient of the divisions as branch admittance in the C1 ladder network

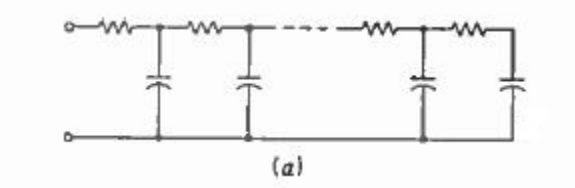

Figure 3.25: Realization of Z_{RC} in C1 form [53].

3.8.4 Realization of Z_{RC} in Cauer 2 Form:

Expansion of Z_{RC} leads to the circuit configuration in Figure 3.26.
Realization of Z_{RC} in C2 form is summarized as following:

1. Arrange the numerator and denominator polynomials in ascending order.
2. perform continued division
3. Assign the quotient of the divisions as branch admittance in the C2 ladder network

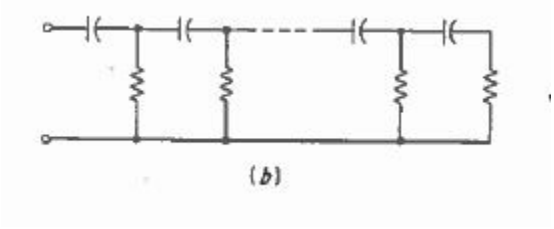

Figure 3.26: Realization of Z_{RC} in C2 form [53].

3.8.5 Realization of Z_{RL} in Foster 1 Form:

Expansion of Z_{Rl} leads to the circuit configuration in Figure 3.27.
Realization of Z_{RL} in F1 form is summarized as following:

1. Expand $\frac{1}{s}.Z_{RL}$ into partial fractions.
2. Form Z_{RL} by multiplying each term of the partial fraction expansion by s.
3. Synthesis Z_{RL} as a series connection of impedance terms in the partial fraction form

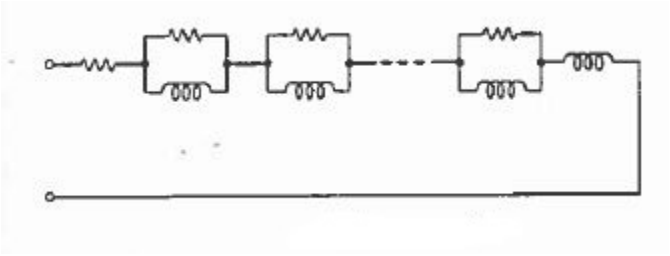

Figure 3.27: Realization of Z_{RL} in F1 form [53].

3.8.6 Realization of Z_{RL} in Foster 2 Form:

Expansion of Z_{RL} leads to the circuit configuration in Figure 3.28.
Realization of Z_{RL} in F2 form is summarized as following:

1. Expand Y_{RL} into partial fractions.
2. Synthesis Z_{RL} as a parallel connection of admittance terms.

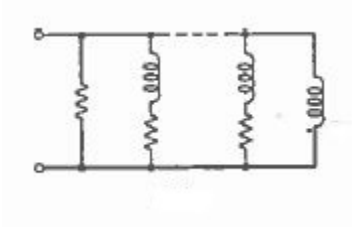

Figure 3.28: Realization of Z_{RL} in F2 form [53].

3.8.7 Realization of Z_{RL} in Cauer 1 Form:

Expansion of Z_{RL} leads to the circuit configuration in Figure 3.29.
Realization of Z_{RL} in C1 form is summarized as following:

1. Expand Y_{RL} into partial fractions.
2. Synthesis Z_{RL} as a parallel connection of admittance terms.

1. Arrange the numerator and denominator polynomials in descending order.
2. perform continued division.
3. Assign the quotient of the divisions as branch admittance in the C1 network.

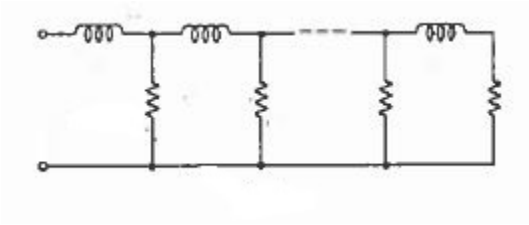

Figure 3.29: Realization of Z_{RL} in C1 form [53].

1. Arrange the numerator and denominator polynomials in ascending order.
2. perform continued division.
3. Assign the reciprocals of the quotients of the divisions as branch admittance in the C2 network.

3.8.8 Realization of Z_{RL} in Cauer 2 Form:

Expansion of Z_{RL} leads to the circuit configuration in Figure 3.30.
Realization of Z_{RL} in C2 form is summarized as following:

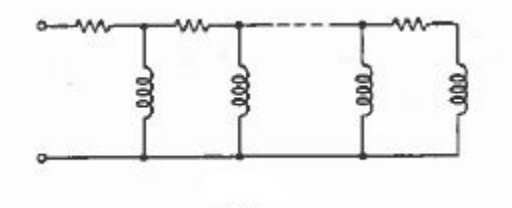

Figure 3.30: Realization of Z_{RL} in C2 form [53].

As shall be discussed in Chapter 4, the Cauer method is adopted for the load circuit synthesis, which results in finding electrical parameters of the load.

Chapter 4

Simulation

In this chapter, we describe simulations conducted on different combination of loads. As explained in Chapter 3, three major eigen-loads, heating (modelled as a resistive), lighting (modelled as an inductive) and motor types (simulated as an equivalent model of an induction motor) are considered in this work. We show that, with having time series information of the voltage and current of the total load, we are able to guess, the contributions of the three eigen-loads, (1) heating load, (2) lighting load and (3) motor load in the total load. As the result, we simulated all different topologies of the load circuit, considering the three mentioned eigen-loads. The significant strength of our method is that, it detects between resistive, inductive and motor loads based on mostly steady Our algorithm developed distinguishable steady state impedance coefficients for different load types. For lower order loads, the steady state section of the voltage and current signals are sampled. While, for higher order loads, the transient section of the voltage and current signals are sample as well. The selection of sampling points, is important because, impedance coefficients are calculated for the sampled portion of voltage and current signals. Sampling rate should be sufficient to capture the essential characteristics of that circuit. Also, the sampling point distance, needs to be at least one cycle of 60 Hz period.
PSCAD as an accurate reliable study tool is selected for this study for the following reasons:

1. PSCAD is the most powerful power system transient simulation tool. For higher order load circuits, we need accurate transient data for the voltage and the current.

2. The main idea behind this research is taking advantage of the discrete time impedance

coefficients. These coefficients are derived from implementing the trapezoidal integration rule on the voltage and current time series data. **PSCAD** is coded based on trapezoidal method, i.e., the output data from PSCAD is a determined resource of data set, to validate our theory with.

This work proves that by looking at the time series voltage and current signals, at real time, we can say how many percent of the total load, is from motor, resistive and inductive type. Simulation based data are examined as described in Sections 4.2.1, 4.2.3, 4.2.4, 4.2.6, 4.2.8, 4.2.10, 4.2.11, 4.2.12, and 4.2.14. Nine different load topologies, including different combination of eigen-loads are simulated in PSCAD and the Output voltage and current time series signals are imported into **Matlab**. The beauty of our algorithm is its capability of deriving the electrical parameters of the load. this will exactly tell, how many percent of the total impedance (or admittance) is from each of the eigen-loads. we employ network synthesis concept to achieve this goal. In order to calculate the exact values of electrical parameters for a load, we need to have whether the impedance or the admittance transfer function. Cauer (Foster) methods are stepped in to design a network which realizes the given Z(s) or Y(s).
Note that we use admittance transfer function in developing our algorithm. We present a method to construct a transfer function for the total impedance of the aggregated load. We have the discrete domain function of impedance by having the values of calculated coefficients as will be discussed in Sections 4.2.1, 4.2.3, 4.2.4, 4.2.6, 4.2.8, 4.2.10, 4.2.11, 4.2.12, and 4.2.14. Obtained impedance coefficients, from the impedance transfer function as shown in Equation 4.1.

$$Z_z = \frac{a_n.Z^n + a_{n-1}.Z^{n-1} + a_{n-2}.Z^{n-2} + \cdots + a_0}{b_m.Z^m + b_{m-1}.Z^{m-1} + B_{m-2}.Z^{m-2} + \cdots + b_0} \tag{4.1}$$

The first step is to convert Equation 4.1 which is in Z domain to S domain as in Equation 4.2.

$$Z_s = \frac{a'_n.S^n + a'_{n-1}.S^{n-1} + a'_{n-2}.S^{n-2} + \cdots + a'_0}{b'_m.S^m + b'_{m-1}.S^{m-1} + B'_{m-2}.S^{m-2} + \cdots + b'_0} \tag{4.2}$$

Cauer method synthesizes admittance Laplacian function $Y_s = 1/Z_s$ in the form of resistances and inductance (RL circuit)or RC circuit.

4.1 Discrete-Continues Transformation

In this section, we briefly explain how to convert the derived impedance discrete domain function to the continue domain function. There are five most common **"discrete-continuous"** mapping techniques namely: backward difference method, forward difference method, bilinear transform method, bilinear transform with pre-warping method and matched-Z method. Since we applied trapezoidal to obtain our impedance discrete coefficients, we employ bilinear transform method.

4.1.1 Bilinear Transform Method

This method is also known as trapezoidal substitution method or Tustin method. The relation between s and z is given by:

$s \leftarrow \frac{2}{T}.\frac{z-1}{z+1}$ $z = e(sT) = \frac{1+sT/2}{1-sT/2}$ where T is the time interval between samples of the discrete-time system. The process consists of using a mapping function to replace every z in the F(z) with the function of s to obtain F(s). The highlighted portion of s plane is mapped inside the unit circle in z-plane as shown in Figure 4.1.

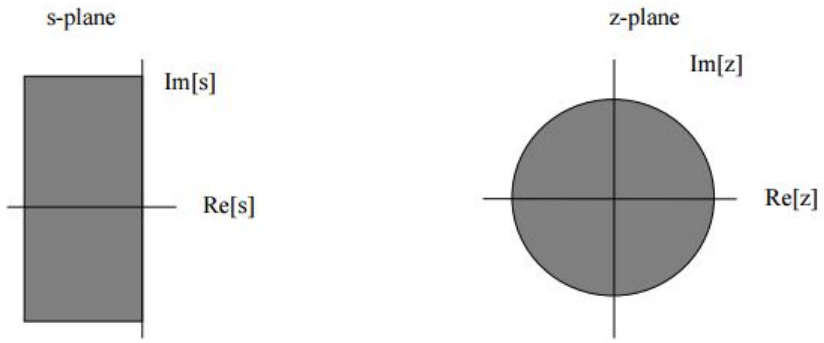

Figure 4.1: Mapping of the s-plane to the z-plane with the bilinear transform method.

The advantage of selected method (Tustin mapping)is that, it does not suffer stability limitations associated with higher order and more complex numerical methods. Therefore, discrete-time derived coefficients(discrete-time digital filter) will be related to the continuous-time (analog filter)through the bilinear transform process. "Network synthesis" block obtains analog coefficients. It applies whether 1st Cauer or 2nd Cauer methods, depending on the load topology determining the **type of the loads** and the **exact values**

of the load's parameters. Sections 4.2.2, 4.2.2, 4.2.2, 4.2.2, 4.2.2, 4.2.2 will demonstrate the process of calculating each simulation load parameters.

4.2 Simulation Results

4.2.1 Simulation One: Parallel Resistive and Inductive Load

As the first example, the simulation case is a parallel steady state **RL** circuit(**representing Resistive load in parallel with an Inductive load**) with sampling rate of $\Delta t = 625\mu s$ (sampling frequency =1600 Hz) and maximum simulation time of $t_{max} = 0.0625s$. As stated, loads are classified into major three groups specified as resistor (R), lamps (modelled as a single inductor), and motors (model as an induction motor). This simulation case, describes the behaviour of a resistive load paralleled with an inductive load. There are 100 samples in total. Voltage magnitude is 230 KV to mimic the city electricity magnitude. No transient sample is selected since the order of the circuit is one and the steady state portions of the voltage and current signals are sufficient to discriminate between inductance and resistance values. Three samples are chosen from the voltage and the current signals. The reason is that this load case is a first order system. (**Note that corresponding voltage and current meters are inserted right after the voltage source, because we need to get the aggregated load's information.**)

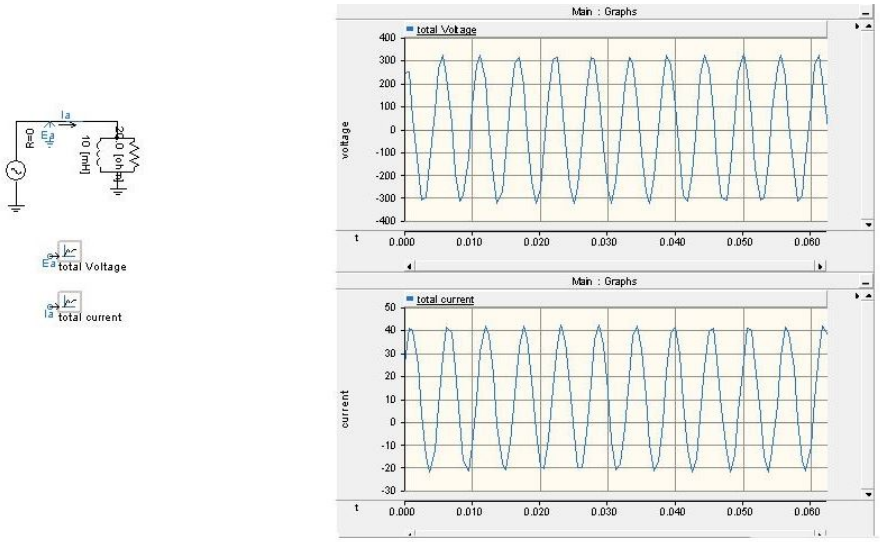

Figure 4.2: Inductive load paralleled with a resistive load.

As proved in Chapter 3, the magnitude of coefficients, $a_0, a_1, \cdots, a_n, b_0, b_1, \cdots, b_n$ will be equal regardless of the sampling points selection pattern. Therefore, for all nine simulation cases, we consider at least two different sampling scenario, (in some cases we illustrated three different sampling scenarios). For each of the sampling schemes, $a_0, a_1, \cdots, a_n$ $b_0, b_1, \cdots, b_n$ coefficients are calculated. We prove that, as for the correct order of the load circuit, the magnitude of these coefficients will be equal. For the wrong choice of load order, the magnitude of these coefficients are diverse.

Simulation One: First Sampling Scenario

In this sampling scheme, the first sampling point is the 76th point of voltage and current waveforms. The distance between each samples is 10 samples. Matrix A describes the values for all current terms and all voltage history terms (refer to Equation 3.4 in Chapter 3). Matrix B contains voltage (V_t) values. First order impedance discrete time series coefficients are calculated and resulted as:
$[a_0, a_1, b_0] = [12.3077 - 12.3077 - 0.2308]$

Table 4.1: Values of current at time t and $t - \Delta t$, voltage at time $t - \Delta t$ for the first sampling scenario in the case of a parallel RL load.

selected sample	$i(t)$	$i(t - \Delta t)$	$v(t - \Delta t)$
sample 76th	-62.9551	-72.1146	-50.8833
sample 86th	95.73191	89.20309	-191.188
sample 96th	-37.726	-19.3333	321.2645

Table 4.2: Values of voltage at time t for the first sampling scenario in the case of a parallel RL load.

selected sample	$v(t)$
sample 76th	124.475
sample 86th	124.475
sample 96th	-300.509

Simulation One: Second Sampling Scenario

In this sampling scheme, the first sampling point is the 20th point of voltage and current waveforms. The distance between each samples is 20 samples. First order discrete time

Table 4.3: Values of current at time t and $t - \Delta t$, voltage at time $t - \Delta t$ for the second sampling scenario in the case of a parallel RL load.

selected sample	$i(t)$	$i(t - \Delta t)$	$v(t - \Delta t)$
sample 20th	-77.1399	-73.7391	147.6691
sample 40th	14.39903	34.66287	289.8169
sample 60th	97.46917	94.06845	-147.669

impedance coefficients are calculated and resulted as:
$[a_0, a_1, b_0] = [12.3077 - 12.3077 - 0.2308]$
For both sets of sampling schemes, derived coefficients $\{a_0, a_1, b_0\}$, have the same values. It confirms that this load case is a first order system. The same process is practice for second order coefficients. Five samples are selected from the voltage and the current signals. $[a_0, a_1, a_2, b_0, b_1]$ coefficient values were different for two individual group of sampling points. It proves that, this load, does not full fill the second order requirements.

Table 4.4: Values of voltage at time t for the second sampling scenario in the case of a parallel RL load.

selected sample	$v(t)$
sample 20th	-75.9326
sample 40th	-316.282
sample 60th	75.93257

Figure 4.3: First order impedance coefficients for the first and second scenarios of a paralleled RL load.

4.2.2 Simulation One: Paralleled RL Load Parameters Calculations

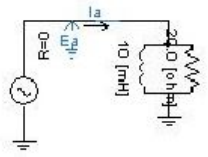

Figure 4.4: Paralleled RL Load

Equation 4.3is resulted from the discrete time impedance coefficients that are derived from PSCAD.

$$\frac{V(z)}{I(z)} = 12.3077I(z) - 12.3077I(z).z^{-1} - 0.2308V(z).z^{-1} \xrightarrow{TustinTransfrom} Z(s) = \frac{s+2000}{20s} \tag{4.3}$$

Tustin method converts Equation 4.3 to Equation 4.4.

$$Z(s) = \frac{s+2000}{20s} \tag{4.4}$$

Applying 2nd Cauer method (**Continued fraction on Z(s)**) determines load's constituent's parameters as following:

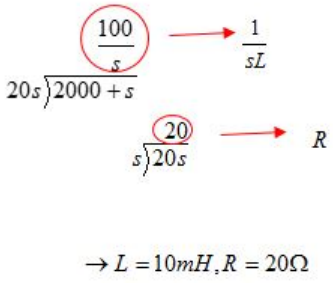

Figure 4.5: Paralleled RL parameters calculation

4.2.3 Simulation Two: Resistor in Series with a Parallel Inductance and Capacitance

Figure 4.6 is predicted to be a second order load based on calculations(refer to Chapter 3). We implement the same process as for Section 4.2.1 to calculate the discrete impedance coefficients for this load as well. We selected $\frac{1}{5}$ of the sample points from slow transient portion of the voltage and current signals. Note that slow transient is simulated with adding the "ramp up time" value to the voltage source setting. The signal will reach to the steady state condition after the ramp up time. Using a switch after the voltage source will also produce the slow transient situation in PSCAD. In this simulation case, sampling rate is $\Delta t = 625\mu s$(sampling frequency =1600 Hz), maximum simulation time is $t_{max} = 0.0625s$

and ramp up time=0.00625. Up to sample number 10, it is all slow transient portion of the signal. Steady state section starts from the 11th sample. One sample is selected from the slow transient samples. All the rest four samples are chosen from the steady state samples. Note that, in Chapter 3, it is proved, knowing the circuit topology, we can guess the order of the load circuit. Thereafter, network synthesis tool as explained in Chapter3, Section 3.5, will solve the load disaggregation problem. It will detect the load's type and determine the loads' parameters. But, In a real system, load's circuit's configuration is unknown, therefore the first and key step is to **predict the order of the load's circuit**.

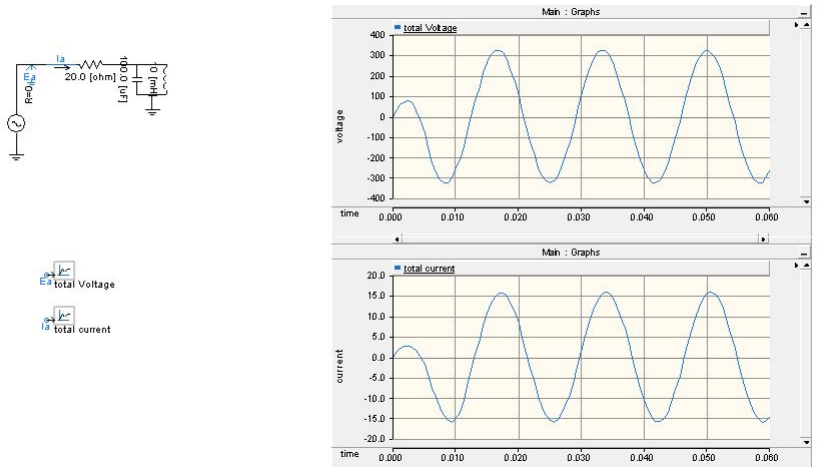

Figure 4.6: Resistive load in series with a paralleled LC.

Figure 4.6, represents a parallel inductance and capacitance which are placed in series with a resistance. Two different sampling scenarios are designated which both have the same initial point, (both start from 8th point of the voltage/current signal)with the different sample points distances.
The process to determine the order of a load circuit is such that, $(a_0, a_1, a_2, \cdots a_n, b_0, b_1, b_2, \cdots, b_n)$ coefficients are calculated for orders=(1,2,...,n) up to the correct order. for the correct predicted order, resulting matrix of $inv(A) * B$ carries the same values for at least two different sampling patterns.

Simulation Two: First Sampling Scenario

In this sampling scheme, the first sampling point is the 8th point of voltage and current waveforms. The distance between each samples is 20 samples. First order discrete time

Table 4.5: Values of current at time t and $t - \Delta t$, voltage at time $t - \Delta t$ for the first sampling scenario in the case of a resistance in series with a paralleled LC load.

selected sample	$i(t)$	$i(t - \Delta t)$	$v(t - \Delta t)$
8th sample	0.221231	1.549666	-30.53
28th sample	15.56777	14.67393	-321.265
48th sample	-2.20467	-5.80907	50.8833

Table 4.6: Values of voltage at time t for the first sampling scenario in the case of a resistance in series with a paralleled LC load.

selected sample	$v(t)$
8th sample	-17.8642
28th sample	324.2664
48th sample	25.52032

impedance coefficients are calculated and resulted as:
$[a_0, a_1, b_0] = [36.3046 - 19.3411 - 0.1335]$

Simulation Two: Second Sampling Scenario

In this sampling scheme, the first sampling point is the 8th point of voltage and current waveforms. The distance between each samples is 35 samples.

Table 4.7: Values of current at time t and $t - \Delta t$, voltage at time $t - \Delta t$ for the second sampling scenario in the case of a resistance in series with a paralleled LC load.

selected sample	$i(t)$	$i(t - \Delta t)$	$v(t - \Delta t)$
8th sample	0.221231	1.549666	-30.53
43th sample	-15.3608	-15.8779	316.2819
78th sample	9.564251	6.340717	-191.188

Table 4.8: Values of voltage at time t for the first sampling scenario in the case of a resistance in series with a paralleled LC load.

selected sample	$v(t)$
8th sample	-17.864
43th sample	-289.816
78th sample	247.336

Discrete time impedance coefficients are calculated and resulted as:
$[a_0, a_1, b_0] = [36.079 - 19.0608 - 0.1209]$ So far, we calculated the first order impedance coefficients for two different sampling scenarios. The magnitude of the two impedance matrices are equal within less than 10% error. Since this load satisfies the 1st order criteria, we will continue to the second order calculation. As explained in Chapter 3, for the second order situation, we will engage five sampling points from the voltage and the current signals.

Simulation Two: First Sampling Scenario For the Second Order Status

In this sampling scheme, the first sampling point is the 8th point of voltage and current waveforms. The distance between each samples is 20 samples.

Table 4.9: Values of current at time t, $t - \Delta t$ and $t - 2\Delta t$, voltage at time $t - \Delta t$ and $t - 2\Delta t$ for the first sampling scenario in the case of a resistance in series with a paralleled LC load.

selected sample	$i(t)$	$i(t - \Delta t)$	$i(t - 2\Delta t)$	$v(t - \Delta t)$	$v(t - 2\Delta t)$
8th sample	0.221231	1.549666	2.336653	-30.53	-62.2376
28th sample	15.56777	14.67393	13.02486	-321.265	-300.509
48th sample	-2.20467	-5.80907	-9.0913	50.8833	124.4751
68th sample	-15.7265	-14.7778	-13.0126	321.2645	300.5095
68th sample	2.200985	5.811509	9.100879	-50.8833	-124.475

Table 4.10: Values of voltage at time t for the first sampling scenario in the case of a parallel RL load.

selected sample	$v(t)$
8th sample	-17.8642
28th sample	324.2664
48th sample	25.52032
68th sample	-324.266
88th sample	-25.5203

Discrete time impedance coefficients are: $[a_0, a_1, a_2, b_0, b_1] = [22.8470 - 32.8826 \quad 17.1530 \quad -1.6441 \quad 1.0000]$

Simulation Two: Second Sampling Scenario For the Second Order Status

In this sampling scheme, the first sampling point is the 8th point of voltage and current waveforms. The distance between each samples is 10 samples.

Table 4.11: Values of current at time t, $t - \Delta t$ and $t - 2\Delta t$, voltage at time $t - \Delta t$ and $t - 2\Delta t$ for the second sampling scenario in the case of a resistance in series with a paralleled LC load.

selected sample	$i(t)$	$i(t-\Delta t)$	$i(t-2\Delta t)$	$v(t-\Delta t)$	$v(t-2\Delta t)$
8th sample	0.221231	1.549666	2.336653	-30.53	-62.2376
18th sample	-13.4113	-15.2336	-15.9516	263.1482	300.5095
28th sample	15.56777	14.67393	13.02486	-321.265	-300.509
38th sample	-9.59291	-6.34855	-2.74361	191.1884	124.4751
48th sample	-2.20467	-5.80907	-9.0913	50.8833	124.4751

Table 4.12: Values of voltage at time t for the second sampling scenario in the case of a resistance in series with a paralleled LC load.

selected sample	$v(t)$
8th sample	-17.8642
18th sample	-211.245
28th sample	324.2664
38th sample	-247.337
48th sample	25.52032

Discrete time impedance coefficients are calculated and resulted as: $[a_0, a_1, a_2, b_0, b_1] = [22.8470 \quad -32.8826 \quad 17.1530 \quad -1.6441 \quad 1.0000]$ Second order derived impedance coefficients are identical. It justifies that this circuit satisfies the second order characteristics. Up to this end, first order and 2nd order discrete time coefficients values for different group of sampling points are equivalent. This forces us to continue the same process for third order.

Simulation Two: First Sampling Scenario For the Third Order Status

In this sampling scheme, the first sampling point is the 5th point of voltage and current waveforms. The distance between each samples is 15 samples. For the third order situation, we need at least 7 sampling points.

Table 4.13: Values of current at time t, $t-\Delta t$, $t-2\Delta t$ and $t-3\Delta t$, voltage at time $t-\Delta t$, $t-2\Delta t$ and $t-3\Delta t$ for the first sampling scenario in the case of a resistance in series with a paralleled LC load.

selected sample	$i(t)$	$i(t-\Delta t)$	$i(t-2\Delta t)$	$i(t-3\Delta t)$	$v(t-\Delta t)$	$v(t-2\Delta t)$	$v(t-3\Delta t)$
5th sample	2.688084	2.664771	2.253407	1.384349	-74.201	-57.9634	-31.6282
20th sample	-7.19437	-10.6446	-13.4113	-15.2336	147.6691	211.2454	263.1482
35th sample	1.014964	4.708302	8.121243	11.05883	-25.5203	-100.514	-169.953
50th sample	5.171216	1.524038	-2.20467	-5.80907	-100.514	-25.5203	50.8833
65th sample	-10.5285	-7.46292	-3.98515	-0.28728	211.2454	147.6691	75.93257
80th sample	14.27682	12.25925	9.564251	6.340717	-289.817	-247.337	-191.188
95th sample	-15.8509	-15.1888	-13.6873	-11.4295	324.2664	309.3493	277.3375

Table 4.14: Values of voltage at time t for the first sampling scenario in the case of a resistance in series with a paralleled LC load.

selected sample	$v(t)$
5th sample	76.47536
20th sample	-75.9326
35th sample	-50.8833
50th sample	169.9526
65th sample	-263.148
80th sample	316.2819
95th sample	-321.265

Discrete time impedance coefficients are calculated and resulted as:

$$[a_0, a_1, a_2, a_3, b_0, b_1, b_2] = [537.1875 \quad -775.8906 \quad 407.2500 \quad -2.0454 \quad 37.210 \quad -61.4375 \quad 32.0879]$$

Simulation Two: Second Sampling Scenario For the Third Order Status

In this sampling scheme, the first sampling point is the 5th point of voltage and current waveforms. The distance between each samples is 10 samples.

Table 4.15: Values of current at time t, $t-\Delta t$, $t-2\Delta t$ and $t-3\Delta t$, voltage at time $t-\Delta t$, $t-2\Delta t$ and $t-3\Delta t$ for the second sampling scenario in the case of a resistance in series with a paralleled LC load.

selected sample	$i(t)$	$i(t-\Delta t)$	$i(t-2\Delta t)$	$i(t-3\Delta t)$	$v(t-\Delta t)$	$v(t-2\Delta t)$	$v(t-3\Delta t)$
5th sample	2.688084	2.664771	2.253407	1.384349	-74.201	-57.9634	-31.6282
15th sample	-15.5555	-14.2037	-12.1923	-9.87563	324.2664	309.3493	277.3375
25th sample	10.6904	7.756909	4.333147	0.562823	-211.245	-147.669	-75.9326
35th sample	1.014964	4.708302	8.121243	11.05883	-25.5203	-100.514	-169.953
45th sample	-11.8722	-14.0006	-15.3608	-15.8779	247.3366	289.8169	316.2819
55th sample	15.85452	15.19178	13.68826	11.42731	-324.266	-309.349	-277.338
65th sample	-10.5285	-7.46292	-3.98515	-0.28728	211.2454	147.6691	75.93257

Table 4.16: Values of voltage at time t for the second sampling scenario in the case of a resistance in series with a paralleled LC load.

selected sample	$v(t)$
5th sample	76.47536
15th sample	-321.265
25th sample	263.1482
35th sample	-50.8833
45th sample	-191.188
455th sample	321.2645
65th sample	-263.148

Discrete time impedance coefficients are calculated and resulted as: $[a_0, a_1, a_2, a_3, b_0, b_1, b_2] = [6.9746 \ -38.082 \ 45.5977 \ \ -21.0547 \ -4.0745 \ \ 4.9507 \ \ -2.2212]$ Different obtained impedance coefficient matrices confirm that this load is not a third order load. The largest order, which resulted to the equal impedance values is two. Note that, Both inductance and capacitance, generate first order history terms and they are set in parallel. Second history terms will be generated when we implement trapezoidal integration on Z_z. We analyse this simulation load case with a different $Deltat$ value as well. The new value of Δt is 0.0022 seconds. $t_{max} = 0.4s$ and ramp up time=0.044(slow transient ends at sample 22). $[a_0, a_1, a_2, b_0, b_1] = [24.9774 \ \ 3.8009 \ \ 15.0226 \ \ 0.1900 \ \ 1.0000]$ For the second order conditions, we considered two different sampling scenarios. The two scenarios resulted in two identical impedance matrices for $t = t, t - \Delta t, t - 2\Delta t$ time stamps. this proves our statement in Chapter 3 that says, different Δt values will result in equal discrete impedance coefficients. In other word, the sampling rate will not impact our algorithm.

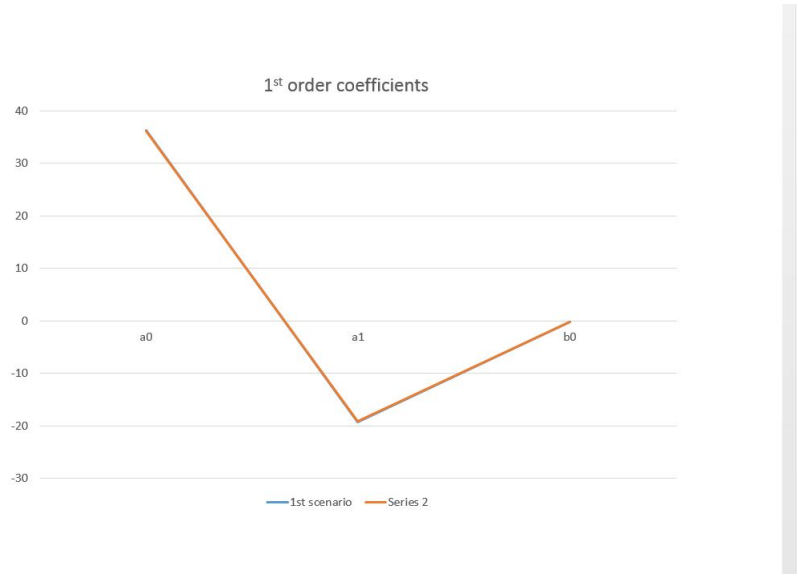

Figure 4.7: First order impedance coefficients for the first and second scenarios of a resistance in series with a paralleled LC load.

Figure 4.8: Second order impedance coefficients for the first and second scenarios of a resistance in series with a paralleled LC load.

Figure 4.9: Third order impedance coefficients for the first and second scenarios of a resistance in series with a paralleled LC load.

Figures 4.7 and 4.7 demonstrate first order and 2nd order impedance coefficient values for both scenarios. This confirms that two graphs are exactly matched while in Figure 4.9, we see two different patterns of coefficients.

4.2.4 Simulation Three: Motor Load

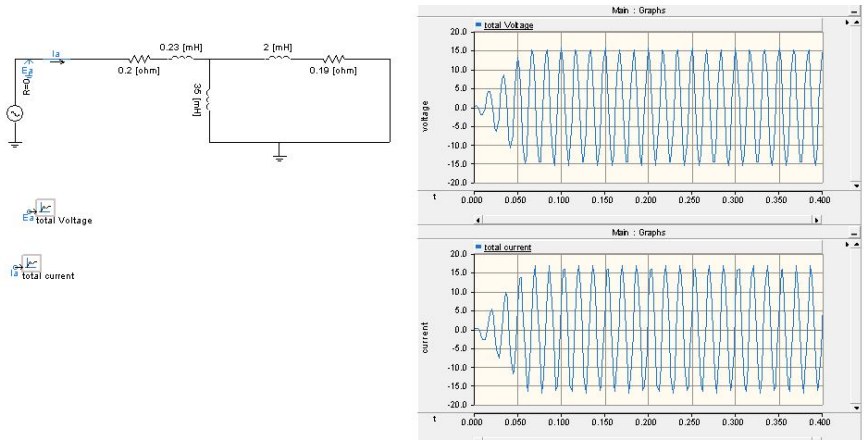

Figure 4.10: Motor load case.

This simulation case describes the behaviour of a motor type load. We assume motor loads as the second order systems based on calculations in Chapter 3. Simulation data confirms this fact. In this simulation case, sampling rate is $\Delta t = 2200\mu s$, maximum simulation time is $t_{max} = 0.4seconds$ and ramp up time is 0.066 seconds. Following analysis starts with order=1. It calculates (a_0, a_1, b_0) coefficients for at least two different sets of voltage and current samples. the same process is continued for higher orders until we get the correct order of the circuit. We selected one sampling point from transient portion of the voltage and the current signal.

Simulation Three: First Sampling Scenario

In this sampling scheme, the first sampling point is the 25th point of voltage and current waveforms. The distance between each samples is 20 samples.

Table 4.17: Values of current at time t and $t - \Delta t$, voltage at time $t - \Delta t$ for the first sampling scenario for a single motor load

selected sample	$i(t)$	$i(t - \Delta t)$	$v(t - \Delta t)$
25th sample	13.1152	7.969328	-11.6227
45th sample	-11.9759	-16.7281	6.975206
65th sample	-1.39197	11.37702	6.267753

Table 4.18: Values of voltage at time t for the first sampling scenario for a single motor load.

selected sample	$v(t)$
25th sample	6.132031
45th sample	5.544468
65th sample	-14.7334

Discrete time impedance coefficients are calculated and resulted as:
$[a_0, a_1, b_0] = [2.3049 - 1.56431.0007]$

Simulation Three: Second Sampling Scenario

In this sampling scheme, the first sampling point is the 25th point of voltage and current waveforms. The distance between each samples is 32 samples.

Table 4.19: Values of current at time t and $t - \Delta t$, voltage at time $t - \Delta t$ for the second sampling scenario for a single motor load

selected sample	$i(t)$	$i(t - \Delta t)$	$v(t - \Delta t)$
25th sample	13.1152	7.969328	-11.6227
57th sample	4.449092	14.92126	0.976791
89th sample	-15.2177	-5.10202	15.47781

Table 4.20: Values of voltage at time t for the second sampling scenario for a single motor load.

selected sample	$v(t)$
25th sample	6.132031
57th sample	-12.11
89th sample	-11.6041

Discrete coefficients are calculated and resulted as:
$[a_0, a_1, b_0] = [2.1643 - 1.51450.8789]$

Simulation Three: Third Sampling Scenario

In this sampling scheme, the first sampling point is the 40th point of voltage and current waveforms. The distance between each samples is 32 samples.

Table 4.21: Values of current at time t and $t - \Delta t$, voltage at time $t - \Delta t$ for the third sampling scenario for a single motor load

selected sample	$i(t)$	$i(t - \Delta t)$	$v(t - \Delta t)$
40th sample	16.33137	8.214105	-15.4778
72th sample	6.438923	15.75991	-0.97679
104th sample	-14.2184	-3.06126	15.16008

Table 4.22: Values of voltage at time t for the third sampling scenario for a single motor load.

selected sample	$v(t)$
40th sample	9.301219
72th sample	-10.7907
104th sample	-12.8112

Discrete coefficients are calculated and resulted as:
$[a_0, a_1, b_0] = [2.1643 - 1.51450.8789]$ Looking at the three obtained matrices for $[a_0, a_1, b_0]$, all are equivalent. We will continue with second order analysis:

Simulation Three: First Sampling Scenario For the Second Order Status

In this sampling scheme, the first sampling point is the 25th point of voltage and current waveforms. The distance between each samples is 20 samples.

Table 4.23: Values of current at time t, $t - \Delta t$ and $t - 2\Delta t$, voltage at time $t - \Delta t$ and $t - 2\Delta t$ for the first sampling scenario for a single motor load.

selected sample	$i(t)$	$i(t - \Delta t)$	$i(t - 2\Delta t)$	$v(t - \Delta t)$	$v(t - 2\Delta t)$
25th sample	13.1152	7.969328	-1.69501	-11.6227	-9.39485
45th sample	-11.9759	-16.7281	-10.6144	6.975206	14.96564
65th sample	-1.39197	11.37702	16.75935	6.267753	-6.26775
85th sample	13.75697	2.231712	-10.7419	-14.9656	-6.97521
105th sample	-16.1424	-14.2184	-3.06126	12.81116	15.16008

Table 4.24: Values of voltage at time t for the first sampling scenario in the case of a single motor load

selected sample	$v(t)$
25th sample	6.132031
45th sample	5.544468
65th sample	-14.7334
85th sample	13.23837
105th sample	-2.14351

Discrete time series coefficients are calculated and resulted as:
$[a_0, a_1, a_2, b_0, b_1] = [2.2981 \; -3.8341 \;\; 1.5405 \;\; 0.0112 \; -0.9888]$

Simulation Three: Second Sampling Scenario For the Second Order Status

In this sampling scheme, the first sampling point is the 25th point of voltage and current waveforms. The distance between each samples is 32 samples.

Table 4.25: Values of current at time t, $t - \Delta t$ and $t - 2\Delta t$, voltage at time $t - \Delta t$ and $t - 2\Delta t$ for the second sampling scenario for a single motor load.

selected sample	$i(t)$	$i(t-\Delta t)$	$i(t-2\Delta t)$	$v(t-\Delta t)$	$v(t-2\Delta t)$
25th sample	13.1152	7.969328	-1.69501	-11.6227	-9.39485
57th sample	4.449092	14.92126	15.70543	0.976791	-10.7907
89th sample	-15.2177	-5.10202	8.327259	15.47781	9.301219
121th sample	-9.39709	-16.5789	-12.9948	4.057742	13.81616
153th sample	12.16258	-0.2891	-12.5526	-14.1579	-4.80718

Table 4.26: Values of voltage at time t for the second sampling scenario in the case of a single motor load

selected sample	$v(t)$
25th sample	6.132031
57th sample	-12.11
89th sample	-11.6041
121th sample	8.335509
153th sample	14.31545

Discrete time series coefficients are calculated and resulted as:
$[a_0, a_1, a_2, b_0, b_1] = [2.2980 - 3.83391.54040.0112 - 0.9887]$

Simulation Three: Third Sampling Scenario For the Second Order Status

In this sampling scheme, the first sampling point is the 15th point of voltage and current waveforms. The distance between each samples is 40 samples.

Table 4.27: Values of current at time t, $t - \Delta t$ and $t - 2\Delta t$, voltage at time $t - \Delta t$ and $t - -2\Delta t$ for the third sampling scenario for a single motor load.

selected sample	$i(t)$	$i(t - \Delta t)$	$i(t - 2\Delta t)$	$v(t - \Delta t)$	$v(t - 2\Delta t)$
15th sample	-3.3824	-6.74192	-5.57201	1.429158	5.375798
55th sample	15.70543	6.29245	-7.2055	-15.5514	-10.2141
95th sample	2.804772	14.07973	16.21294	2.530041	-9.61164
135th sample	-16.7539	-11.5663	1.132217	14.60327	13.81616
175th sample	3.476008	-9.74306	-16.6352	-8.0028	4.433859

Table 4.28: Values of voltage at time t for the third sampling scenario in the case of a single motor load

selected sample	$v(t)$
15th sample	4.192964
55th sample	10.79071
95th sample	-13.0289
135th sample	-5.90798
175th sample	15.24297

Discrete time series coefficients are calculated and resulted as:
$[a_0, a_1, a_2, b_0, b_1] = [2.2981 - 3.83411.54050.0112 - 0.9888]$
Motor circuit full fills 2nd order principals because all three matrices
$\begin{bmatrix} A = 2.2981 & -3.8341 & 1.5405 & 0.0112 & -0.9888 \end{bmatrix}$
$\begin{bmatrix} B = 2.2980 & -3.8339 & 1.5404 & 0.0112 & -0.9887 \end{bmatrix}$
$\begin{bmatrix} C = 2.2980 & -3.8339 & 1.5404 & 0.0112 & -0.9887 \end{bmatrix}$ are equivalent as shown in figure 4.12. Additionally, since it is determined that motor circuit is satisfying the second order characteristics, we analyse the case with the third order criteria. It resulted in different impedance coefficients. This interprets that third order and higher orders cannot be the correct order for the single motor load.

Figure 4.11: First order impedance coefficients for three different scenarios of a single motor load.

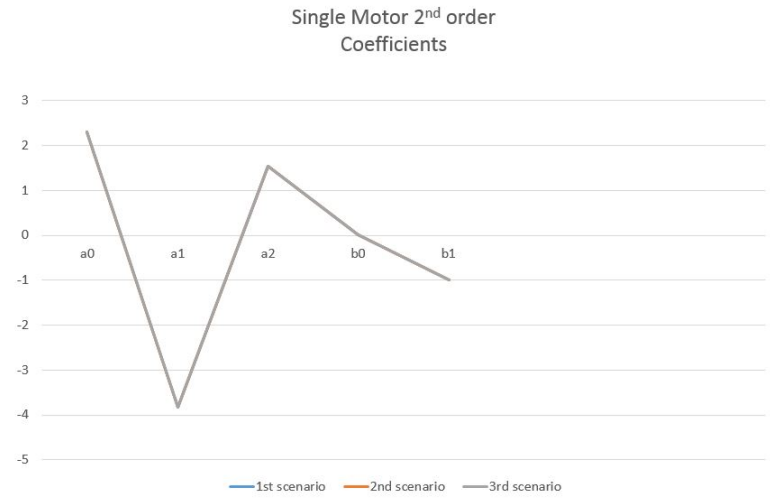

Figure 4.12: Second order impedance coefficients for three different scenarios of a single motor load.

4.2.5 Simulation Three: Single Motor Load Parameters Calculations

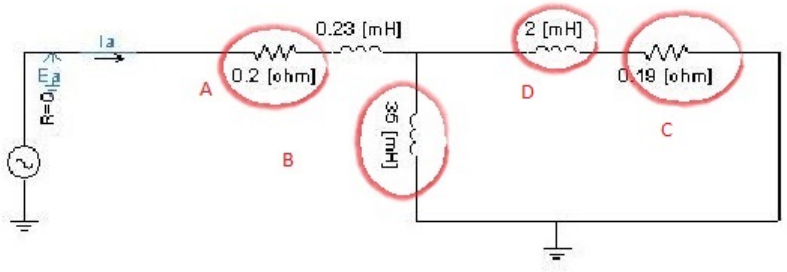

Figure 4.13: Single motor load.

Y(s)is the results from converting the discrete time coefficients to the continuous domain.

$$y(s) = \frac{I(s)}{V(s)} = \frac{0.002122s^2 + 0.3809s + 1.028}{s + 5.12}$$

$\rightarrow$

$$5.12 + s \overline{)1.028 + 0.3809 + 0.00212s^2} \quad 0.2007 \rightarrow \text{A=R}$$

$$0.18s + 0.00212s^2 \overline{)5.12 + s} \quad \frac{28.44}{s} \rightarrow \text{B=1/Lms}$$

$$0.9396s \overline{)0.18s + 0.002122s^2} \quad 0.19157 \rightarrow \text{C=R2}$$

$$0.00212s^2 \overline{)0.9396s} \quad \frac{442.78}{s} \rightarrow \text{D=1/L2s}$$

Figure 4.14: Motor load parameter calculation.

As shown in Figure 4.14, in every step of the division, the quotients are R and L values of the load circuit. The first quotient is Z_s which is a series arm and is equivalent to R_1. Second quotient is Y_s which indicates shunt arm and is equivalent to L_m. Third quotient shows R_2 and the last quotient is the value of L_2. L_1 value is not synthesized.

We captured four parameters of a single motor load. Note that we have to continue the division as yet we get zero in the remainder.

4.2.6 Simulation Four: Paralleled Resistive and a Motor

This simulation, evaluates the behaviour of an aggregated load including a single motor load in parallel with a resistive load. We will consider all combinations of heating (resistive), lighting (inductive) and motor loads , because these are the three major eigneloads we considered in this work. We will prove that we can distinguish between these three types In this simulation case, sampling rate is $\Delta t = 2200\mu s$(sampling frequency =1600

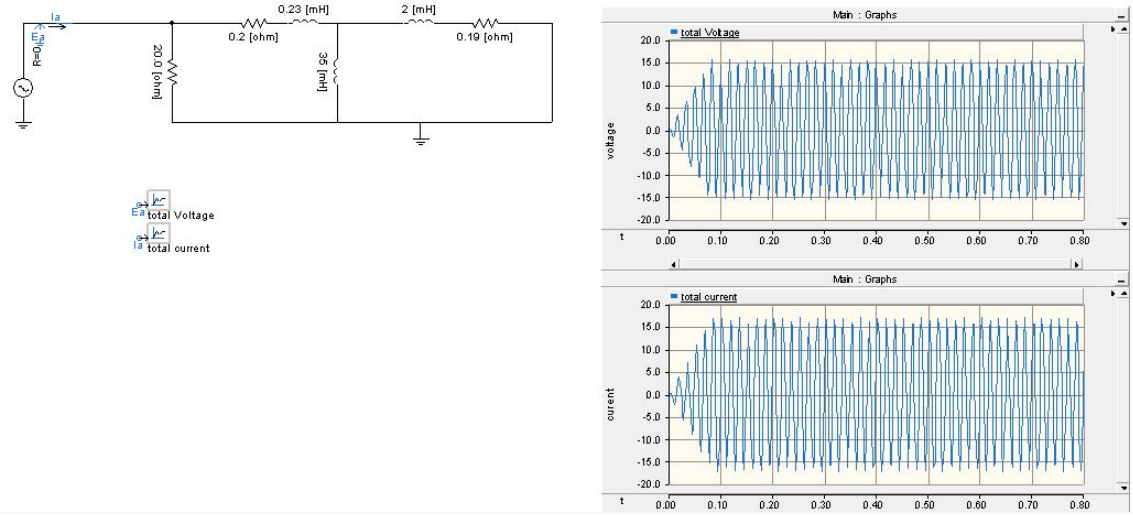

Figure 4.15: Paralleled resistive and a motor.

Hz), maximum simulation time is $t_{max} = 0.8s(totalsamples : 367)$ and ramp up time=0.08. Theoretically, this circuit is also supposed to be 2nd order. Because, resistance does not generate any history terms. Motor load is also confirmed to be a second order system in Section **??**. It may seem that this algorithm is not able to discern between a case of the single motor load and a case of the paralleled motor and resistance since both systems are second order. But in fact, due to different obtained discrete coefficients, network synthesis will result in two different topologies which determines whether there is a single motor or a paralleled motor and resistance.

Simulation Four: First Sampling Scenario

In this sampling scheme, the first sampling point is the 25th point of voltage and current waveforms. The distance between each samples is 20 samples.

Table 4.29: Values of current at time t and $t - \Delta t$, voltage at time $t - \Delta t$ for the first sampling scenario in the case of a paralleled resistance and a motor.

selected sample	$i(t)$	$i(t - \Delta t)$	$v(t - \Delta t)$
25th sample	11.07299	7.054133	-9.58875
45th sample	-11.6826	-17.0501	6.975206
65th sample	-2.13397	11.05827	6.267753

Table 4.30: Values of voltage at time t for the first sampling scenario in the case of a paralleled resistance and a motor.

selected sample	$v(t)$
25th sample	5.058925
45th sample	5.544468
65th sample	-14.7334

Discrete time series coefficients are calculated and resulted as:
$[a_0, a_1, b_0] = [2.0939 \; -1.4113 \;\; 0.8522]$

Simulation Four: Second Sampling Scenario

In this sampling scheme, the first sampling point is the 25th point of voltage and current waveforms. The distance between each samples is 32 samples.

Table 4.31: Values of current at time t and $t - \Delta t$, voltage at time $t - \Delta t$ for the second sampling scenario in the case of a paralleled resistance and a motor.

selected sample	$i(t)$	$i(t - \Delta t)$	$v(t - \Delta t)$
25th sample	11.07299	7.054133	-9.58875
57th sample	3.838176	14.86706	0.976791
89th sample	-15.8025	-5.88056	15.47781

Table 4.32: Values of voltage at time t for the second sampling scenario in the case of a paralleled resistance and a motor.

selected sample	$v(t)$
25th sample	5.058925
57th sample	-12.11
89th sample	-11.6041

Discrete time series coefficients are calculated and resulted as:
$[a_0, a_1, b_0] = [2.0772 \quad -1.4058 \quad 0.8369]$

Simulation Four: Third Sampling Scenario

In this sampling scheme, the first sampling point is the 30th point of voltage and current waveforms. The distance between each samples is 40 samples.

Table 4.33: Values of current at time t and $t - \Delta t$, voltage at time $t - \Delta t$ for the third sampling scenario in the case of a paralleled resistance and a motor.

selected sample	$i(t)$	$i(t - \Delta t)$	$v(t - \Delta t)$
30th sample	-7.47218	-12.8154	3.986642
70th sample	15.44856	5.059682	-15.3798
110th sample	4.256216	15.0745	0.586322

Table 4.34: Values of voltage at time t for the third sampling scenario in the case of a paralleled resistance and a motor.

selected sample	$v(t)$
30th sample	5.839642
70th sample	12.11003
110th sample	-11.8608

Discrete time series coefficients are calculated and resulted as:
$[a_0, a_1, b_0] = [2.1281 \quad -1.4220 \quad 0.8824]$

Considering three calculated coefficient matrices:

$$\begin{bmatrix} A = 2.0667 & -1.4027 & 0.8271 \end{bmatrix}$$

$$\begin{bmatrix} B = 2.0717 & -1.4043 & 0.8317 \end{bmatrix}$$

$$\begin{bmatrix} C = 2.1110 & -1.4168 & 0.8672 \end{bmatrix}$$

They are all equivalent. We will continue with order=2.

Simulation Four: First Sampling Scenario For The Second Order Condition

In this sampling scheme, the first sampling point is the 25th point of voltage and current waveforms. The distance between each samples is 40 samples.

Table 4.35: Values of current at time t, $t - \Delta t$ and $t - 2\Delta t$, voltage at time $t - \Delta t$ and $t - 2\Delta t$for the first sampling scenario in the case of a parallel resistance and a motor resistance

selected sample	$i(t)$	$i(t - \Delta t)$	$i(t - 2\Delta t)$	$v(t - \Delta t)$	$v(t - 2\Delta t)$
25th sample	11.07299	7.054133	-1.01084	-9.58875	-7.75075
65th sample	-2.13397	11.05827	17.06735	6.267753	-6.26775
105th sample	-16.2537	-14.8632	-3.82351	12.81116	15.16008
145th sample	8.217491	-5.49593	-15.6423	-11.0689	0.586322
185th sample	13.16801	16.91667	9.679471	-8.66295	-15.3798

Table 4.36: Values of voltage at time t for the first sampling scenario in the case of a paralleled resistance and a motor

selected sample	$v(t)$
25th sample	5.058925
65th sample	-14.7334
105th sample	-2.14351
145th sample	15.5367
185th sample	-3.67906

Discrete time series coefficients are calculated and resulted as:

$[a_0, a_1, a_2, b_0, b_1] = [2.0612 - 3.4389 \;\; 1.3817 - 0.1619 - 0.8178]$

Simulation Four: Second Sampling Scenario For The Second Order Condition

In this sampling scheme, the first sampling point is the 15th point of voltage and current waveforms. The distance between each samples is 50 samples.

Table 4.37: Values of current at time t, $t-\Delta t$ and $t-2\Delta t$, voltage at time $t-\Delta t$ and $t-2\Delta t$for the second sampling scenario in the case of a parallel resistance and a motor resistance.

selected sample	$i(t)$	$i(t-\Delta t)$	$i(t-2\Delta t)$	$v(t-\Delta t)$	$v(t-2\Delta t)$
15th sample	-2.61752	-5.62104	-4.81866	1.179055	4.435033
65th sample	-2.13397	**11.05827**	17.06735	6.267753	-6.26775
115th sample	11.68301	-1.30108	-13.4423	-13.4395	-3.29806
165th sample	-16.7807	-8.9643	4.671463	15.47781	11.60412
215th sample	15.46045	15.79731	5.875347	-11.6041	-15.4778

Table 4.38: Values of voltage at time t for the second sampling scenario in the case of a paralleled resistance and a motor.

selected sample	$v(t)$
15th sample	3.459195
65th sample	-14.7334
115th sample	14.85421
165th sample	-9.30122
215th sample	0.195482

Impedance coefficients are calculated and resulted as:
$[a_0, a_1, a_2, b_0, b_1] = [2.0612 - 3.4389 \;\; 1.3817 - 0.1618 - 0.8178]$

Simulation Four: Third Sampling Scenario For The Second Order Condition

In this sampling scheme, the first sampling point is the 20th point of voltage and current waveforms. The distance between each samples is 50 samples.

Table 4.39: Values of current at time t, $t-\Delta t$ and $t-2\Delta t$, voltage at time $t-\Delta t$ and $t-2\Delta t$for the third sampling scenario in the case of a parallel resistance and a motor resistance.

selected sample	$i(t)$	$i(t-\Delta t)$	$i(t-2\Delta t)$	$v(t-\Delta t)$	$v(t-2\Delta t)$
20th sample	-4.67116	2.140791	6.900771	5.479104	-0.27411
70th sample	15.44856	5.059682	-8.6172	-15.3798	-8.66295
120th sample	-16.7856	-13.6895	-1.70625	13.81616	14.60327
170th sample	11.70028	17.07949	11.367	-6.97521	-14.9656
220th sample	-2.15386	-13.9538	-16.6941	-2.53004	9.61164

Table 4.40: Values of voltage at time t for the third sampling scenario in the case of a paralleled resistance and a motor.

selected sample	$v(t)$
20th sample	-8.11793
70th sample	12.11003
120th sample	-4.05774
170th sample	-5.54447
220th sample	13.02888

Discrete time series coefficients are calculated and resulted as:
$[a_0, a_1, a_2, b_0, b_1] = [2.0604 - 3.4383 \;\; 1.3819 - 0.1629 - 0.8171]$ Motor in parallel with Resistance also full fills second order principals, because all three obtained matrices:

$$\begin{bmatrix} A = 2.0615 & -3.4394 & 1.3820 & -0.1618 & -0.8180 \end{bmatrix}$$
$$\begin{bmatrix} B = 2.0613 & -3.4396 & 1.3823 & -0.1622 & -0.8179 \end{bmatrix}$$
$$\begin{bmatrix} C = 2.0652 & -3.4422 & 1.3811 & -0.1566 & -0.8214 \end{bmatrix}$$

are equivalent. This is shown in Figures 4.16 and 4.17.

Figure 4.16: First order impedance coefficients for three scenarios of a paralleled motor and resistance

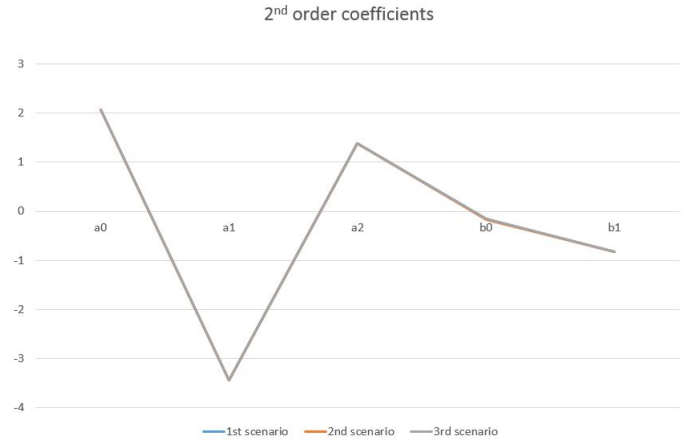

Figure 4.17: Second order impedance coefficients for three scenarios of a paralleled motor and resistance

4.2.7 Simulation One: Paralleled Motor and Resistance Load Parameters Calculations

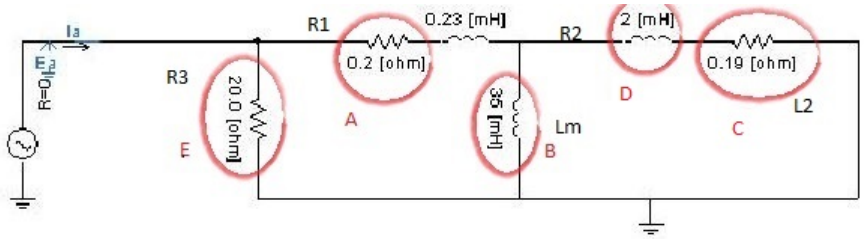

Figure 4.18: Paralleled motor and resistance.

This case determines a motor type in parallel with resistance. As described in Section 4.2.6, this load is a second order load.

$$y(s) = \frac{20.02s^2 + 3594s + 9856}{s^2 + 9614s + 4.856e4}$$

$\rightarrow$

0.202 → A=R1

$4.856e4 + 9614s + s^2 \overline{)\, 9856 + 3594s + 20.02s^2}$

$29.56/s$ → B=1/Lms

$164.69s + 19.81s^2 \overline{)\, 4.856e4 + 9614s + s^2}$

0.181 → C=R2

$9028s + s^2 \overline{)\, 1642.69s + 19.81s^2}$

$459/s$ → D=1/L2s

$19.628s^2 \overline{)\, 9028s + s^2}$

19.628 → E=R3

$s^2 \overline{)\, 19.628s^2}$

Figure 4.19: Motor load in parallel with a resistive load parameter calculation.

Note that, PSCAD discrete time coefficients are different for a **Motor** load and a **Motor+Resistance** load cases, although, the circuit order and the number of coefficients are the same.

Following case products five steps of division prior to getting a remainder of zero whereas in Section 4.2.5, we get zero in remainder after continuing the long division for four consecutive stages. The first four quotients, determine motor's parameters, $R_1, L_m, R_2 \& L_2$ and the fifth quotient is the value of parallel resistance.

4.2.8 Simulation Five: Single Motor in Parallel with One Resistance and One Inductance

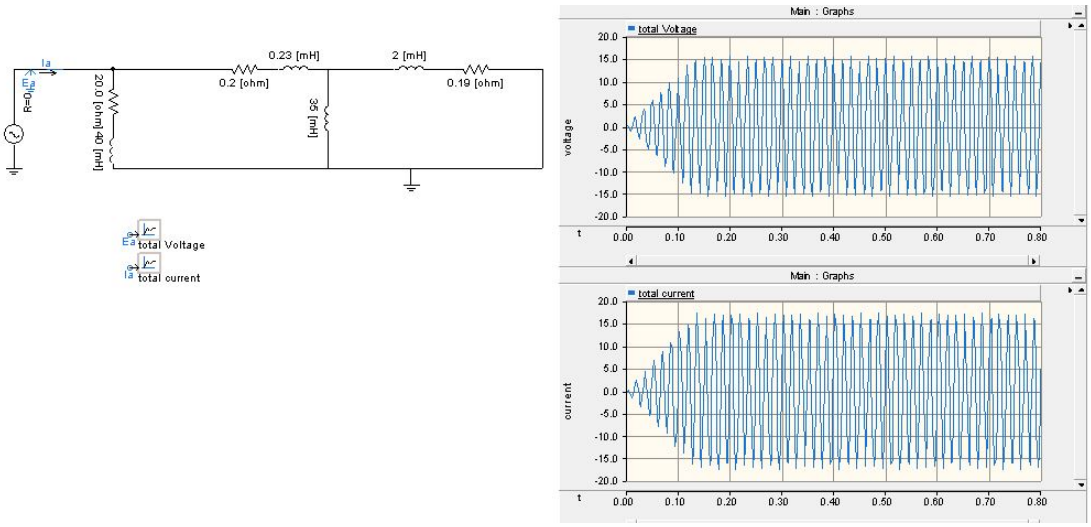

Figure 4.20: Single motor in parallel with one resistance and one inductance load.

In this simulation case, sampling rate is $\Delta t = 2200\mu s$(sampling frequency =1600 Hz), maximum simulation time is $t_{max} = 0.8s$ and ramp up time=0.132s. This case describes an aggregated load combining of motor, inductance and resistance. As discussed in Chapter 3, induction motor load is a 2nd order system. Inductance is a first order system. Therefore, a parallel circuit including both will have the characteristics of a third order system. We calculated impedance discrete time coefficients for first and second order situation. Resulted discrete time coefficients were within 10% equivalence. Thus, we need to move on to the third order analysis. In Following you will see the results earned from order=3 analysis.

Simulation Five: First Sampling Scenario For The Third Order Status

In this sampling scheme, the first sampling point is the 35th point of voltage and current waveforms. The distance between each samples is 10 samples.

Table 4.41: Values of current at time t, $t-\Delta t$, $t-2\Delta t$ and $t-3\Delta t$, voltage at time $t-\Delta t$, $t-2\Delta t$ and $t-3\Delta t$ for the first sampling scenario in the case of a motor load in parallel with an inductance and a resistance.

selected sample	$i(t)$	$i(t-\Delta t)$	$i(t-2\Delta t)$	$i(t-3\Delta t)$	$v(t-\Delta t)$	$v(t-2\Delta t)$	$v(t-3\Delta t)$
35th sample	-3.6274	4.025515	8.683997	7.590059	5.286402	-1.34935	-6.73159
45th sample	-8.59834	-12.2633	-7.98461	1.151465	4.998898	10.47595	9.046218
55th sample	14.64574	6.203539	-5.87806	-13.7587	-13.7371	-8.8522	1.492288
65th sample	-1.65254	11.63228	17.44466	12.04937	6.267753	-6.26775	-14.7334
75th sample	-14.8389	-16.5727	-7.54313	6.387411	10.21408	15.55144	10.79071
85th sample	14.35952	2.584053	-10.8687	-17.2634	-14.9656	-6.97521	5.544468
70th sample	2.614842	14.37684	16.80403	8.320351	2.530041	-9.61164	-15.5122

Table 4.42: Values of voltage at time t for the first sampling scenario in the case of a motor load in parallel with an inductance and a resistance.

selected sample	$v(t)$
35th sample	-8.79022
45th sample	4.065943
55th sample	9.711642
65th sample	-14.7334
75th sample	1.755633
85th sample	13.23837
70th sample	-13.0289

Discrete time series coefficients are calculated and resulted as:

$$\text{A}=\begin{bmatrix}2.2080 & -4.3249 & 2.5497 & -0.4297 & -0.2943 & -0.9923 & 0.3021\end{bmatrix}$$

Simulation Five: Second Sampling Scenario For The Third Order Status

In this sampling scheme, the first sampling point is the 20th point of voltage and current waveforms. The distance between each samples is 15 samples.

Table 4.43: Values of current at time t, $t-\Delta t$, $t-2\Delta t$ and $t-3\Delta t$, voltage at time $t-\Delta t$, $t-2\Delta t$ and $t-3\Delta t$ for the second sampling scenario in the case of a motor load in parallel with an inductance and a resistance.

selected sample	$i(t)$	$i(t-\Delta t)$	$i(t-2\Delta t)$	$i(t-3\Delta t)$	$v(t-\Delta t)$	$v(t-2\Delta t)$	$v(t-3\Delta t)$
20th sample	-2.73869	1.437729	4.278048	4.175772	3.320669	-0.16612	-3.16289
35th sample	-3.6274	4.025515	8.683997	7.590059	5.286402	-1.34935	-6.73159
50th sample	-3.44124	7.511785	13.2344	10.30246	6.402241	-3.47319	-10.7268
65th sample	-1.65254	11.63228	17.44466	12.04937	6.267753	-6.26775	-14.7334
80th sample	0.451432	13.05818	17.18663	10.15616	4.433859	-8.0028	-15.243
95th sample	2.614842	14.37684	16.80403	8.320351	2.530041	-9.61164	-15.5122
110th sample	4.737216	15.46906	16.15683	6.353933	0.586322	-11.0689	-15.5367

Table 4.44: Values of voltage at time t for the first sampling scenario in the case of a motor load in parallel with an inductance and a resistance.

selected sample	$v(t)$
20th sample	-4.91996
35th sample	-8.79022
50th sample	-12.4484
65th sample	-14.7334
80th sample	-13.9915
95th sample	-13.0289
110th sample	-11.8608

Discrete time series coefficients are calculated and resulted as:

B=$\begin{bmatrix} 2.2080 & -4.3250 & 2.5498 & -0.4298 & -0.2944 & -0.9923 & 0.3021 \end{bmatrix}$

Matrices A and B equal. Thus, third order properties match with this load's properties. **Worth mentioning, for higher order systems, to be able to detect the correct load's components, more samples from the slow transient section of the voltage and the current**

signals need to be selected.

Order=4 is also verified not to be the correct order for this load circuit, since it results in non-equal impedance coefficients, for the two different sampling scenarios as following:

Simulation Five: First Sampling Scenario For The Fourth Order Status

In this sampling scheme, the first sampling point is the 30th point of voltage and current waveforms. The distance between each samples is 10 samples. Impedance coefficients are:

$$A=\begin{bmatrix}1.4781 & -1.8820 & -0.2716 & 0.8721 & -0.1931 & -0.6313 & 0.4679 & -1.1464 & 0.4666\end{bmatrix}$$

Simulation Five: Second Sampling Scenario For The Fourth Order Status

In this sampling scheme, the first sampling point is the 20th point of voltage and current waveforms. The distance between each samples is 15 samples.

$$B=\begin{bmatrix}0.8023 & -3.2489 & 4.2122 & -2.0933 & 0.3266 & -2.5863 & 2.2977 & -0.8562 & 0.4071\end{bmatrix}$$

Figure 4.21: Third order impedance coefficients for three different scenarios of a motor load in parallel with an inductance and a resistance.

Figure 4.22: Fourth order impedance coefficients for three different scenarios of a motor load in parallel with an inductance and a resistance.

4.2.9 Simulation Five: Single Motor in Parallel with One Resistance and One Inductance Parameters Calculations

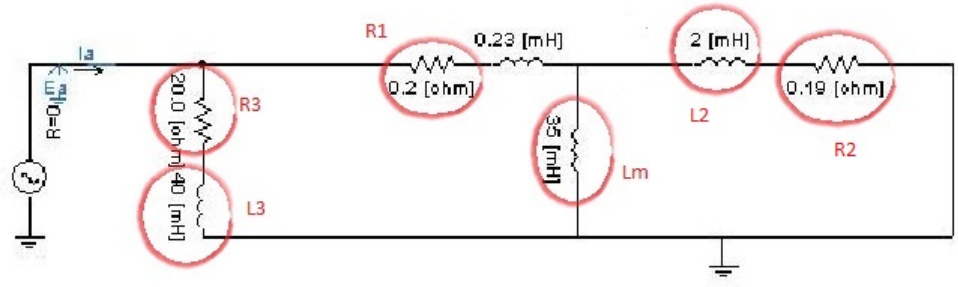

Figure 4.23: Single motor in parallel with one resistance and one inductance

This case determines an induction motor type in parallel with an inductance. Following Y_s is derived from the third order discrete time coefficients which have been analysed in Section 4.2.8. Figure 4.24 indicates six stages of continued division, prior to getting a remainder of zero.

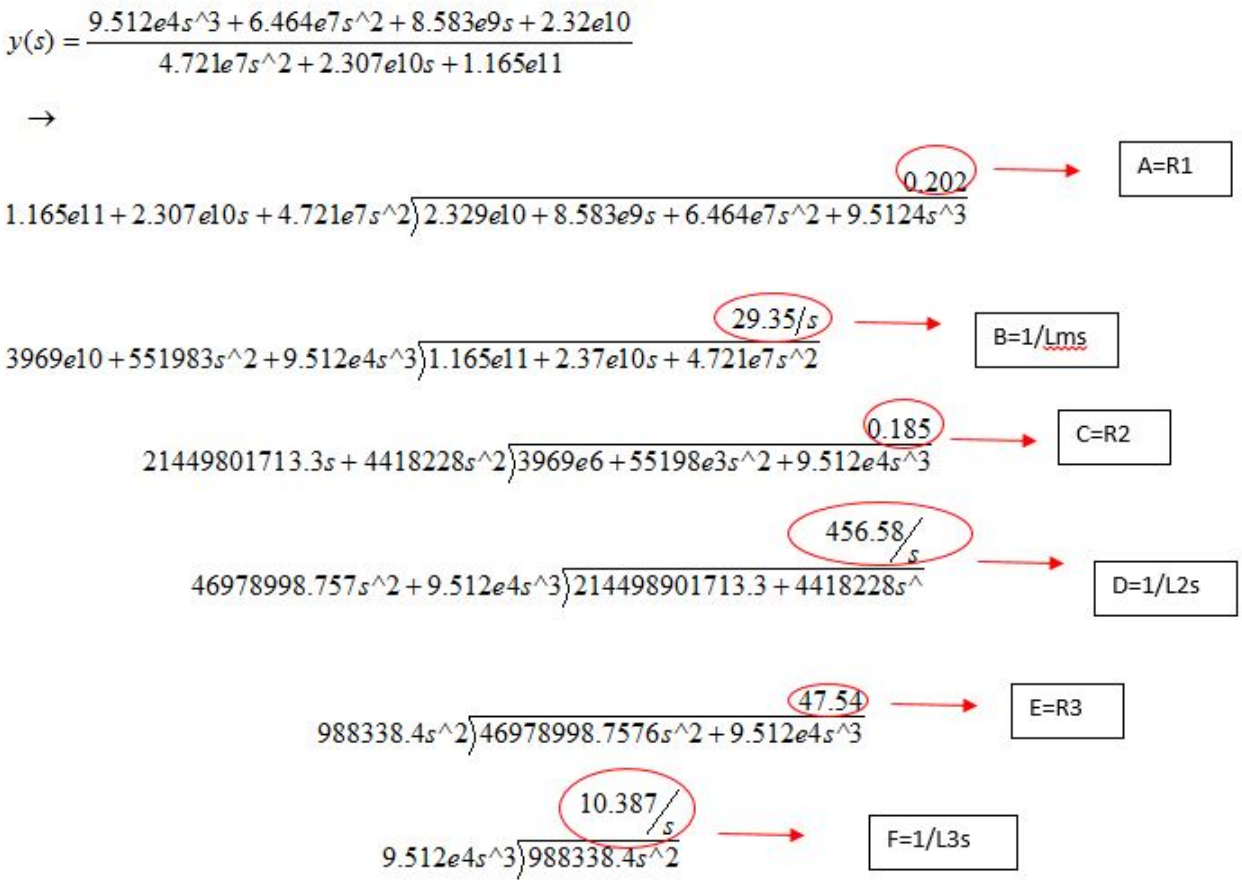

Figure 4.24: Motor in parallel with an inductive and a resistive load parameter calculation.

The first four quotients correspond to the motor's parameters, $R_1, L_m, R_2 \& L_2$ and 5th and 6th quotients, are the values of individual **resistance** and **inductance**.

4.2.10 Simulation Six: Two Series Motor in Parallel with a Resistive and an Inductive Load

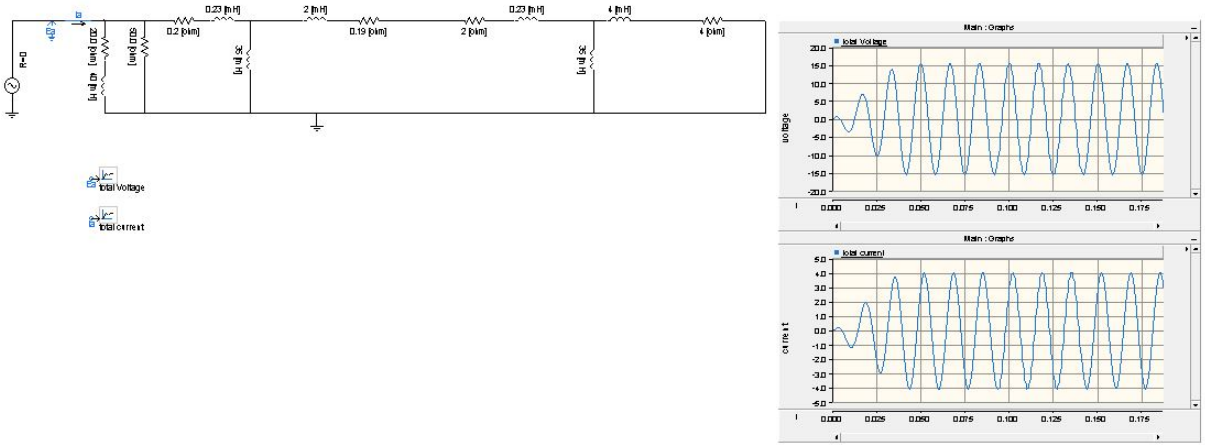

Figure 4.25: Two series motor in parallel with a resistive and an inductive load.

In this simulation case, sampling rate is $\Delta t = 625\mu s$(sampling frequency =1600 Hz), maximum simulation time is $t_{max} = 0.1875s$, ramp up time=0.0375s (slow transient ends at sample number 60). This simulation describes two series motor loads in parallel with a resistance and an inductance. Although, in real power system, loads are connected in parallel from a distribution feeder. But we analysed a higher order case in this section. Sometimes, some power electronic loads have more complex circuit structures which leads to the higher orders. We proved that our algorithm is capable of detecting the higher order loads as well.

Simulation Six: First Sampling Scenario For The Third Order Status

In this sampling scheme, the first sampling point is the 20th point of voltage and current waveforms. The distance between each samples is 10 samples.

Table 4.45: Values of current at time t, $t-\Delta t$, $t-2\Delta t$ and $t-3\Delta t$, voltage at time $t-\Delta t$, $t-2\Delta t$ and $t-3\Delta t$ for the first sampling scenario in the case of two series motor in parallel with a resistive and an inductive Load.

selected sample	$i(t)$	$i(t-\Delta t)$	$i(t-2\Delta t)$	$i(t-3\Delta t)$	$v(t-\Delta t)$	$v(t-2\Delta t)$	$v(t-3\Delta t)$
20th sample	-1.08422	-1.18047	-1.20521	-1.1643	2.11873	2.862528	3.356094
30th sample	1.847889	1.670556	1.409224	1.084638	-6.90432	-6.97878	-6.65809
40th sample	-1.63121	-1.07295	-0.48892	0.086761	8.778512	7.294637	5.486276
50th sample	-0.58222	-1.30023	-1.92157	-2.41571	-3.84574	-0.95609	1.865721
60th sample	3.152638	3.541393	3.719616	3.684601	-6.82702	-9.59789	-11.7463
70th sample	-4.04172	-3.75978	-3.27442	-2.6127	14.79497	15.50839	15.36482
80th sample	2.216767	1.375249	0.45409	-0.49584	-13.8608	-11.8291	-9.14379

Table 4.46: Values of voltage at time t for the first sampling scenario in the case of two series motor in parallel with a resistive and an inductive Load.

selected sample	$v(t)$
20th sample	-1.14999
30th sample	6.410918
40th sample	-9.83224
50th sample	6.638006
60th sample	3.571032
70th sample	-13.264
80th sample	15.12653

Discrete time series coefficients are calculated and resulted as:

$$\text{A}=\begin{bmatrix}10.7906 & -28.2620 & 24.2639 & -6.7923 & -1.7882 & 0.6953 & 0.0954\end{bmatrix}$$

Simulation Six: Second Sampling Scenario For The Third Order Status

In this sampling scheme, the first sampling point is the 10th point of voltage and current waveforms. The distance between each samples is 15 samples.

Table 4.47: Values of current at time t, $t-\Delta t$, $t-2\Delta t$ and $t-3\Delta t$, voltage at time $t-\Delta t$, $t-2\Delta t$ and $t-3\Delta t$ for the second sampling scenario in the case of two series motor in parallel with a resistive and an inductive Load.

selected sample	$i(t)$	$i(t-\Delta t)$	$i(t-2\Delta t)$	$i(t-3\Delta t)$	$v(t-\Delta t)$	$v(t-2\Delta t)$	$v(t-3\Delta t)$
10th sample	-0.07954	0.03305	0.109863	0.15053	0.640957	0.142396	-0.24335
25th sample	0.339286	-0.03408	-0.37887	-0.67713	-3.87283	-2.58956	-1.27105
40th sample	-1.63121	-1.07295	-0.48892	0.086761	8.778512	7.294637	5.486276
55th sample	3.023137	2.447016	1.754769	0.989035	-13.6991	-12.8223	-11.2744
70th sample	-4.04172	-3.75978	-3.27442	-2.6127	14.79497	15.50839	15.36482
85th sample	3.889271	3.97408	3.835769	3.481958	-11.8291	-13.8608	-15.1265
100th sample	-3.39011	-3.83106	-4.0635	-4.07461	7.062435	10.10304	12.58535

Table 4.48: Values of voltage at time t for the second sampling scenario in the case of two series motor in parallel with a resistive and an inductive Load.

selected sample	$v(t)$
10th sample	-1.21923
25th sample	5.03414
40th sample	-9.83224
55th sample	13.82834
70th sample	-13.264
85th sample	9.143793
100th sample	-3.63156

Discrete time series coefficients are calculated and resulted as:

B=$\begin{bmatrix} 10.7411 & -27.0579 & 22.4343 & -6.1140 & -1.7042 & 0.6530 & 0.0644 \end{bmatrix}$

It is important to note that, since this circuit is a higher order circuit, more transient samples are selected in compare with the lower order loads. In this specific example, four sampling points are selected from point 1 to 60, which are considered as the transient data. We will analyse 4th order coefficients since third order coefficients satisfy our assumptions.

Simulation Six: First Sampling Scenario For The Fourth Order Status

n this sampling scheme, the first sampling point is the 20th point of voltage and current waveforms. The distance between each samples is 10 samples.

Table 4.49: Values of current at time t, $t-\Delta t$, $t-2\Delta t$, $t-3\Delta t$ and $t-4\Delta t$, voltage at time $t-\Delta t$, $t-2\Delta t$, $t-3\Delta t$ and $t-4\Delta t$ for the first sampling scenario in the case of two series motor in parallel with a resistive and an inductive Load.

selected sample	$i(t)$	$i(t-\Delta t)$	$i(t-2\Delta t)$	$i(t-3\Delta t)$	$i(t-4\Delta t)$	$v(t-\Delta t)$	$v(t-2\Delta t)$	$v(t-3\Delta t)$	$v(t-4\Delta t)$
20th sample	-1.08422	-1.18047	-1.20521	-1.1643	-1.06742	2.11873	2.86E+00	3.356094	3.593048
30th sample	1.847889	1.670556	1.409224	1.084638	0.719978	-6.90432	-6.97878	-6.65809	-5.98841
40th sample	-1.63121	-1.07295	-0.48892	0.086761	0.622167	8.778512	7.294637	5.486276	3.472675
50th sample	-0.58222	-1.30023	-1.92157	-2.41571	-2.76055	-3.84574	-0.95609	1.865721	4.464868
60th sample	3.152638	3.541393	3.719616	3.684601	3.445646	-6.82702	-9.59789	-11.7463	-13.1745
70th sample	-4.04172	-3.75978	-3.27442	-2.6127	-1.81158	14.79497	15.50839	15.36482	14.37219
80th sample	2.216767	1.375249	0.45409	-0.49584	-1.42207	-13.8608	-11.8291	-9.14379	-5.95316
90th sample	0.68201	1.587901	2.402648	3.081205	3.586052	4.807176	1.220537	-2.43355	-5.95316
100th sample	-3.39011	-3.83106	-4.0635	-4.07461	-3.8638	7.062435	10.10304	12.58535	14.37219

Table 4.50: Values of voltage at time t for the first sampling scenario in the case of two series motor in parallel with a resistive and an inductive Load.

selected sample	$v(t)$
20th sample	-1.14999
30th sample	6.410918
40th sample	-9.83224
50th sample	6.638006
60th sample	3.571032
70th sample	-13.264
80th sample	15.12653
90th sample	-8.12817
100th sample	-3.63156

Discrete time series coefficients are calculated and resulted as:

$$\text{A}=\begin{bmatrix}5.4039 & -17.4479 & 20.7260 & -10.7033 & 2.0216 & -3.1295 & 3.7334 & -2.0526 & 0.4507\end{bmatrix}$$

Simulation Six: Second Sampling Scenario For The Fourth Order Status

In this sampling scheme, the first sampling point is the 30th point of voltage and current waveforms. The distance between each samples is 5 samples.

Table 4.51: Values of current at time t, $t-\Delta t$, $t-2\Delta t$, $t-3\Delta t$ and $t-4\Delta t$, voltage at time $t-\Delta t$, $t-2\Delta t$, $t-3\Delta t$ and $t-4\Delta t$ for the second sampling scenario in the case of two series motor in parallel with a resistive and an inductive Load.

selected sample	$i(t)$	$i(t-\Delta t)$	$i(t-2\Delta t)$	$i(t-3\Delta t)$	$i(t-4\Delta t)$	$v(t-\Delta t)$	$v(t-2\Delta t)$	$v(t-3\Delta t)$	$v(t-4\Delta t)$
30th sample	1.847889	1.670556	1.409224	1.084638	0.719978	-6.90432	-6.97878	-6.65809	-5.98841
35th sample	1.08932	1.46565	1.73506	1.888555	1.92441	-0.6713	-2.56383	-4.19955	-5.5
40th sample	-1.63121	-1.07295	-0.48892	0.086761	0.622167	8.778512	7.294637	5.486276	3.472675
45th sample	-2.94331	-2.96092	-2.8198	-2.53509	-2.1294	8.477551	9.702566	10.33646	10.3709
50th sample	-0.58222	-1.30023	-1.92157	-2.41571	-2.76055	-3.84574	-0.95609	1.865721	4.464868
55th sample	3.023137	2.447016	1.754769	0.989035	0.195007	-13.6991	-12.8223	-11.2744	-9.16667
60th sample	3.152638	3.541393	3.719616	3.684601	3.445646	-6.82702	-9.59789	-11.7463	-13.1745
65th sample	-0.91593	0.023743	0.953767	1.819716	2.568313	10.10304	7.062435	3.631558	-4.10E-13
70th sample	-4.04172	-3.75978	-3.27442	-2.6127	-1.81158	14.79497	15.50839	15.36482	14.37219

Table 4.52: Values of voltage at time t for the second sampling scenario in the case of two series motor in parallel with a resistive and an inductive Load.

selected sample	$v(t)$
30th sample	6.410918
35th sample	-1.37901
40th sample	-9.83224
45th sample	-6.70545
50th sample	6.638006
55th sample	13.82834
60th sample	3.571032
65th sample	-12.5854
70th sample	-13.264

Discrete time series coefficients are calculated and resulted as:

B=$\begin{bmatrix} 5.2638 & -16.9958 & 20.1887 & -10.4259 & 1.9692 & -3.1492 & 3.7865 & -2.1002 & 0.4650 \end{bmatrix}$

Resulted coefficients matrices as for order =4 are equivalent which confirms that this load

is a 4th order load.

Simulation Six: First Sampling Scenario For The Fifth Order Status

In this sampling scheme, the first sampling point is the 20th point of voltage and current waveforms. The distance between each samples is 5 samples. Discrete time series coefficients are calculated and resulted as:

$[a0, a1, a2, a3, a4, a5, b0, b1, b2, b3, b4] =$

$$\begin{bmatrix} 14.74 & -31.096 & 3.26 & 34.092 & -27.1717 & 6.173 & -0.5759 & -2.310 & 2.0379 & 0.2863 & -0.4369 \end{bmatrix}$$

Simulation Six: Second Sampling Scenario For the Fifth Order Status

In this sampling scheme, the first sampling point is the 10th point of voltage and current waveforms. The distance between each samples is 10 samples. Discrete time series coefficients are calculated and resulted as:

$[a0, a1, a2, a3, a4, a5, b0, b1, b2, b3, b4] =$

$$\begin{bmatrix} 8.89 & -26.292 & 26.25 & -8.26 & -1.502 & 0.912 & -2.582 & 2.537 & -1.470 & 0.710 & -0.192 \end{bmatrix}$$

Coefficients values for 5th order mismatch. Therefore, the largest order which results in equal coefficients is four.

4.2.11 Simulation Seven: Three Series Motor in Parallel with a Resistive and an Inductive Load

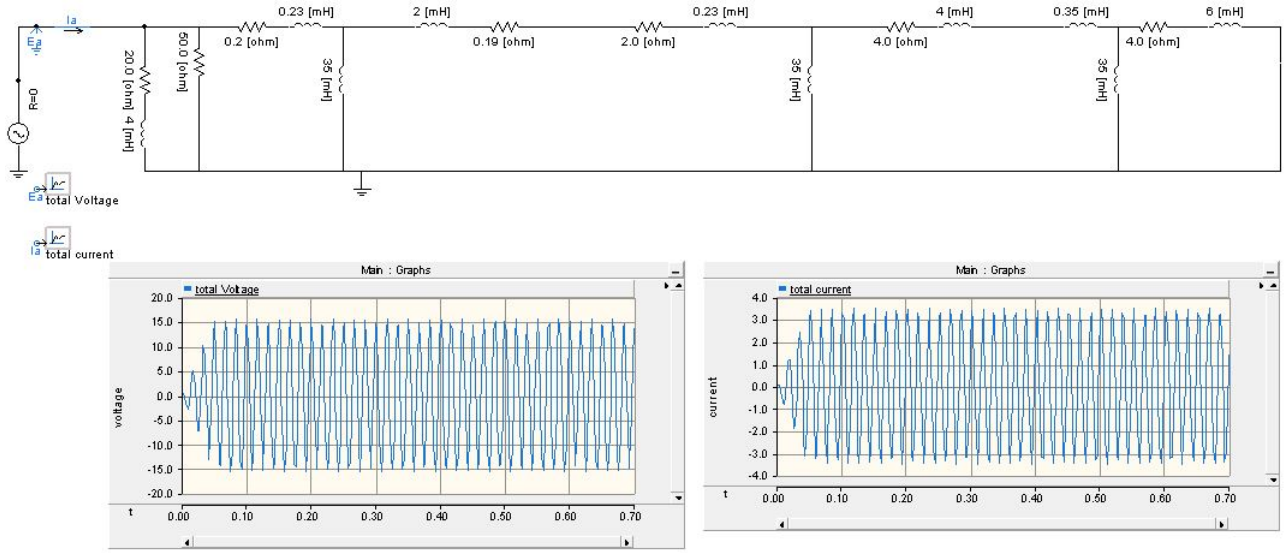

Figure 4.26: Three series motor in parallel with resistive and inductive load.

In this simulation case, sampling rate is $\Delta t = 2200\mu s$. $\{t_{max} = 0.7 seconds$ and $Ramp up time = 0.05$ (slow transient ends at sample number 22). This simulation describes two series motor loads in parallel with a resistance and an inductance.

Simulation Seven: First Sampling Scenario For the Fifth Order Status

In this sampling scheme, the first sampling point is the 10th point of voltage and current waveforms. The distance between each samples is 5 samples.

Table 4.53: Values of current at time t, $t-\Delta t$, $t-2\Delta t$, $t-3\Delta t$, $t-4\Delta t$ and $t-5\Delta t$, voltage at time $t-\Delta t$, $t-2\Delta t$, $t-3\Delta t$, $t-4\Delta t$ and $t-5\Delta t$ for the first sampling scenario in the case of three series motors in parallel with a resistive and an inductive load

selected sample	$i(t)$	$i(t-\Delta t)$	$i(t-2\Delta t)$	$i(t-3\Delta t)$	$i(t-4\Delta t)$	$i(t-5\Delta t)$	$v(t-\Delta t)$	$v(t-2\Delta t)$	$v(t-3\Delta t)$	$v(t-4\Delta t)$	$v(t-5\Delta t)$
10th sample	1.193384	1.112585	0.358973	-0.45581	-0.82461	-0.65301	-5.14035	-4.25538	-1.07124	1.833812	2.695656
15th sample	-0.31091	-1.69494	-1.88942	-0.94974	0.368754	1.193384	1.886488	7.096053	7.189436	2.914371	-2.33956
20th sample	-2.31235	-0.18528	1.803115	2.431806	1.463945	-0.31091	8.766567	-0.43857	-8.35002	-10.1862	-5.53471
25th sample	3.403337	3.010995	0.694947	-1.90806	-3.11962	-2.31235	-15.1601	-12.4012	-1.98061	8.726071	12.98868
30th sample	-0.95577	-3.11054	-3.2285	-1.22808	1.58982	3.403337	5.177457	14.31545	14.15793	4.807176	-7.66504
35th sample	-2.29308	0.39524	2.838765	3.451327	1.836957	-0.95577	9.61164	-2.53004	-13.0289	-15.0676	-7.32243
40th sample	3.46756	2.74645	0.250337	-2.3994	-3.48173	-2.29308	-15.4778	-11.6041	-0.19548	11.34009	15.51215
45th sample	-1.38373	-3.29701	-3.0628	-0.83291	1.945039	3.46756	6.975206	14.96564	13.23837	2.914969	-9.30122
50th sample	-1.95381	0.819001	3.065566	3.327291	1.434418	-1.38373	8.002801	-4.43386	-13.9915	-14.4639	-5.54447
55th sample	3.503459	2.446064	-0.19479	-2.70418	-3.45255	-1.95381	-15.5514	-10.2141	1.755633	12.58535	15.24297
60th sample	-1.77804	-3.41712	-2.83301	-0.40488	2.290679	3.503459	8.662952	15.37981	12.11003	0.976791	-10.7907

Table 4.54: Values of voltage at time t for the first sampling scenario in the case of a three series motors in parallel with a resistive and an inductive load

selected sample	$v(t)$
10th sample	2.339559
15th sample	5.534712
20th sample	-12.9887
25th sample	7.665039
30th sample	7.322435
35th sample	-15.5122
40th sample	9.301219
45th sample	5.544468
50th sample	-15.243
55th sample	10.79071
60th sample	3.679061

Discrete time series coefficients are calculated and resulted as:

$[a0, a1, a2, a3, a4, a5, b0, b1, b2, b3, b4] =$

A=$\begin{bmatrix} 2.261 & -4.796 & 1.66 & 2.1376 & -1.330 & 0.067 & -1.918 & 1.553 & -0.484 & 0.050 & 0.1637 \end{bmatrix}$

Simulation Seven: Second Sampling Scenario For The Fifth Order Status

In this sampling scheme, the first sampling point is the 15th point of voltage and current waveforms. The distance between each samples is 5 samples.

Table 4.55: Values of current at time t, $t-\Delta t$, $t-2\Delta t$, $t-3\Delta t$, $t-4\Delta t$ and $t-5\Delta t$, voltage at time $t-\Delta t$, $t-2\Delta t$, $t-3\Delta t$, $t-4\Delta t$ and $t-5\Delta t$ for the second sampling scenario in the case of three series motors in parallel with a resistive and an inductive load

selected sample	$i(t)$	$i(t-\Delta t)$	$i(t-2\Delta t)$	$i(t-3\Delta t)$	$i(t-4\Delta t)$	$i(t-5\Delta t)$	$v(t-\Delta t)$	$v(t-2\Delta t)$	$v(t-3\Delta t)$	$v(t-4\Delta t)$	$v(t-5\Delta t)$
15th sample	-0.31091	-1.69494	-1.88942	-0.94974	0.368754	1.193384	1.886488	7.096053	7.189436	2.914371	-2.33956
20th sample	-2.31235	-0.18528	1.803115	2.431806	1.463945	-0.31091	8.766567	-0.43857	-8.35002	-10.1862	-5.53471
25th sample	3.403337	3.010995	0.694947	-1.90806	-3.11962	-2.31235	-15.1601	-12.4012	-1.98061	8.726071	12.98868
30th sample	-0.95577	-3.11054	-3.2285	-1.22808	1.58982	3.403337	5.177457	14.31545	14.15793	4.807176	-7.66504
35th sample	-2.29308	0.39524	2.838765	3.451327	1.836957	-0.95577	9.61164	-2.53004	-13.0289	-15.0676	-7.32243
40th sample	3.46756	2.74645	0.250337	-2.3994	-3.48173	-2.29308	-15.4778	-11.6041	-0.19548	11.34009	15.51215
45th sample	-1.38373	-3.29701	-3.0628	-0.83291	1.945039	3.46756	6.975206	14.96564	13.23837	2.914969	-9.30122
50th sample	-1.95381	0.819001	3.065566	3.327291	1.434418	-1.38373	8.002801	-4.43386	-13.9915	-14.4639	-5.54447
55th sample	3.503459	2.446064	-0.19479	-2.70418	-3.45255	-1.95381	-15.5514	-10.2141	1.755633	12.58535	15.24297
60th sample	-1.77804	-3.41712	-2.83301	-0.40488	2.290679	3.503459	8.662952	15.37981	12.11003	0.976791	-10.7907
65th sample	-1.57773	1.236617	3.251941	3.159695	1.019851	-1.77804	6.267753	-6.26775	-14.7334	-13.6321	-3.67906

Table 4.56: Values of voltage at time t for the second sampling scenario in the case of a three series motors in parallel with a resistive and an inductive load.

selected sample	$v(t)$
15th sample	5.534712
20th sample	-12.9887
25th sample	7.665039
30th sample	7.322435
35th sample	-15.5122
40th sample	9.301219
45th sample	5.544468
50th sample	-15.243
55th sample	10.79071
60th sample	3.679061
65th sample	-14.7334

Discrete time series coefficients are calculated and resulted as:

$[a0, a1, a2, a3, a4, a5, b0, b1, b2, b3, b4] =$

B=$\begin{bmatrix} 2.2236 & -4.714 & 1.632 & 2.1014 & -1.3074 & 0.066 & -1.9253 & 1.576 & -0.4994 & 0.050 & 0.1667 \end{bmatrix}$

Two derived impedance coefficient matrices are equivalent for the 5th order analysis. Also, 6th order calculations yield to two different impedance matrices. Thus, this load is a 5th order system.

4.2.12 Simulation Eight: Two Parallel Motors Loads

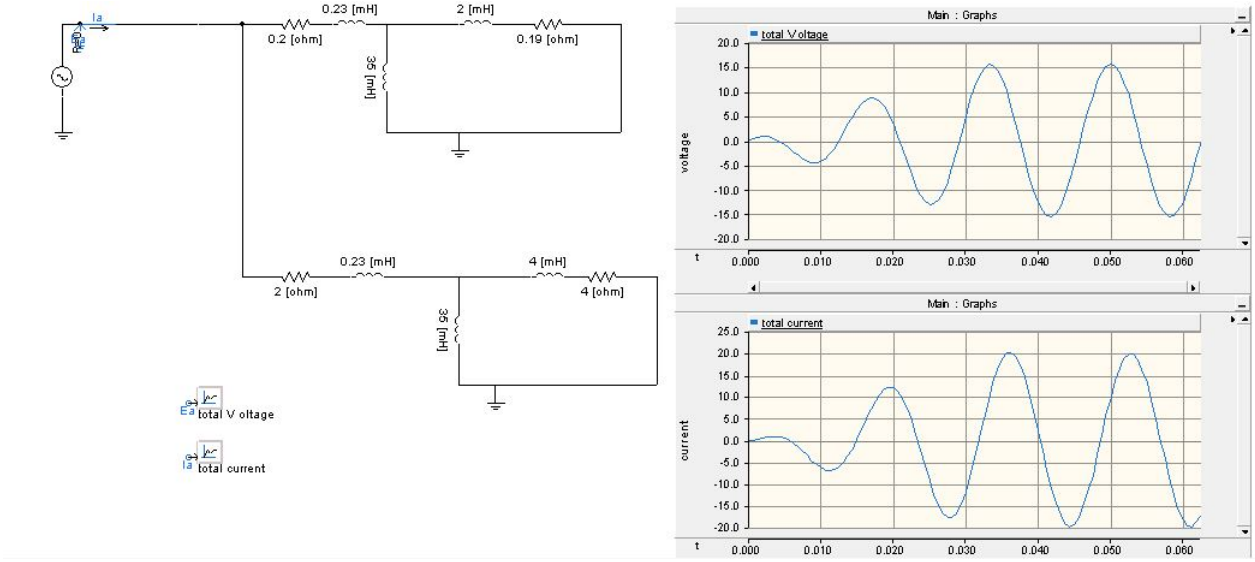

Figure 4.27: Two parallel motors loads.

This example illustrates an aggregated load constituting of two parallel motor loads. In this simulation case, sampling rate is $\Delta t = 625\mu s$(sampling frequency =1600 Hz), maximum simulation time is $t_{max} = 0.0625s$ and ramp up time=0.03(slow transient ends at sample number 48).

Simulation Eight: First Sampling Scenario For The Third Order Status

In this sampling scheme, the first sampling point is the 30th point of voltage and current waveforms. The distance between each samples is 4 samples.

Table 4.57: Values of current at time t, $t-\Delta t$, $t-2\Delta t$ and $t-3\Delta t$, voltage at time $t-\Delta t$, $t-2\Delta t$ and $t-3\Delta t$ for the first sampling scenario in the case of two parallel motors.

selected sample	$i(t)$	$i(t-\Delta t)$	$i(t-2\Delta t)$	$i(t-3\Delta t)$	$v(t-\Delta t)$	$v(t-2\Delta t)$	$v(t-3\Delta t)$
30th sample	10.61917	9.017144	7.040091	4.826744	-8.6304	-8.72347	-8.32261
34th sample	11.15864	12.0443	12.22007	11.72101	-3.20478	-5.24944	-6.875
38th sample	1.289478	4.522545	7.326548	9.56945	6.857844	4.340844	1.723764
42th sample	-12.313	-9.21498	-5.77706	-2.20721	12.96362	12.2903	10.97314
46th sample	-17.7378	-17.7059	-16.7179	-14.8728	8.38181	10.59694	12.12821
50th sample	-8.25894	-11.9136	-14.8025	-16.7668	-4.80718	-1.19511	2.332151
54th sample	9.265115	4.953669	0.424436	-4.06529	-14.795	-13.264	-11

Table 4.58: Values of voltage at time t for the first sampling scenario in the case of two parallel motors.

selected sample	$v(t)$
30th sample	8.013647
34th sample	0.839119
38th sample	-9.1183
42th sample	-12.9206
46th sample	-5.58108
50th sample	8.12817
54th sample	15.50839

Discrete time series coefficients are calculated and resulted as:

$$\text{A}=\begin{bmatrix}5.0677 & -11.4741 & 8.1121 & -1.7024 & -0.5052 & -0.9970 & 0.51539\end{bmatrix}$$

Simulation Eight: Second Sampling Scenario For The Third Order Status

In this sampling scheme, the first sampling point is the 40th point of voltage and current waveforms. The distance between each samples is 4 samples.

Table 4.59: Values of current at time t, $t-\Delta t$, $t-2\Delta t$ and $t-3\Delta t$, voltage at time $t-\Delta t$, $t-2\Delta t$ and $t-3\Delta t$ for the second sampling scenario in the case of two parallel motors.

selected sample	$i(t)$	$i(t-\Delta t)$	$i(t-2\Delta t)$	$i(t-3\Delta t)$	$v(t-\Delta t)$	$v(t-2\Delta t)$	$v(t-3\Delta t)$
40th sample	-5.77706	-2.20721	1.289478	4.522545	10.97314	9.118296	6.857844
44th sample	-16.7179	-14.8728	-12.313	-9.21498	12.12821	12.92057	12.96362
48th sample	-14.8025	-16.7668	-17.7378	-17.7059	2.332151	5.581085	8.38181
52th sample	0.424436	-4.06529	-8.25894	-11.9136	-11	-8.12817	-4.80718
56th sample	16.28371	13.11448	9.265115	4.953669	-15.3648	-15.5084	-14.795
60th sample	19.32273	20.15932	19.91034	18.59294	-7.06243	-10.103	-12.5854
64th sample	6.816886	11.01555	14.62358	17.44378	7.062435	3.631558	-4.10E-13

Table 4.60: Values of voltage at time t for the second sampling scenario in the case of two parallel motors.

selected sample	$v(t)$
40th sample	-12.2903
44th sample	-10.5969
48th sample	1.195109
52th sample	13.26397
56th sample	14.37219
60th sample	3.631558
64th sample	-10.103

Discrete time series coefficients are calculated and resulted as:

B=$\begin{bmatrix} 5.0644 & -11.4930 & 8.1528 & -1.7211 & -0.5136 & -0.9904 & 0.5159 \end{bmatrix}$

Impedance coefficient values for $t=t, t-\Delta t, t-2\Delta t, t-3\Delta t$ are equal for the two sampling scenarios. Therefore, we will proceed with order=4 coefficient calculation. Three different sampling sets are selected.

Simulation Eight: First Sampling Scenario For The Fourth Order Status

In this sampling scheme, the first sampling point is the 20th point of voltage and current waveforms. The distance between each samples is 5 samples.

Table 4.61: Values of current at time t, $t-\Delta t$, $t-2\Delta t$ and $t-3\Delta t$ and $t-4\Delta t$, voltage at time $t-\Delta t$, $t-2\Delta t$, $t-3\Delta t$ and $t-4\Delta t$ for the first sampling scenario in the case of two parallel motors.

selected sample	$i(t)$	$i(t-\Delta t)$	$i(t-2\Delta t)$	$i(t-3\Delta t)$	$i(t-4\Delta t)$	$v(t-\Delta t)$	$v(t-2\Delta t)$	$v(t-3\Delta t)$	$v(t-4\Delta t)$
20th sample	-6.79403	-7.00161	-6.82318	-6.31469	-5.54857	2.648413	3.57816	4.195117	4.49131
25th sample	0.258391	-1.83327	-3.64976	-5.11123	-6.16645	-4.84104	-3.23695	-1.58881	1.74E-13
30th sample	10.61917	9.017144	7.040091	4.826744	2.52011	-8.6304	-8.72347	-8.32261	-7.48552
35th sample	9.56945	11.15864	12.0443	12.22007	11.72101	-0.83912	-3.20478	-5.24944	-6.875
40th sample	-5.77706	-2.20721	1.289478	4.522545	7.326548	10.97314	9.118296	6.857844	4.340844
45th sample	-17.7059	-16.7179	-14.8728	-12.313	-9.21498	10.59694	12.12821	12.92057	12.96362
50th sample	-8.25894	-11.9136	-14.8025	-16.7668	-17.7378	-4.80718	-1.19511	2.332151	5.581085
55th sample	13.11448	9.265115	4.953669	0.424436	-4.06529	-15.5084	-14.795	-13.264	-11
60th sample	19.32273	20.15932	19.91034	18.59294	16.28371	-7.06243	-10.103	-12.5854	-14.3722

Table 4.62: Values of voltage at time t for the first sampling scenario in the case of two parallel motors.

selected sample	$v(t)$
20th sample	-1.43749
25th sample	6.292675
30th sample	8.013647
35th sample	-1.72376
40th sample	-12.2903
45th sample	-8.38181
50th sample	8.12817
55th sample	15.36482
60th sample	3.631558

Discrete time series coefficients are calculated and resulted as:

$$[a0, a1, a2, a3, a4, b0, b1, b2, b3] =$$
$$\begin{bmatrix} 5.0678 & -16.4878 & 19.4712 & -9.7424 & 1.6912 & -1.4958 & -0.4912 & 1.4957 & -0.5087 \end{bmatrix}$$

Simulation Eight: Second Sampling Scenario For The Fourth Order Status

In this sampling scheme, the first sampling point is the 30th point of voltage and current waveforms. The distance between each samples is 5 samples.

Table 4.63: Values of current at time t, $t-\Delta t$, $t-2\Delta t$ and $t-3\Delta t$ and $t-4\Delta t$, voltage at time $t-\Delta t$, $t-2\Delta t$, $t-3\Delta t$ and $t-4\Delta t$ for the second sampling scenario in the case of two parallel motors.

selected sample	$i(t)$	$i(t-\Delta t)$	$i(t-2\Delta t)$	$i(t-3\Delta t)$	$i(t-4\Delta t)$	$v(t-\Delta t)$	$v(t-2\Delta t)$	$v(t-3\Delta t)$	$v(t-4\Delta t)$
30th sample	10.61917	9.017144	7.040091	4.826744	2.52011	-8.6304	-8.72347	-8.32261	-7.48552
35th sample	9.56945	11.15864	12.0443	12.22007	11.72101	-0.83912	-3.20478	-5.24944	-6.875
40th sample	-5.77706	-2.20721	1.289478	4.522545	7.326548	10.97314	9.118296	6.857844	4.340844
45th sample	-17.7059	-16.7179	-14.8728	-12.313	-9.21498	10.59694	12.12821	12.92057	12.96362
50th sample	-8.25894	-11.9136	-14.8025	-16.7668	-17.7378	-4.80718	-1.19511	2.332151	5.581085
55th sample	13.11448	9.265115	4.953669	0.424436	-4.06529	-15.5084	-14.795	-13.264	-11
60th sample	19.32273	20.15932	19.91034	18.59294	16.28371	-7.06243	-10.103	-12.5854	-14.3722
65th sample	2.257668	6.816886	11.01555	14.62358	17.44378	10.10304	7.062435	3.631558	-4.10E-13
70th sample	-17.2642	-14.5713	-11.0641	-6.93537	-2.41191	14.79497	15.50839	15.36482	14.37219

Table 4.64: Values of voltage at time t for the second sampling scenario in the case of two parallel motors.

selected sample	$v(t)$
30th sample	8.013647
35th sample	-1.72376
40th sample	-12.2903
45th sample	-8.38181
50th sample	8.12817
55th sample	15.36482
60th sample	3.631558
65th sample	-12.5854
70th sample	-13.264

Discrete time series coefficients are calculated and resulted as:

$$[a0, a1, a2, a3, a4, b0, b1, b2, b3] =$$
$$\begin{bmatrix} 5.0678 & -16.4825 & 19.4589 & -9.7335 & 1.6892 & -1.4947 & -0.4918 & 1.4947 & -0.5081 \end{bmatrix}$$

Simulation Eight: Third Sampling Scenario For The Fourth Order Status

In this sampling scheme, the first sampling point is the 40th point of voltage and current waveforms. The distance between each samples is 5 samples.

Table 4.65: Values of current at time t, $t-\Delta t$, $t-2\Delta t$ and $t-3\Delta t$ and $t-4\Delta t$, voltage at time $t-\Delta t$, $t-2\Delta t$, $t-3\Delta t$ and $t-4\Delta t$ for the third sampling scenario in the case of two parallel motors.

selected sample	$i(t)$	$i(t-\Delta t)$	$i(t-2\Delta t)$	$i(t-3\Delta t)$	$i(t-4\Delta t)$	$v(t-\Delta t)$	$v(t-2\Delta t)$	$v(t-3\Delta t)$	$v(t-4\Delta t)$
40th sample	-5.77706	-2.20721	1.289478	4.522545	7.326548	10.97314	9.118296	6.857844	4.340844
45th sample	-17.7059	-16.7179	-14.8728	-12.313	-9.21498	10.59694	12.12821	12.92057	12.96362
50th sample	-8.25894	-11.9136	-14.8025	-16.7668	-17.7378	-4.80718	-1.19511	2.332151	5.581085
55th sample	13.11448	9.265115	4.953669	0.424436	-4.06529	-15.5084	-14.795	-13.264	-11
60th sample	19.32273	20.15932	19.91034	18.59294	16.28371	-7.06243	-10.103	-12.5854	-14.3722
65th sample	2.257668	6.816886	11.01555	14.62358	17.44378	10.10304	7.062435	3.631558	-4.10E-13
70th sample	-17.2642	-14.5713	-11.0641	-6.93537	-2.41191	14.79497	15.50839	15.36482	14.37219
75th sample	-15.2861	-17.7612	-19.2498	-19.6691	-18.9951	1.220537	4.807176	8.12817	11
80th sample	5.666001	1.092029	-3.53966	-7.97276	-11.9619	-13.8608	-11.8291	-9.14379	-5.95316

Table 4.66: Values of voltage at time t for the third sampling scenario in the case of two parallel motors.

selected sample	$v(t)$
40th sample	-12.2903
45th sample	-8.38181
50th sample	8.12817
55th sample	15.36482
60th sample	3.631558
65th sample	-12.5854
70th sample	-13.264
75th sample	2.433549
80th sample	15.12653

Discrete time series coefficients are calculated and resulted as:

$[a0, a1, a2, a3, a4, b0, b1, b2, b3] =$

$$\begin{bmatrix} 5.0678 & -16.4670 & 19.4235 & -9.7082 & 1.6839 & -1.4916 & -0.4937 & 1.4919 & -0.5066 \end{bmatrix}$$

Fifth order impedance coefficients are not equivalent for two selected sampling patterns. The largest order which results in the equal impedance coefficients is 4. Usually, in the case of parallel motors, if they are not identical, each single motor will increase the total order of the circuit, by two. In other words, if n motor loads are connected to a feeder, the

aggregated load will be a $2n$ order system.

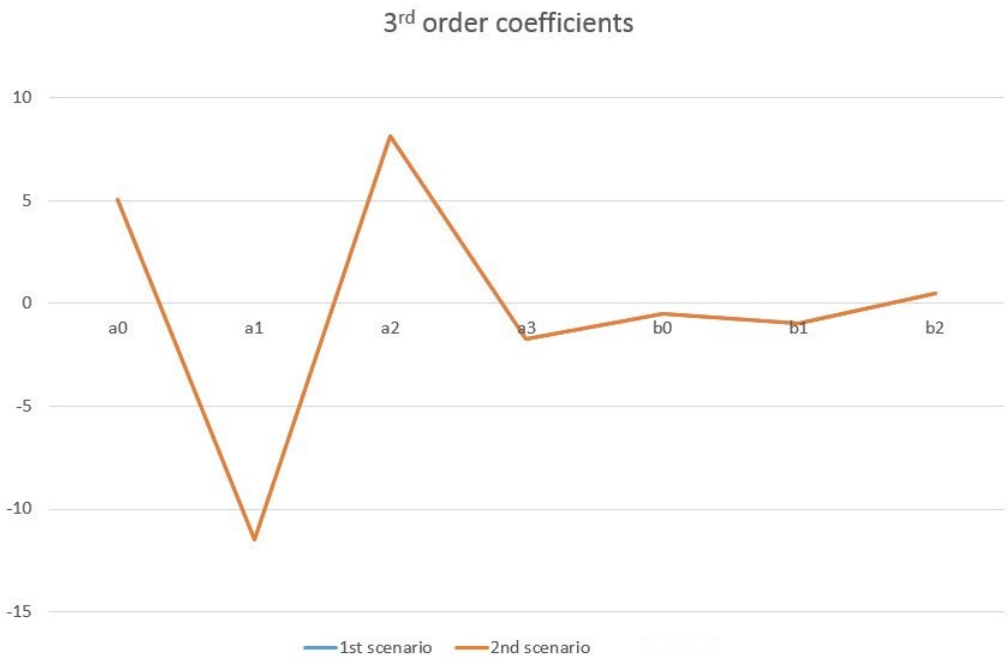

Figure 4.28: Third order impedance coefficients for two different sampling scenarios of two parallel motor loads.

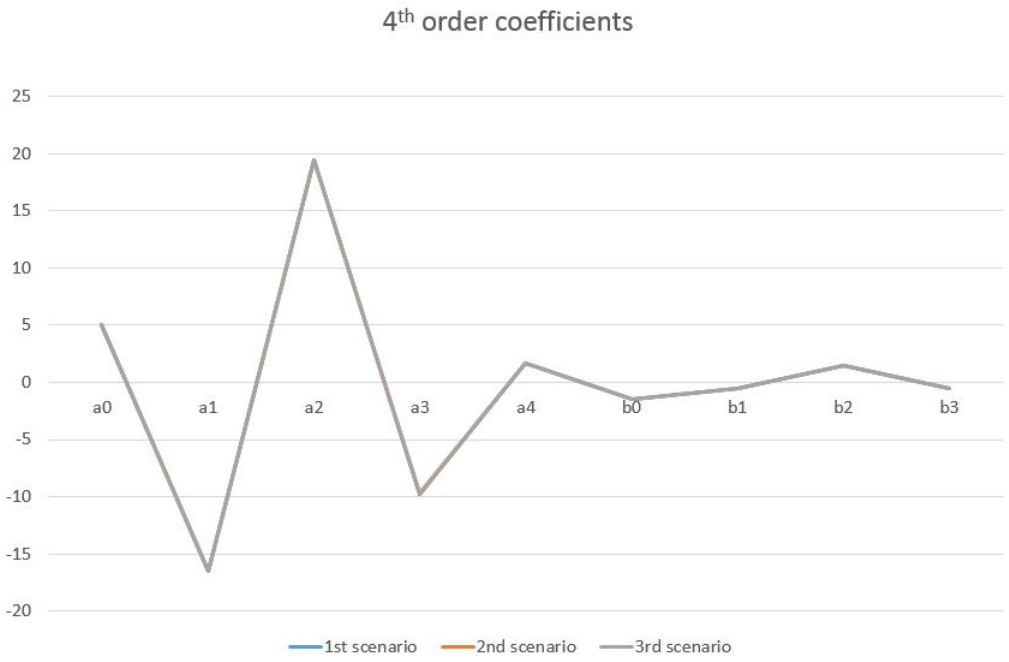

Figure 4.29: Fourth order impedance coefficients for three different sampling scenarios of two parallel motor loads.

4.2.13 Simulation Eight: Two Parallel Motors Load Parameters Calculations

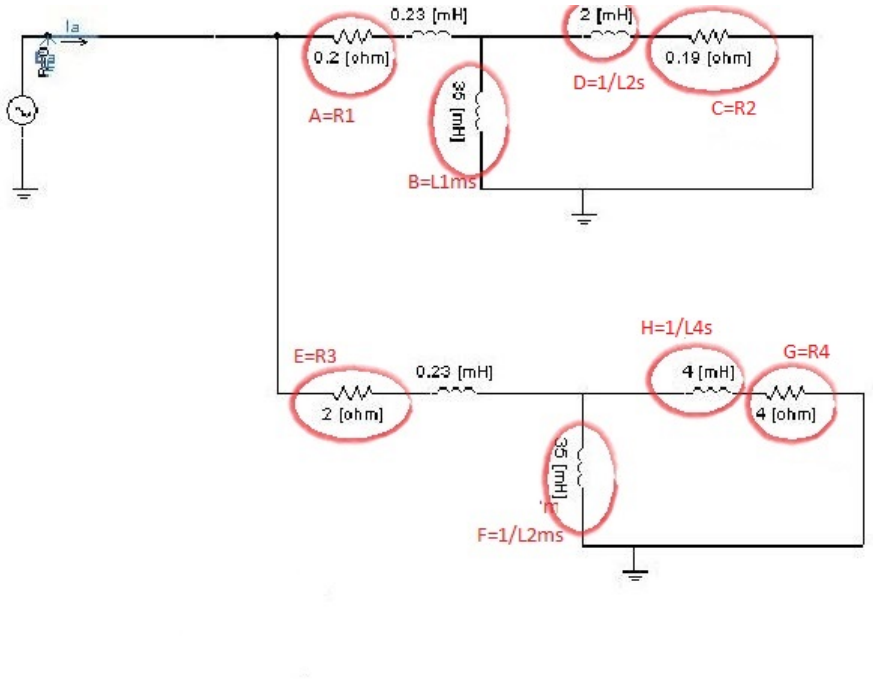

Figure 4.30: Two parallel motors.

Y_s in Figure 4.31 is derived from the 4th order calculated discrete impedance coefficients. Following division products 8 steps of division prior to getting a remainder of zero
The first eight quotients are indicating two motor's parameters respectively, R_1, L_m, R_2&L_2 & R_3, L_{2m}, R_4&L_4.

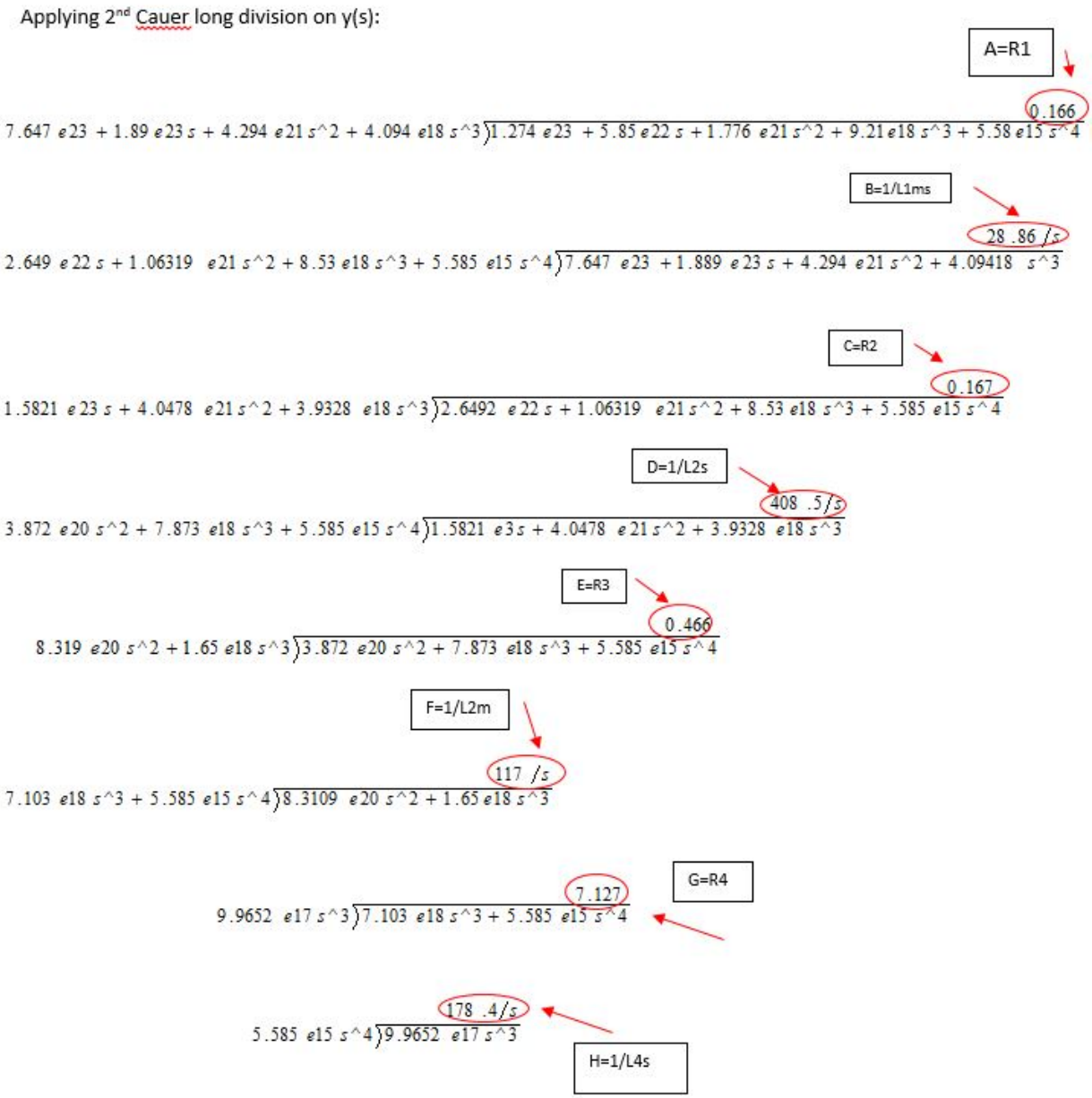

Figure 4.31: Two parallel motors load parameter calculation.

4.2.14 Simulation Nine: Two Parallel Motors in Parallel with One Resistive Load

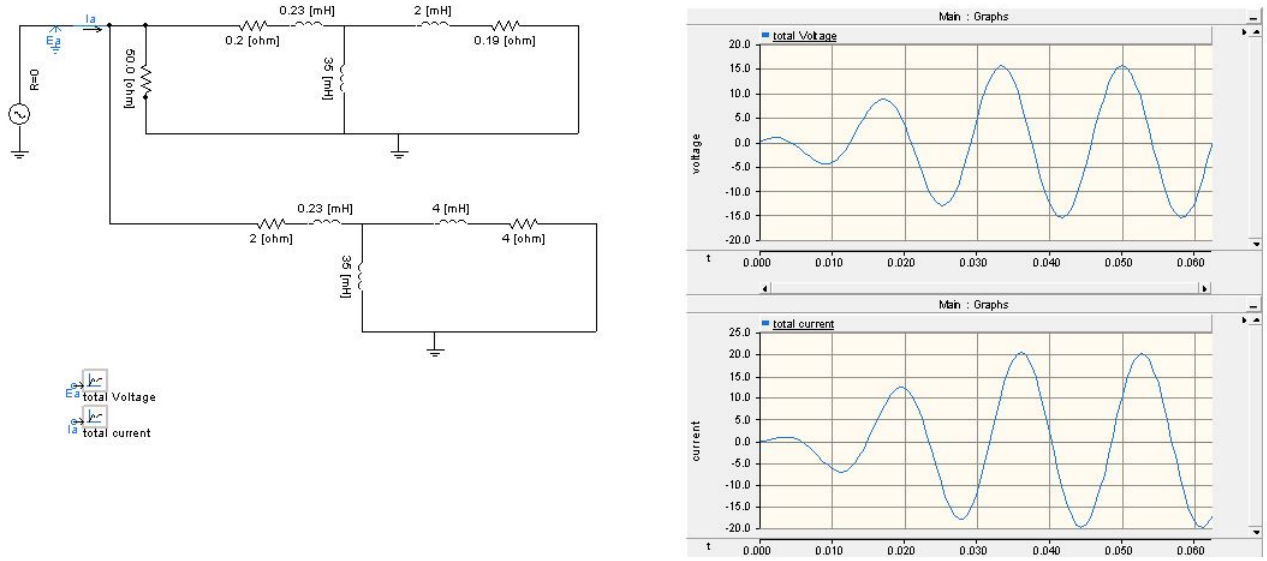

Figure 4.32: Two parallel motor in parallel with one resistive load.

In this simulation case, sampling rate is $\Delta t = 625\mu s$(sampling frequency =1600 Hz), maximum simulation time is $t_{max} = 0.0625s$ and ramp up time=0.03 (slow transient ends at sample number 48). For this case, since resistor does not change the total order of the aggregated circuit, this load is a 4th order load same as Section 4.2.12.

Simulation Nine: First Sampling Scenario For The Fourth Order Status

In this sampling scheme, the first sampling point is the 30th point of voltage and current waveforms. The distance between each samples is 5 samples.

Table 4.67: Values of current at time t, $t-\Delta t$, $t-2\Delta t$, $t-3\Delta t$ and $t-4\Delta t$, voltage at time $t-\Delta t$, $t-2\Delta t$, $t-3\Delta t$ and $t-4\Delta t$ for the first sampling scenario in the case of two parallel motors in parallel with a resistive load.

selected sample	$i(t)$	$i(t-\Delta t)$	$i(t-2\Delta t)$	$i(t-3\Delta t)$	$i(t-4\Delta t)$	$v(t-\Delta t)$	$v(t-2\Delta t)$	$v(t-3\Delta t)$	$v(t-4\Delta t)$
30th sample	10.77944	9.189752	7.21456	4.993196	2.67E+00	-8.6304	-8.72347	-8.32261	-7.48552
35th sample	9.534974	11.17542	12.1084	12.32506	11.85851	-0.83912	-3.20478	-5.24944	-6.875
40th sample	-6.02286	-2.42667	1.107112	4.385388	7.239731	10.97314	9.118296	6.857844	4.340844
45th sample	-17.8735	-16.9299	-15.1153	-12.5714	-9.47426	10.59694	12.12821	12.92057	12.96362
50th sample	-8.09637	-11.8174	-14.7786	-16.8134	-17.8494	-4.80718	-1.19511	2.332151	5.581085
55th sample	13.42177	9.575283	5.249569	0.689716	-3.84529	-15.5084	-14.795	-13.264	-11
60th sample	19.39536	20.30056	20.1124	18.84465	16.57115	-7.06243	-10.103	-12.5854	-14.3722
65th sample	2.005961	6.614825	10.8743	14.55095	17.44378	10.10304	7.062435	3.631558	-4.10E-13
70th sample	-17.5295	-14.8672	-11.3743	-7.24266	-2.69935	14.79497	15.50839	15.36482	14.37219

Table 4.68: Values of voltage at time t for the second sampling scenario in the case of two parallel motors in parallel with a resistive load.

selected sample	$v(t)$
30th sample	8.013647
35th sample	-1.72376
40th sample	-12.2903
45th sample	-8.38181
50th sample	8.12817
55th sample	15.36482
60th sample	3.631558
65th sample	-12.5854
70th sample	-13.264

Discrete time series coefficients are calculated and resulted as:

$$\text{B=}\begin{bmatrix}4.6014 & -14.9632 & 17.6626 & -8.8337 & 1.5329 & -1.6559 & -0.0936 & 1.1800 & -0.4305\end{bmatrix}$$

Simulation Nine: Second Sampling Scenario For The Fourth Order Status

In this sampling scheme, the first sampling point is the 40th point of voltage and current waveforms. The distance between each samples is 5 samples.

Table 4.69: Values of current at time t, $t-\Delta t$, $t-2\Delta t$, $t-3\Delta t$ and $t-4\Delta t$, voltage at time $t-\Delta t$, $t-2\Delta t$, $t-3\Delta t$ and $t-4\Delta t$ for the second sampling scenario in the case of two parallel motors in parallel with a resistive load.

selected sample	$i(t)$	$i(t-\Delta t)$	$i(t-2\Delta t)$	$i(t-3\Delta t)$	$i(t-4\Delta t)$	$v(t-\Delta t)$	$v(t-2\Delta t)$	$v(t-3\Delta t)$	$v(t-4\Delta t)$
40th sample	-6.02286	-2.42667	1.107112	4.385388	7.239731	10.97314	9.12E+00	6.857844	4.340844
45th sample	-17.8735	-16.9299	-15.1153	-12.5714	-9.47426	10.59694	12.12821	12.92057	12.96362
50th sample	-8.09637	-11.8174	-14.7786	-16.8134	-17.8494	-4.80718	-1.19511	2.332151	5.581085
55th sample	13.42177	9.575283	5.249569	0.689716	-3.84529	-15.5084	-14.795	-13.264	-11
60th sample	19.39536	20.30056	20.1124	18.84465	16.57115	-7.06243	-10.103	-12.5854	-14.3722
65th sample	2.005961	6.614825	10.8743	14.55095	17.44378	10.10304	7.062435	3.631558	-4.10E-13
70th sample	-17.5295	-14.8672	-11.3743	-7.24266	-2.69935	14.79497	15.50839	15.36482	14.37219
75th sample	-15.2374	-17.7856	-19.3459	-19.8316	-19.2151	1.220537	4.807176	8.12817	11
80th sample	5.968531	1.369245	-3.30308	-7.78988	-11.8428	-13.8608	-11.8291	-9.14379	-5.95316

Table 4.70: Values of voltage at time t for the second sampling scenario in the case of two parallel motors in parallel with a resistive load.

selected sample	$v(t)$
40th sample	-12.2903
45th sample	-8.38181
50th sample	8.12817
55th sample	15.36482
60th sample	3.631558
65th sample	-12.5854
70th sample	-13.264
75th sample	2.433549
80th sample	15.12653

Discrete time series coefficients are calculated and resulted as:

$$\text{B=}\begin{bmatrix}4.6014 & -14.9667 & 17.6706 & -8.8395 & 1.5341 & -1.6567 & -0.0930 & 1.1806 & -0.4308\end{bmatrix}$$

Figure 4.33: Third order impedance coefficients for two different sampling scenarios of two parallel motors in parallel with one resistance load.

Figure 4.34: Fourth order impedance coefficients for two different sampling scenarios of two parallel motors in parallel with one resistance load.

Figure 4.35: Fifth order impedance coefficients for two different sampling scenarios of two parallel motors in parallel with one resistance load.

4.2.15 Simulation Nine: Two Parallel Motors in Parallel with A Resistive Load Parameters Calculations

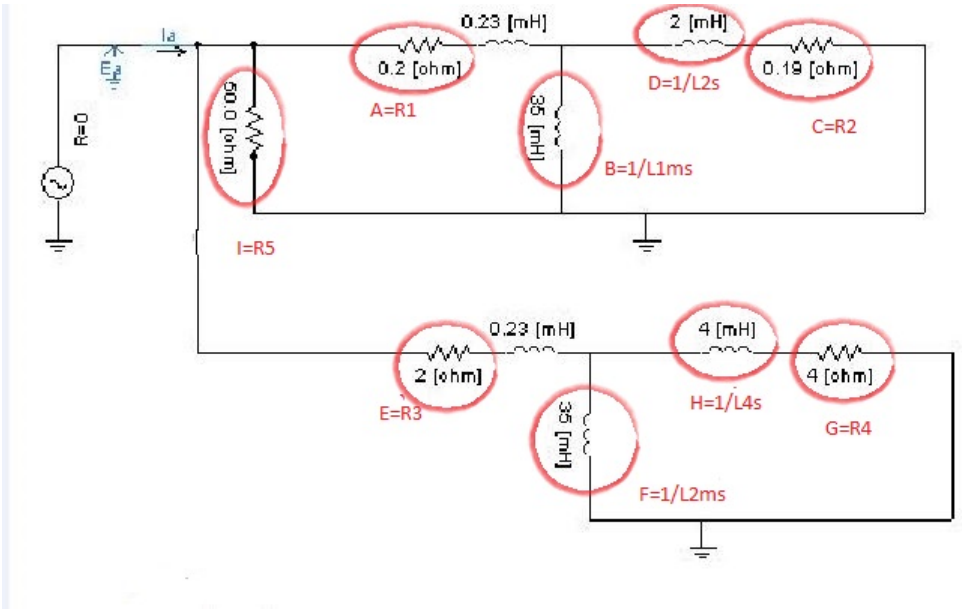

Figure 4.36: Two parallel motors in parallel with a resistive load.

In Figure 4.37, Y_s is derived from the 4th order impedance coefficients. In this case, we see 9 stages of division before we reach zero in remainder. The first eight quotients are the values of the 2 motors parameters respectively, $R_1, L_m, R_2 \& L_2$ & $R_3, L_{2m}, R_4 \& L_4$ and the last quotient is the value of paralleled resistance.

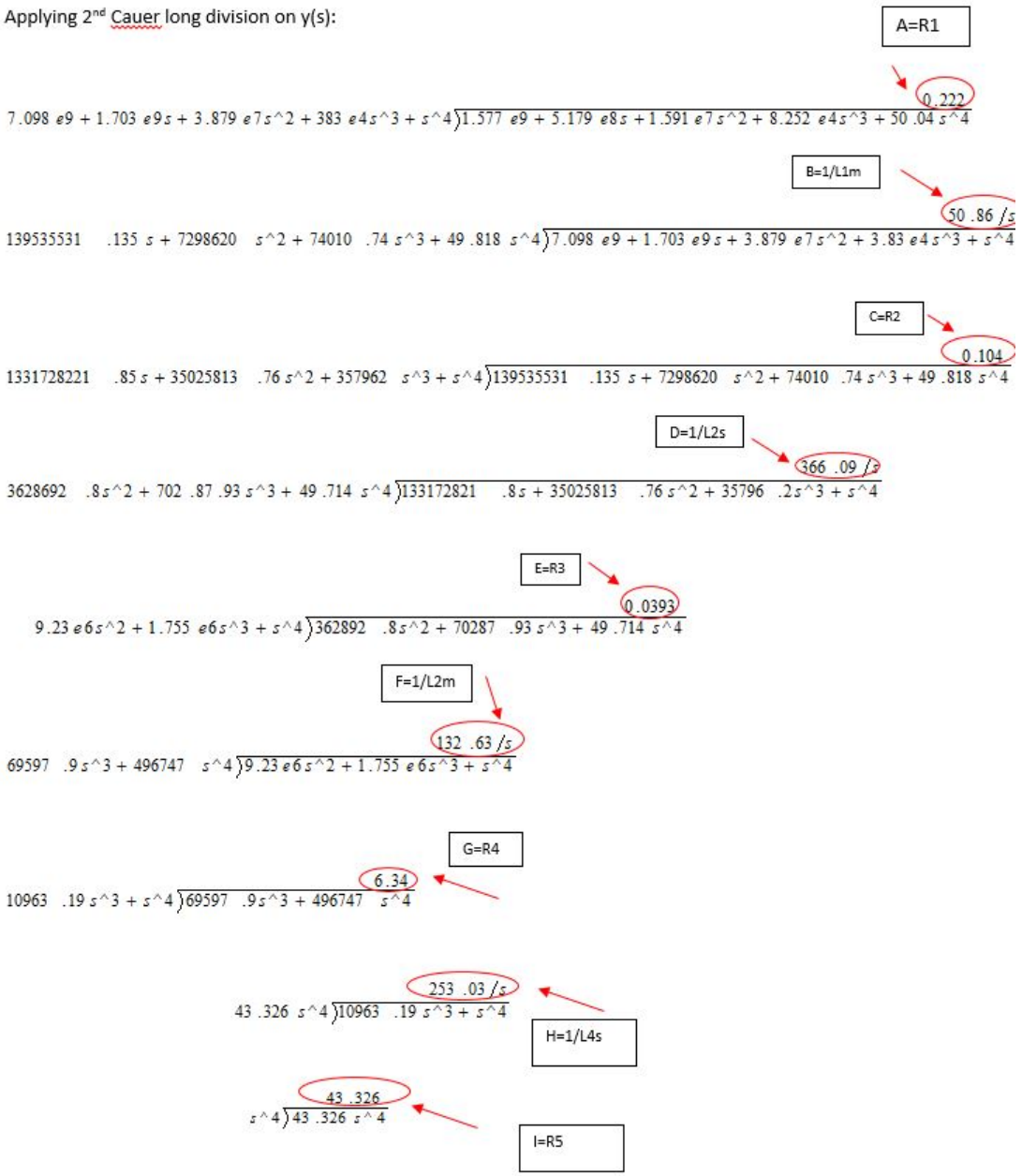

Figure 4.37: Two parallel motors load parameter calculation.

4.2.16 Simulation Ten: Two Parallel Motors in Parallel with A Resistive and An Inductive Load Parameters Calculations

In this section, we describe two parallel motors in parallel with a resistive and inductive load. The load is a 5th order load. Since inductance generates 1st order history terms, it increase the total order of the aggregated load circuit by one. According to our algorithm, the order of an aggregated load combining of motor loads and inductive loads in parallel is formulated as:(number of inductive loads)*1+(number of motor loads *2)

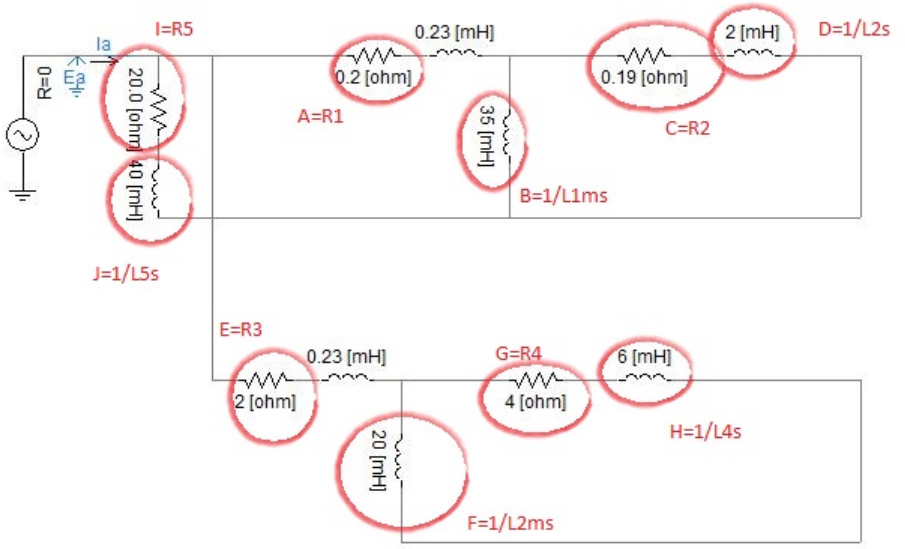

Figure 4.38: Two Parallel motors in parallel with a resistive and an inductive load.

This case determines an inductor type in parallel with two induction motors. In Figure 4.39, Y_s is derived from the 5th order discrete time impedance coefficients. This load scenario products ten steps of long division before reaching to zero in remainder.

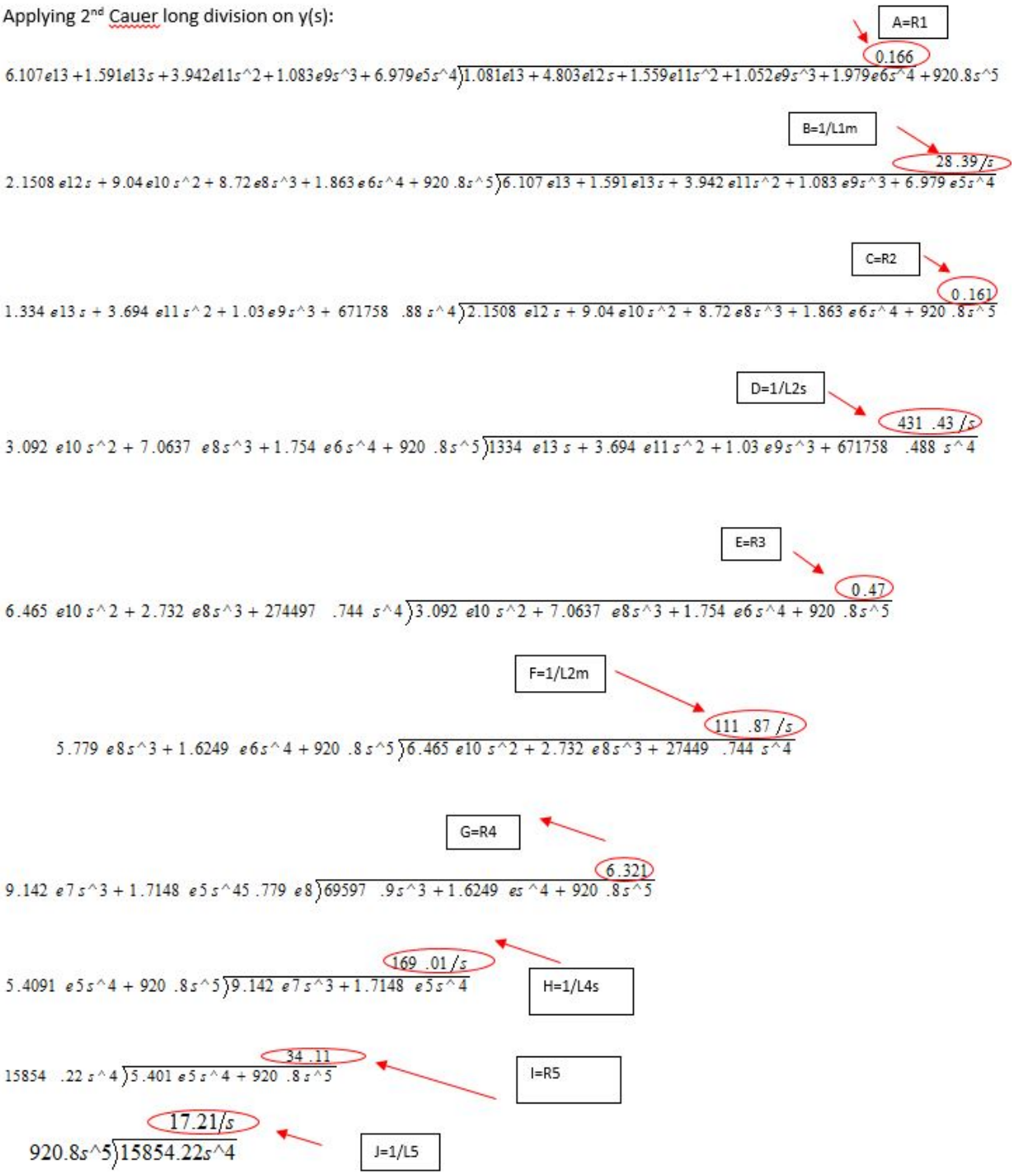

Figure 4.39: Two parallel motors in parallel with a series RL load parameter calculation.

The first eight quotients are 2 motors parameters respectively namely, $R_1, L_m, R_2 \& L_2$ & $R_3, L_{2m}, R_4 \& L_4$. The $9th$ and the $10th$ quotients are the values of paralleled **Resistor** and **inductor** within some errors. In conclusion, having the electrical parameters of an aggregated load, and the types of its constituent eigenloads, will determine, what type of loads are connected to the feeder at each time stamp. Figure 4.40 demonstrates the general overview of our load disaggregation algorithm.

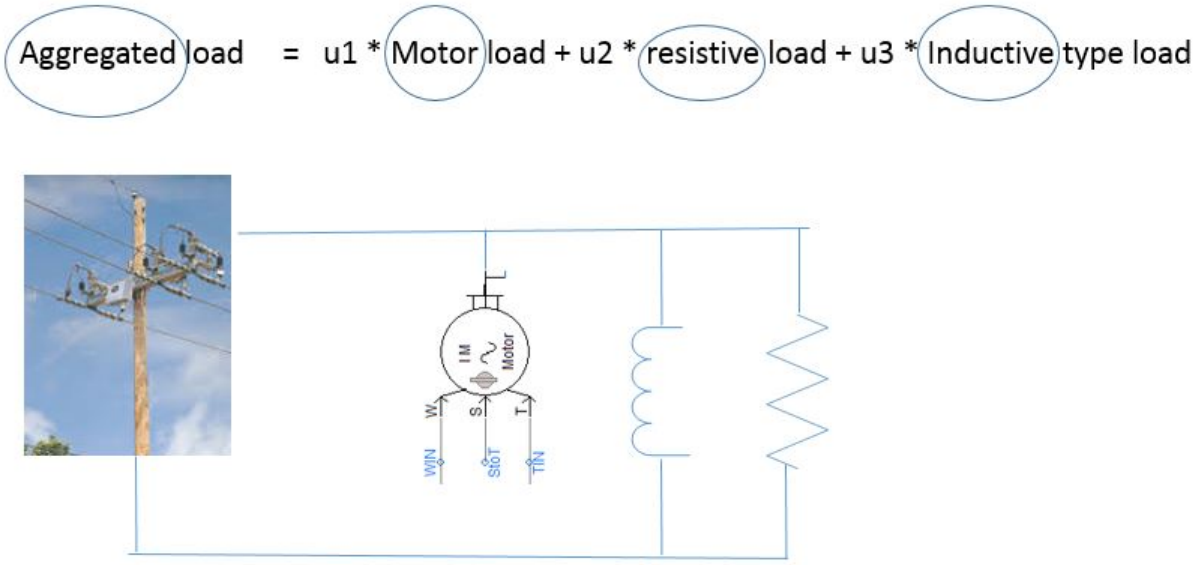

Figure 4.40: General overview of or work.

In which u_1, u_2 and u_3 are the contributions of each eigen-loads in the total load.

Chapter 5

Experimental Results

The proposed "Load decomposition" algorithm is validated with real experimental data accomplished on a number of different appliance types at "UBC Power Lab". As discussed in Chapter 3, voltage and current signals in near-real time domain, are the inputs of the proposed algorithm. The main goal of this chapter is to verify the proposed method with real measurements. A number of electric appliances were analysed in the lab and current and voltage waveforms were recorded for a period of few seconds. Sampling frequency is 10KHz. A current and voltage probe (different probe) were attached to an oscilloscope for measuring the voltage and current waveforms. Table 5.1 summarizes the list of appliances which have been tested.

5.1 Appliances Electrical Load Types and Classification

In this section, we briefly explain about four major category of appliances according to their characteristics.

5.1.1 Resistive Loads

Loads consisting of any type of heating elements such as conventional electric heating appliances (without power electronic interfaces), iron, heater, toaster, oven, kettles, electric rice cookers, electric hair curlers and even incandescent lights are categorized as resistive loads. These type of loads have negligible reactive power.

Table 5.1: Experimental appliances list.

Appliance type	order of the load/type of the load
Compact Florescent Lamp with magnetic ballast	1st order-inductive
Fan	2nd order-Motor load
Refrigerator	2nd order-Motor Load
Hair Dryer	2nd order-Motor Load
LCD Samsung	power electronics
iphone charger	power electronics
HTC charger	power electronics
Asus charger	power electronics
Razor	2nd order and Motor
Vacuum Cleaner	2nd order and Motor type
Iron	resistive load
incandescent lamp	purely Resistive

5.1.2 Inductive Loads

An example of this group are florescent lamps which convert the electromagnetic radiation to the light.

5.1.3 Motor Loads

Induction motors have the most appearance among the household appliances. Fan, vacuum cleaner, dishwasher and refrigerator are examples of motor loads.

5.1.4 Non-Linear Loads

These loads do not draw the sinusoidal current pattern. The most predominant ones are power electronic loads such as charger, TV and desktop computer. Figure 5.1 shows the measured voltage at the outlet. To obtain the aggregated voltage value, we measured the voltage between the outlet and appliances. Note that, in order to mimic the similar situation as in real power gird, all loads are directly connected to the 120 volt outlet. We use the same voltage signal for all the appliances.

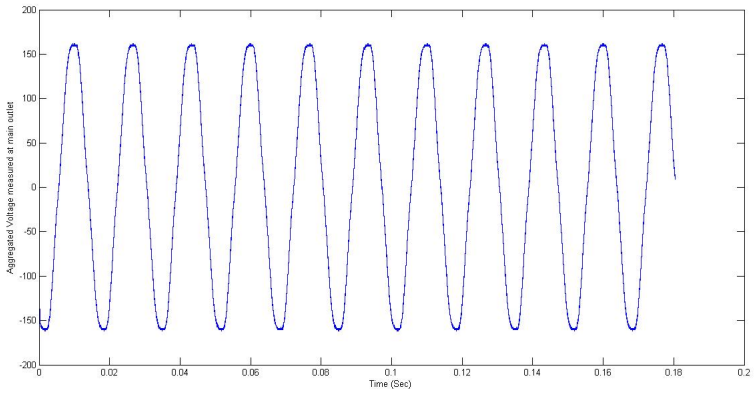

Figure 5.1: Voltage measured at main outlet.

5.2 Measuring General Observations

Some loads such as the vacuum cleaners exhibit a fairly constant frequency over the time. While the magnitude of current has a decaying component (inrush current). Some loads have multiple stages from the starting moment to the steady state. The current waveform of a HTC laptop charger as shown in Figure 5.5, has this characteristic. Current has the higher frequency components at the middle stage and then starts damping after a few cycles.

5.2.1 Fan

Figure 5.2 indicates the current waveform for a table fan captured on-line while it was connected to the city electricity.

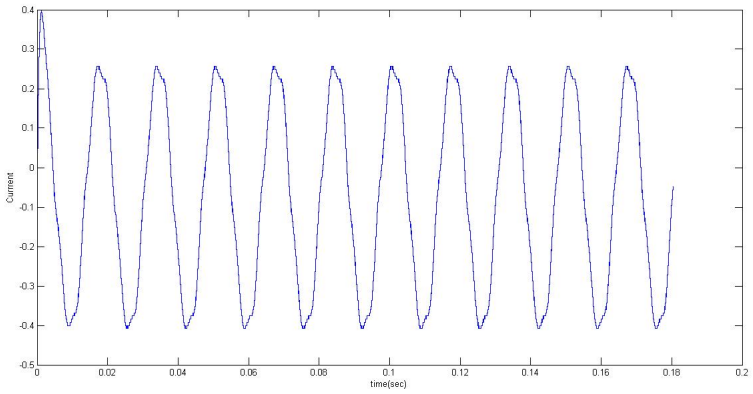

Figure 5.2: Current waveform in time for a fan.

5.2.2 Fan Parameters Calculation

As the first step, we need to choose at least two different sampling scenarios or two different harmonic data sets. We extracted the 60 Hz instantaneous voltage and current signals. Additionally, two sampling patterns were selected due to calculating the impedance coefficients. Both v_t and i_t are sampled with sampling rate of Δt = 1.6e-06 seconds. As discussed in Chapter 3, from Equation 3.4, we derive the second order impedance coefficients for two different sampling scenarios as following.

First Sampling Scenario For the Second Order Status
$A = [a_0, a_1, a_2, b_0, b_1] = \begin{bmatrix} 257.1647 & -499.2356 & 242.3976 & -1.9700 & 0.9726 \end{bmatrix}$

Second Sampling Scenario For the Second Order Status
$B = [a_0, a_1, a_2, b_0, b_1] = \begin{bmatrix} 259.2187 & -499.2816 & 240.2983 & -1.9631 & 0.9653 \end{bmatrix}$
Matrices A and B are equivalent within 10% error. We also, analysed the third order coefficients. The derived values were not equivalent for two different sampling schemes. Implementing second Cauer synthesis method on the continuous admittance function of the fan leads to:
$R_1 = 107 ohm$
$L_m = 11.02 mH$

$R_2 = 419.43ohm$
$L_2 = 11.02mH$

5.2.3 Florescent Lamp

Figure 5.3 demonstrates the current waveform of a magnetic ballast florescent lamp. There are some noise and also harmonics embedded in the current waveform. We extracted 60Hz component and implemented our method on the instantaneous voltage and current data. Florescent lamp was confirmed to be a first order load based on real voltage and current data.

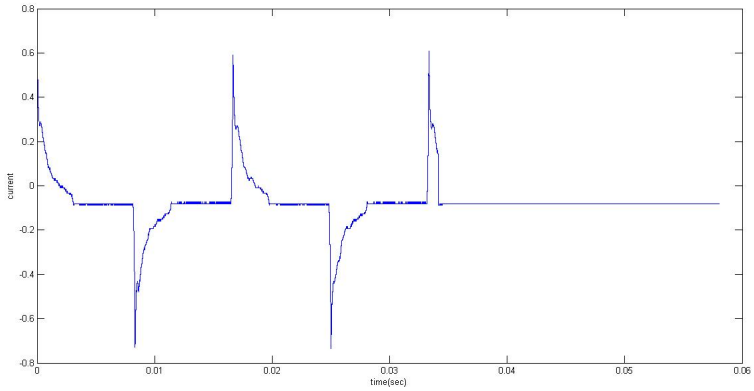

Figure 5.3: Current waveform in time for a florescent lamp

5.2.4 Florescent Parameters Calculation

As the first step, we need to choose at least two different sampling scenarios or two different harmonic data sets. We extracted the 60 Hz instantaneous voltage and current signals. Additionally, two sampling patterns were selected due to calculating the impedance coefficients. Both v_t and i_t are sampled with sampling rate of $\Delta t =$ 8e-07 seconds. As discussed by Equation 3.4, we derive the first order impedance coefficients for two different sampling scenarios as following.

First Sampling Scenario For the First Order Status
$A = [a_0, a_1, b_0] = \begin{bmatrix} 1567.7 & -1567.8 & -1 \end{bmatrix}$

Second Sampling Scenario For the First Order Status
$B = [a_0, a_1, a_2, b_0, b_1] = \begin{bmatrix} 1567.5 & -1567.5 & -1 \end{bmatrix}$
Matrices A and B are equivalent within 10% error. We also, analysed the second order coefficients. The derived values were not equivalent for two different sampling schemes. Implementing second Cauer synthesis method on the continuous admittance function of the fan leads to:
$L = 0.637mH$

5.2.5 Fan in Parallel With Florescent Lamp Parameters Calculation

We put the fan and the florescent lamp in parallel for this case and aggregated voltage and current are measured.

5.2.6 Parallel Florescent and Fan Parameters Calculation

As the first step, we need to choose at least two different sampling scenarios or two different harmonic data sets. We extracted the 60 Hz instantaneous voltage and current signals. Additionally, two sampling patterns were selected due to calculating the impedance coefficients. Both v_t and i_t are sampled with sampling rate of Δt = 1.6e-06 seconds. As discussed in Chapter 3, from Equation 3.4, we derive the second order impedance coefficients for two different sampling scenarios as following.

First Sampling Scenario For the Second Order Status
$A = [a_0, a_1, a_2, b_0, b_1] = \begin{bmatrix} 351.25 & -703.5 & -352 & -2 & 1 \end{bmatrix}$

Second Sampling Scenario For the Second Order Status
$B = [a_0, a_1, a_2, b_0, b_1] = \begin{bmatrix} 347.2160 & -694.2740 & 347.0588 & -1.9993 & .9993 \end{bmatrix}$
Matrices A and B are equivalent within 10% error. This confirms that **this parallel load topology**, at least satisfies the second order circuit requirements. Therefore the next proposed order is order number three. As shown by Equation 3.4, we derive the third order impedance coefficients for two different sampling scenarios as following.

First Sampling Scenario For the Third Order Status Since the selected order is three, we need at least seven coefficients. $A = [a_0, a_1, a_2, a_3, b_0, b_1, b_2] =$
$\begin{bmatrix} 365 & -1094.3 & 1093.6 & -364.3 & 3 & -3 & 1 \end{bmatrix}$

Second Sampling Scenario For the Third Order Status $B = [a_0, a_1, a_2, a_3, b_0, b_1, b_2] = \begin{bmatrix} 368.5 & -1104.5 & 1103.6 & -376.6 & 3 & -3 & 1 \end{bmatrix}$

Matrices A and B are equivalent within 10% error. This confirms that **this parallel load topology**, at least satisfies the third order circuit requirements. Therefore the next proposed order is order number four. Fourth order nine impedance coefficients including $[a_0, a_1, a_2, a_3, a_4, b_0, b_1, b_2, b_3]$ received different values for the two different group of 60 Hz voltage and current samples. This proves that a parallel fan and florescent lamp load is a third order system. Note, as described in Chapter 3, motors are second order loads and inductive loads are first order loads. Whenever, we have an odd number for the aggregated load, there has to be some motor and some inductance. But, in the case of the even orders, total load can either be a combination of motors, or parallel motor and resistances. We concluded that a parallel fan and florescent lamp is a third order load. This implies that there is a second order motor load and a first order inductive load in parallel. Sections 5.2.1 and 5.2.3, already proved that a fan is a motor load and a florescent lamp is an inductive load type. Therefore, the parallel combination will be a third order load.

5.2.7 Hair Dryer

Figure 5.4 shows the current waveform of a current waveform. The current signal is in phase with voltage signal which confirms that, hair dryer is a resistive load. We also verified this with our algorithm.

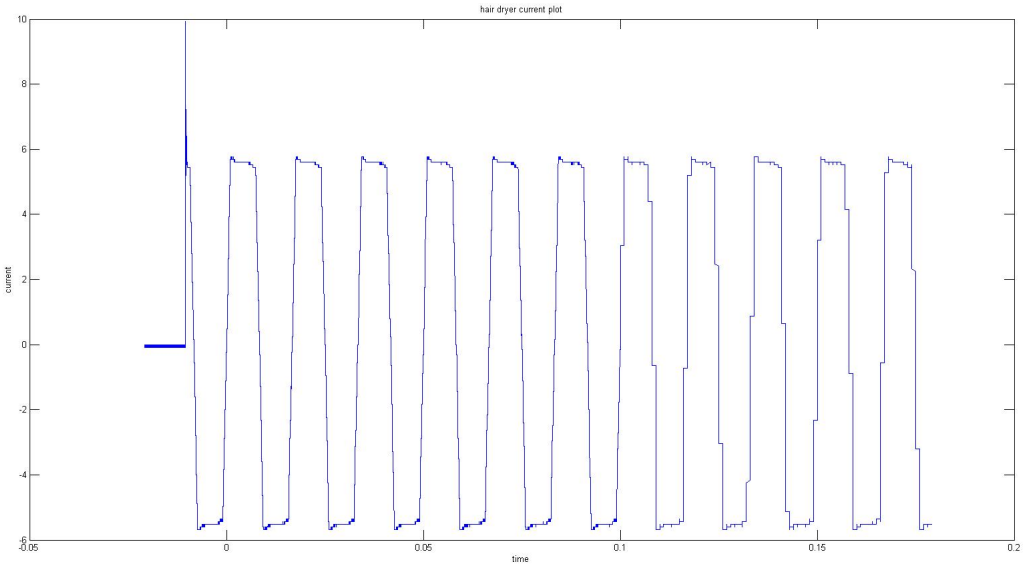

Figure 5.4: Current waveform in time for a hair-dryer.

This thesis for the hair dryer, did not cover finding circuit parameters. However, based our theory and simulation results in Section 3.4, we believe, hair dryer is a first order load.

5.2.8 HTC Charger

HTC charger as discussed before is a power electronic load. For the power electronic loads, we extract at least two different frequency components from the voltage and the current signals. Impedance coefficients are calculated for each set of two harmonics.

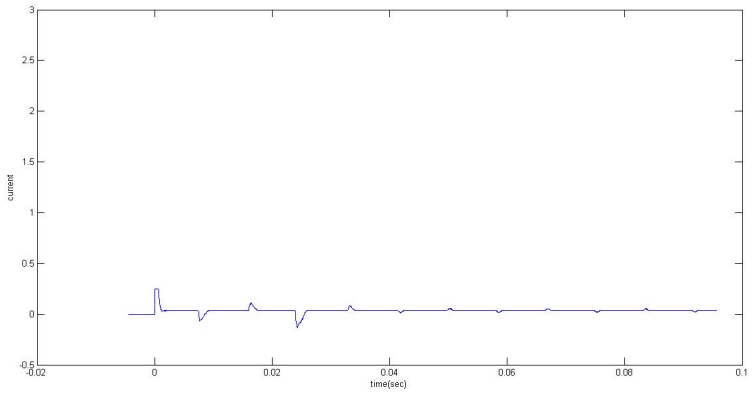

Figure 5.5: Current waveform in time for an HTC laptop charger.

This thesis does not cover power electronic load analysis.

5.2.9 Refrigerator

Refrigerator is an induction motor type of load. It is widely used for heavy duty applications requiring high starting torques.

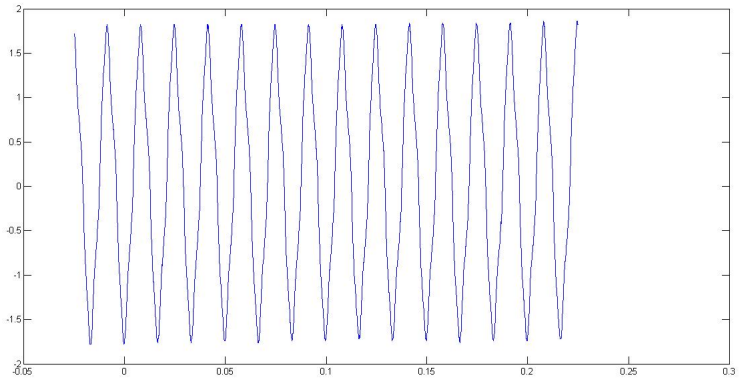

Figure 5.6: Current waveform in time for a refrigerator.

For the refrigerator, we did not cover finding circuit parameters. However, based our theory and simulation results in Section 3.4, we believe, refrigerator is a second order

load.

5.3 Chapter Summary

In this chapter, we validated our method with some real measurements, which have been conducted on a few home electrical appliances. This proved that the method is implementable to BC-Hydro distribution feeders.

Chapter 6

Conclusions and Future Work

6.1 Summary

In this thesis, we devised an innovative solution for the load disaggregation challenges. So far, most researches in this domain, looked at load's active and reactive power waveforms to extract the distinctive patterns for individual load types. But this thesis exploits smart meter voltage and current load information to discern between different type of loads. Our algorithm is able to distinguish between motor, heating and lighting loads. We proposed an EMTP based solution to solve the load disaggregation problem. The most important breakthrough is that we are able to recognize the type and the value of the loads at any level in distribution network. The result of this research is an input feeding the linear power flow technique provided in paper [11]. LPF, assumes a linear voltage-power dependency for all the load categories. Since, the dependency factor is different for each type of load, we need to know the load type before solving a LPF problem.

First chapter, introduced the concept of load disaggregation and its applications in smart distribution system. It also covered the definition of DMS, smart meter, and VVO. Chapter 2 summarized literature review. Most researchers employed machine learning techniques to classify different loads. Third chapter is the main body of this research. It explained, how to derive the discrete time values of the impedance matrix for each type of load. Network synthesis is integrated into our algorithm to calculate load's electrical circuit parameters. In Chapter 4, we analysed some of PSCAD simulation load cases. Three major type of loads, (1) motor, (2) inductive, and (3) resistive are accounted in our technique. Total loads are synthesized from different combinations of these eigen-loads.

For this reason, simulation examples covered different circuit topologies including R and L elements in the form of a motor, pure inductance and pure resistance. In Chapter 5, we validate our method with real measurement data.

6.2 Future Work

The following are suggested areas for future work and improvement to this thesis:

1. This method is implementable on data received from BC-Hydro smart meters.

2. This thesis can be coupled with Shifted Frequency Analysis (SFA) models and employed by PSCAD. The shifted system is then numerically integrated to obtain dynamic phasor solutions, which are more easily understood by power system operators and planners than instantaneous time domain results. SFA allows the exact simulation of frequencies within a band centred around a fundamental frequency using large time steps in a discrete-time EMTP type of solution environment [54]. This powerful tool, gives us the freedom to choose the sampling rate from the load voltage and current signals.

3. The other future's improvement is to expand the selection of eigen-loads. One can consider different category of induction motors, as an example. For instance, adopting another circuit synthesis method, may result in more exact determination of load circuit parameters.

4. The other extension can be the process of converting a discrete time impedance function to a continuous time impedance function. There is always a compromise between accuracy and stability in all the discrete-continuous mapping methods.

5. One last limitation of this thesis is in its incapability of detecting individual inductance values and resistance components in total load. This work only reported the aggregated value for R and L. Working toward this challenge is another future work.

Bibliography

[1] S.S. Venkata and H. Rudnick. Distribution systems [guest editorial]. *Power and Energy Magazine, IEEE*, 5(4):16–22, July 2007. → pages 1

[2] EDISON utlity. 2014 pv distribution system modeling workshop, May 2010. → pages xiv, 3

[3] BC-Hydro. 35 kv and below interconnection requirements for power generators, May 2010. → pages 4

[4] World energy needs and nuclear power, May 2015. → pages 5

[5] key world energy statistics 2014, May 2014. → pages xiv, 5

[6] H. Farhangi. The path of the smart grid. *Power and Energy Magazine, IEEE*, 8(1):18–28, January 2010. → pages 6

[7] Jixuan Zheng, D.W. Gao, and Li Lin. Smart meters in smart grid: An overview. In *Green Technologies Conference, 2013 IEEE*, pages 57–64, April 2013. → pages 6

[8] BC-Hydro. Epri technical executive discusses the importance of distribution management, April 2012. → pages 7

[9] Robert Uluski. Grid modernization, 2015. → pages xiv, 7

[10] US department of energy report. Application of automated controls for voltage and reactive power management, December 2012. → pages 8

[11] J.R. Marti, H. Ahmadi, and L. Bashualdo. Linear power-flow formulation based on a voltage-dependent load model. *Power Delivery, IEEE Transactions on*, 28(3):1682–1690, July 2013. → pages 9, 10, 11, 55, 145

[12] A. Ellis, D. Kosterev, and A. Meklin. Dynamic load models: Where are we? In *Transmission and Distribution Conference and Exhibition, 2005/2006 IEEE PES*, pages 1320–1324, May 2006. → pages 9

[13] A. Dwyer, R.E. Nielsen, J. Stangl, and N.S. Markushevich. Load to voltage dependency tests at b.c. hydro. *Power Systems, IEEE Transactions on*, 10(2):709–715, May 1995. → pages 9

[14] UBC. Local voltage stability assessment for variable load characteristics, May 2009. → pages 11

[15] Effects of reduced voltage on the operation and efficiency of electric loads), Sep 1981. → pages 11

[16] Non-intrusive load monitoring approaches for disaggregated energy sensing: A survey, 2012. → pages xiv, 12, 19, 20

[17] Stephen Makonin. Nonintrusive load monitoring, December 2014. → pages 13

[18] G.W. Hart. Nonintrusive appliance load monitoring. *Proceedings of the IEEE*, 80(12):1870–1891, Dec 1992. → pages xiv, 13, 15

[19] V. Amenta, S. Gagliano, G.M. Tina, G. Di Modica, and O. Tomarchio. Web interactive non intrusive load disaggregation system for energy consumption awareness. In *AEIT Annual Conference, 2013*, pages 1–6, Oct 2013. → pages xiv, 14

[20] M. Zeifman and K. Roth. Nonintrusive appliance load monitoring: Review and outlook. *Consumer Electronics, IEEE Transactions on*, 57(1):76–84, February 2011. → pages 15

[21] A. Marchiori, D. Hakkarinen, Qi Han, and L. Earle. Circuit-level load monitoring for household energy management. *Pervasive Computing, IEEE*, 10(1):40–48, Jan 2011. → pages 15, 17

[22] W.L. Chan, A.T.P. So, and L.L. Lai. Wavelet feature vectors for neural network based harmonics load recognition. In *Advances in Power System Control, Operation and Management, 2000. APSCOM-00. 2000 International Conference on*, volume 2, pages 511–516 vol.2, Oct 2000. → pages 16, 18, 29

[23] At the flick of a switch: Detecting and classifying unique electrical events on the residential power line (nominated for the best paper award), May 2010. → pages 16, 17, 31

[24] A. Cole and A. Albicki. Nonintrusive identification of electrical loads in a three-phase environment based on harmonic content. In *Instrumentation and Measurement Technology Conference, 2000. IMTC 2000. Proceedings of the 17th IEEE*, volume 1, pages 24–29 vol.1, 2000. → pages 16, 29

[25] something that i do not know. → pages 16, 17, 27

[26] T. Hassan, F. Javed, and N. Arshad. An empirical investigation of v-i trajectory based load signatures for non-intrusive load monitoring. *Smart Grid, IEEE Transactions on*, 5(2):870–878, March 2014. → pages xiv, 16, 17, 18, 24, 25

[27] A-Zoha. Non-intrusive load monitoring approaches for disaggregated energy sensing: A survey, May 2010. → pages xiv, 16

[28] M. Zeifman. Disaggregation of home energy display data using probabilistic approach. *Consumer Electronics, IEEE Transactions on*, 58(1):23–31, February 2012. → pages xiv, 17, 23, 24

[29] Ching-Lung Lin Hsueh-Hsien Chang, Hong-Tzer Yang. Load identification in neural networks for a non-intrusive monitoring of industrial electrical loads, December 2014. → pages 18

[30] Yizheng Xu. Artificial intelligence based methodology for load disaggregation at bulk supply point, December 2014. → pages 18

[31] Daniel Kroening. Computer aided verification, May 2014. → pages 18

[32] D. Egarter, V.P. Bhuvana, and W. Elmenreich. Paldi: Online load disaggregation via particle filtering. *Instrumentation and Measurement, IEEE Transactions on*, 64(2):467–477, Feb 2015. → pages 19, 20

[33] M. Figueiredo, B. Ribeiro, and A. de Almeida. Electrical signal source separation via nonnegative tensor factorization using on site measurements in a smart home. *Instrumentation and Measurement, IEEE Transactions on*, 63(2):364–373, Feb 2014. → pages 19, 20

[34] Albeik. Unsupervised disaggregation of low frequency power measurements, May 2010. → pages 19, 23

[35] J.Zico Kolter and Matthew J. Johnson. Download page for GAISLER IP Cores, May 2011. → pages xiv, 20, 21

[36] M. Figueiredo, B. Ribeiro, and A. de Almeida. Electrical signal source separation via nonnegative tensor factorization using on site measurements in a smart home. *Instrumentation and Measurement, IEEE Transactions on*, 63(2):364–373, Feb 2014. → pages xiv, 23

[37] Hsueh-Hsien Chang. Non-intrusive demand monitoring and load identification for energy management systems based on transient feature analyses, May 2010. → pages xiv, xv, 26, 27, 28, 29

[38] Christopher Laughman. Ieee power and energy magazine feature analyses, May 2010. → pages xv, 27, 30

[39] H.W. Dommel. Digital computer solution of electromagnetic transients in single-and multiphase networks. *Power Apparatus and Systems, IEEE Transactions on*, PAS-88(4):388–399, April 1969. → pages 33, 34, 38

[40] A comprehensive resource for emtdc transient analysis for pscad power system simulation. → pages 34

[41] Charles A. Thompson. A study of numerical integration techniques for use in the companion circult method of transient circuit analysis. → pages xv, 36, 37, 38

[42] Jorge Hollman. Step by step eigenvalue analysis with emtp discrete time solutions. → pages xv, 41, 43

[43] G. Groenewold. Optimal ladder filters. *Circuits and Systems II: Express Briefs, IEEE Transactions on*, 56(2):147–151, Feb 2009. → pages 56

[44] K.L. Su. *Analog Filters*. K.L. Su, K.L. Su, 2002. → pages 56

[45] Henry Ruston. *Analog Filters using MATLAB*. ML. Wanhammar, L. Wanhammarl, 2009. → pages 56

[46] Active and passive filter synthesis using matlab. → pages 56

[47] K. Murthy and R.E. Bedford. Transformation between foster and cauer equivalent networks. *Circuits and Systems, IEEE Transactions on*, 25(4):238–239, Apr 1978. → pages 56

[48] J.N. Davidson, D.A. Stone, and M.P. Foster. Required cauer network order for modelling of thermal transfer impedance. *Electronics Letters*, 50(4):260–262, February 2014. → pages 56

[49] L. Codecasa. Canonical forms of one-port passive distributed thermal networks. *Components and Packaging Technologies, IEEE Transactions on*, 28(1):5–13, March 2005. → pages 56

[50] modern synthesis. → pages 56

[51] The electrical engineering handbook. → pages 57, 58, 60

[52] Synthesis of analogue circuits. → pages xv, 59

[53] Henry Ruston. *Electric Networks*. McGraw-Hill, McGraw-Hill, 1966. → pages xv, xvi, 62, 63, 64, 65, 66

[54] Peng Zhang. Shifted frequency analysis for emtp simulation of power system dynamics, December 2009. → pages 146